26881

National Library of Canada / Bibliothèque nationale du Canada

CANADIAN THESES ON MICROFICHE / THÈSES CANADIENNES SUR MICROFICHE

NAME OF AUTHOR/NOM DE L'AUTEUR PETER H. L. PANG

TITLE OF THESIS/TITRE DE LA THÈSE STUDIES OF "FORBIDDEN" TRANSITIONS IN $Mp^4$ ELEMENTS.

UNIVERSITY/UNIVERSITÉ Univ. of Alberta

DEGREE FOR WHICH THESIS WAS PRESENTED/ GRADE POUR LEQUEL CETTE THÈSE FUT PRÉSENTÉE Ph. D.

YEAR THIS DEGREE CONFERRED/ANNÉE D'OBTENTION DE CE GRADE 1975

NAME OF SUPERVISOR/NOM DU DIRECTEUR DE THÈSE Dr. T. A. Kernaghan

Permission is hereby granted to the NATIONAL LIBRARY OF CANADA to microfilm this thesis and to lend or sell copies of the film.

The author reserves other publication rights, and neither the thesis nor extensive extracts from it may be printed or otherwise reproduced without the author's written permission.

*L'autorisation est, par la présente, accordée à la BIBLIOTHÈQUE NATIONALE DU CANADA de microfilmer cette thèse et de prêter ou de vendre des exemplaires du film.*

*L'auteur se réserve les autres droits de publication; ni la thèse ni de longs extraits de celle-ci ne doivent être imprimés ou autrement reproduits sans l'autorisation écrite de l'auteur.*

DATED/DATÉ August 1975 SIGNED/SIGNÉ Peter Pang

PERMANENT ADDRESS/RÉSIDENCE FIXE Physics Dept
Univ. of Alberta
Edmonton, Alberta

NL-91 (3-74)

THE UNIVERSITY OF ALBERTA

# STUDIES OF "FORBIDDEN" TRANSITIONS IN $np^4$ ELEMENTS

by

PETER H. L. PANG

A THESIS

SUBMITTED TO THE FACULTY OF GRADUATE STUDIES AND RESEARCH

IN PARTIAL FULFILLMENT OF THE REQUIREMENTS FOR THE DEGREE

OF DOCTOR OF PHILOSOPHY

DEPARTMENT OF PHYSICS

EDMONTON, ALBERTA

FALL, 1975

THE UNIVERSITY OF ALBERTA

FACULTY OF GRADUATE STUDIES AND RESEARCH

The undersigned certify that they have read, and recommend to the Faculty of Graduate Studies and Research, for acceptance, a thesis entitled STUDIES OF "FORBIDDEN" TRANSITIONS IN $np^4$ ELEMENTS submitted by Peter H. L. Pang in partial fulfillment of the requirements for the degree of Doctor of Philosophy.

J. A. Kernahan
Supervisor

Date: August 12/75

## ABSTRACT

Transitions within the ground configuration of the first three $np^4$ elements (O, S and Se), which are "forbidden" under electric dipole selection rules, have been studied. A comprehensive survey of the theoretical methods, based on atomic structure calculations, for determining the Einstein A-coefficients of these "forbidden" lines has also been carried out. Using a technique based on simultaneous absolute intensity and optical line-absorption measurements, experiments were conducted to determine the absolute A-values of these forbidden transitions, produced under laboratory conditions and lying in the wavelength range 2900-7800 Å. Theoretical considerations based on atomic and molecular spectroscopy have also been used to provide mechanisms for the formation of these metastable states and thus of the "forbidden" lines. Applications of the results of this work to certain studies in astrophysics, upper atmospheric and laser physics have also been undertaken.

ACKNOWLEDGEMENTS

After having suggested this project to me, my supervisor, Dr. J. A. Kernahan, provided encouragement, guidance and, at the same time, allowed me the freedom to pursue my own ideas during the work. I, therefore, wish to express my deep gratitude to him and also to thank him for many helpful discussions during the write-up of this thesis.

I would also like to thank Mr. E. A. Foster for his expert technical help in the design and construction of the miscellaneous pieces of equipment, and to Mr. J. H. Woolley for helping me in the setting up of the apparatus used in this work. Pertaining to the apparatus, I wish to thank Dr. E. H. Pinnington for the use of the vacuum monochromator and the uv photomultiplier.

I am particularly grateful to my beloved wife, Aline, for her painstaking typing of this thesis and her moral support throughout the project. I deeply appreciate her understanding in allowing me to devote many evenings and week-ends to experimentation.

Finally, it is a pleasure to acknowledge partial financial support from the University of Alberta and that provided by a postgraduate scholarship from the National Research Council of Canada while undertaking this project.

TABLE OF CONTENTS


| | | Page |
|---|---|---|
| CHAPTER I | INTRODUCTION | 1 |
| CHAPTER II | THEORETICAL CONSIDERATIONS | 11 |
| | 2.1 Electric Dipole (ED), Electric Quadrupole (EQ) and Magnetic Dipole (MD) Radiation | 11 |
| | 2.2 Identification of Multipole Transitions | 15 |
| | 2.3 Transition Probabilities for Stimulated Emission, Absorption and Spontaneous Emission | 19 |
| | 2.4 Derivation of Transition Probabilities | 21 |
| | 2.5 The Selection Rules | 29 |
| | 2.6 Theoretical Calculations of the Spontaneous Transition Probabilities for the "Forbidden" Lines of $np^4$ Elements | 31 |
| CHAPTER III | EQUIPMENT | 55 |
| CHAPTER IV | THEORIES OF THE EXPERIMENTAL METHOD | 73 |
| | 4.1 Excitation Mechanisms | 73 |
| | 4.2 Absorption-Line Theories | 81 |
| | 4.3 Spontaneous Transition Probabilities of "Forbidden" Lines | 94 |
| | 4.4 The Absolute Intensity Measurement | 97 |
| | 4.5 Obtaining the Absolute Transition Probability $A_{ij}$ from its Implicit Relationship with the Measured Quantities in this Project | 104 |

| | | Page |
|---|---|---|
| CHAPTER V | EXPERIMENTAL TECHNIQUES | 106 |
| | 5.1 Techniques in the Production of Forbidden Lines | 106 |
| | 5.2 Temperature Measurement | 113 |
| | 5.3 Photon-Counting Technique | 116 |
| | 5.4 Geometrical Limitations | 126 |
| CHAPTER VI | RESULTS AND DISCUSSION | 130 |
| | 6.1 General Remarks | 130 |
| | 6.2 The Spectra (Oxygen) | 133 |
| | 6.3 Results and Analysis on the Forbidden OI Lines at λλ5577 Å and 2972 Å | 135 |
| | 6.4 Results and Analysis on the Forbidden OI Lines at λλ6300 Å and 6364 Å | 166 |
| | 6.5 The Spectra (Sulphur) | 196 |
| | 6.6 Results and Analysis on the Forbidden Lines of Atomic Sulphur at λλ4589 and 7725 Å | 196 |
| | 6.7 The Spectra (Selenium) | 216 |
| | 6.8 Results and Analysis on the Forbidden SeI Lines at λλ4887 and 7768 Å | 216 |
| CHAPTER VII | SUMMARY | 237 |
| BIBLIOGRAPHY | | 242 |

## LIST OF TABLES


| Table | | Page |
|---|---|---|
| II-1 | The magnetic field vector $\hat{H}$, electric field vector $\hat{E}$ and the Poynting vector $\hat{S}$ for the ED, EQ and MD radiation with the assumption that $r >> \lambda >> \ell$ | 16 |
| II-2 | Zeeman patterns from ED, MD and EQ transitions in a longitudinal ($\alpha = 0$) and a transverse ($\alpha = \pi/2$) magnetic field | 18 |
| III-1 | Operating characteristics of EMR 542-G, EMI 6256S and 9658R | 63 |
| IV-1 | The low-lying metastable levels of the inert gases in eV (from C. E. Moore's Tables on "Atomic Energy Levels") | 80 |
| IV-2 | Spectral radiance $E(\lambda,T)$ in microwatts per (steradian-nanometer-mm$^2$ of source) of lamp No. EPT-1182 operated at 35 Amperes | 101 |
| V-1 | Geometrical Limitations for the "Spex" system | 128 |
| VI-1 | Results on the absolute transition probability A of the green forbidden line | 154 |
| VI-2 | Results for the true intensity ratio I(5577 Å)/I(2972 Å) | 162 |
| VI-3 | Theoretical and experimental results for the A-coefficients of the forbidden OI lines at λλ5577 and 2972 Å ($sec^{-1}$) | 165 |
| VI-4 | Results on the absolute transition probability of the red forbidden OI line at λ6300 Å | 178 |
| VI-5 | Results on the molecular absorption coefficient $k_m$ of OI 1152 Å, assuming a mean A(OI 6300 Å) of $6.29 \times 10^{-3}$ $sec^{-1}$ | 181 |
| VI-6 | Results on the true intensity ratio I(6364 Å)/I(6300 Å) | 183 |

| Table | | Page |
|---|---|---|
| VI-7 | Theoretical and experimental results for the forbidden A-values of OI lines at λλ6300 and 6364 Å (in $sec^{-1} \times 10^{-3}$) | 186 |
| VI-8 | Oxygen abundance results (Holweger Model) | 192 |
| VI-9 | Oxygen abundance results (Mutschlecner Model) | 193 |
| VI-10 | Oxygen abundance results (Utrecht Ref. Model) | 194 |
| VI-11 | Oxygen abundance results from various authors | 195 |
| VI-12 | Results on the absolute transition probability of forbidden SI line at λ4589 Å | 207 |
| VI-13 | Results on the A-ratios of the SI lines at λλ7725 and 4589 Å | 212 |
| VI-14 | Comparison of the previous and present A-values on SI 4589 and 7725 Å (in $sec^{-1}$) | 214 |
| VI-15 | Results on the absolute transition probability of the forbidden SeI line at λ4887 Å | 224 |
| VI-16 | Results on the A-ratios of the forbidden SeI lines at λλ4887 and 7768 Å | 229 |
| VI-17 | Comparison of the experimental and theoretical A-values on SeI 4887 and 7768 Å (in $sec^{-1}$) | 230 |
| VI-18 | Atomic state densities of the ground states of selenium per $cm^3$ | 234 |
| VII-1 | Summary of the forbidden A-values obtained in the present work | 240 |
| VII-2 | Summary of the allowed f-values obtained in the present work | 241 |

LIST OF FIGURES


| Figure | | Page |
|---|---|---|
| 2-1 | The electric dipole | 12 |
| 2-2 | The electric quadrupole | 12 |
| 2-3 | The magnetic dipole | 12 |
| 2-4 | Electron transitions in the non-closed shells | 46 |
| 3-1 | Photograph of the overall experimental set-up | 56 |
| 3-1a | Diagrammatic sketch of the experimental set-up | 56a |
| 3-2 | The discharge tube (DT) | 57 |
| 3-3 | The glass vacuum system | 59 |
| 3-4 | Block diagram of electronics for simultaneous photon-countings | 66 |
| 3-5 | (1) The standard lamp set up with an auxilliary plane mirror on an aluminium optical bench<br>(2) The refrigerated PM chamber attached to the exit end of the Spex 1500 | 70 |
| 3-6 | The AC discharge circuit | 70 |
| 4-1 | An absorption line | 84 |
| 4-2 | The frequency distribution of the absorption coefficient in an absorption line | 84 |
| 4-3 | Diagram of the optical arrangement with $(t + L)2\theta < D$ | 90 |
| 4-4 | $I_L/I_\ell$ vs. $k_0 i$ for oxygen ($L = 2.031i$) | 95 |
| 4-5 | The allowed and the forbidden lines with a common state i | 97 |

| Figure | | Page |
|---|---|---|
| 5-1 | The AC circuit diagram used for exciting forbidden lines of the $np^4$ elements | 108 |
| 5-2 | Temperature-time curves on the external wall of the discharge tube | 110 |
| 5-3 | Spectra of SeI from an impure and a clean discharge | 114 |
| 5-4 | Photoelectric profiles of NeI 4885 Å and SeI 4887 Å | 118 |
| 5-5 | Photoelectric profiles of OI 2972 Å and 5577 Å under the same discharge and slit conditions | 121 |
| 5-6 | The pen-chart profiles of SI 1782 Å and CO 1776 Å from an optimum krypton-sulphur discharge mixture | 125 |
| 5-7 | Illumination of the collimator by a cylindrical discharge through a rectangular slit in (a) section and (b) elevation | 127 |
| 6-1 | Partial term scheme of OI. | 134 |
| 6-2 | The green auroral line when (a) unblended and (b) blended by molecular bands | 137 |
| 6-3 | Potential energy curves for $O_2$ | 144 |
| 6-4 | The intensity of the green auroral line λ5577 Å vs. the electric current of the discharge | 149 |
| 6-5 | Resolution of OI 1218 Å from Lyman α, 1216 Å | 152 |
| 6-6 | Chart-recorded spectra of the forbidden OI lines at λλ2972 and 5577 Å | 160 |
| 6-7 | The red forbidden lines | 167 |
| 6-8 | The intensity of the red auroral line 6300 Å vs. the electric current of the discharge | 171 |

| Figure | | Page |
|---|---|---|
| 6-9 | Resolution of OI 1152 Å from $O_2$ bands | 172 |
| 6-10 | Molecular absorption path | 174 |
| 6-11 | Photographs of the green (5577 Å) and the red (6300/64 Å) forbidden lines of oxygen | 184 |
| 6-12 | Partial term scheme of SI | 197 |
| 6-13 | The forbidden SI line at λ4589 Å in a high pressure discharge medium | 199 |
| 6-14 | The intensity of the forbidden SI line at λ4589 Å vs. the electric current | 203 |
| 6-15 | The spectral scan of sulphur from 1770 Å to 1830 Å | 204 |
| 6-16 | Photographs of the forbidden SI lines at λλ4589 and 7725 Å | 211 |
| 6-17 | Partial term scheme of SeI | 217 |
| 6-18 | Photographs of the forbidden SeI line at λ4887 Å from a Ne-Se discharge which is (a) impure and (b) clean | 219 |
| 6-19 | SeI from a Ne-Se discharge run at 30 mA | 220 |
| 6-20 | Spectrum of a Ne-Se discharge, run at 30 mA, from 7720-7835 Å | 228 |
| 6-21 | The uv SeI lines used in the absorption experiment for determining the atomic state densities of the ground states | 233 |

# CHAPTER I

## INTRODUCTION

It is known that the electric dipole oscillator is the simplest model capable of radiating electromagnetic waves and that such radiation is associated with transitions between stationary atomic states, whence the corresponding spectral lines are produced. Transitions due to electric dipole radiation must satisfy certain selection rules, the most rigorous one being the "Laporte Rule - the parity[†] sum of the two states between which a transition can occur must be odd". Transitions that would violate any of the electric dipole selection rules can nevertheless occur giving rise to the so-called "Forbidden Lines", and they are usually due to electric quadrupole and/or magnetic dipole radiation.

Elements in the $np^4$ ground state configuration, i.e. with four equivalent p electrons and with principal

---

[†]The parity of a state is conventionally even or odd according as the sum of the angular momenta $\Sigma l_i$ of the electrons denoted in the state configuration, is even or odd respectively.

quantum number n, have in the LS-coupling† scheme, the following spectroscopic terms:

$$^1S_0,\ ^1D_2,\ ^3P_0,\ ^3P_1,\ ^3P_2$$

Since these terms belong to the same ground state configuration, the parity sum of any two of them will therefore be even, and any transitions among these levels will violate the strict electric dipole selection rule, thus giving rise to forbidden lines.

Historically, at the beginning of the 1920's, certain lines in nebular and auroral sources could not be identified with any known emission or absorption lines produced at that time in the laboratory. They were assumed to have originated from elements as yet undiscovered on earth or from some unknown spectra of existing elements. Then in 1925 (Mc 25) the green auroral line (5577 Å) and in 1930 (Pa 30) the red auroral lines (6300 Å and 6364 Å) of atomic oxygen were produced under laboratory conditions. It was soon realised that the wave numbers for the lines in the auroral and nebular sources coincided exactly with the differences in energy between low-lying metastable levels

---

†LS-coupling, also called Russell-Saunders coupling, is valid when the interactions between the spin and the orbit angular momenta of different electrons are greater than the interaction between the spin of each electron with its own orbit, whereby the electrostatic (rather than the magnetic) energy predominates.

and the ground state of the OI (Mc 28, Pa 30), OII, OIII, SII and NII (Bo 28) configurations. A proposal (Mr 44) to base the concept of "forbidden" lines on the smallness of the corresponding transition probability† ($\leq 10^2$ sec$^{-1}$) was not accepted (Ru 44). Explanations based on second order multipole radiation (magnetic dipole and electric quadrupole) were then put forward to account for the "forbidden" lines, and the corresponding selection rules have since been formulated and firmly established. These lines were also termed "multipole lines" by Rubinowicz (Ru 44).

The interest in forbidden lines and the problems associated with them are evidenced by the extensive list of careful investigations that have been published on them: For example,

(1) The strong and persistent presence of the green and red auroral lines of oxygen in the upper atmosphere, have led to the following studies: (i) Atomic processes, such as the role played by the metastable energy levels

---

†The "Transition Probability" or the Einstein A-coefficient of a line is the number of spontaneous downward transitions per second per atom between the two stationary states which bound the line. Hence, if N is the population density of the upper state of the transition and $\nu$ its frequency, then its intensity will be given by $I = NAh\nu$.

of the exciting or buffer agents (deactivation), or that played by thermal collisions (dissociative recombination) and so on, in the excitation mechanism of the forbidden lines (Mc 25, Se 54, Wa 59, Da 67, Re 67, Gi 69, Zi 69, Mc 70 and Wa 72). (ii) Atmospheric temperature measurement through the thermal Doppler broadening of the lines. The forbidden lines are used advantageously here because first, they are among the most prominent in the most easily accessible wavelength region; secondly, the excited, metastable states of atomic oxygen have lifetimes which are long enough to ensure that thermal equilibrum with the atmosphere is restored if it is disturbed by the excitation process; and thirdly, the self-absorption of these lines is negligible (Om 71, Hi 66, Mi 61, Tu 62). (iii) Altitude and latitude variations of aurorae with respect to the intensity ratios of forbidden lines. Reliable rocket data for altitude vs. the OI 5577 Å/6300 Å intensity ratio were obtained by Murcray (Mc 69) and for latitude vs. OI 6300 Å/$N^+$ 4278 Å intensity by Eather (Ea 69).

(2) In the determination of element abundances, such as those of sulphur and oxygen, in the solar photosphere, the relevant data on their forbidden lines could be employed. In fact, it was found by Müller (Mü 68) and Malia (Ma 68) that there are a number of advantages in using forbidden lines rather than the high-excitation permitted lines. The

former, being within the ground configuration with small excitation potential ($\leq$ 5.0 eV) at the lower level, should not be sensitive to the model atmospheres, and their equivalent widths† are independent of turbulence and damping constants. The weak permitted lines, on the other hand, are found at a depth in the solar disk where the temperature is not well known, and are very sensitive to the actual temperature adopted, while the equivalent widths of strong permitted lines are affected by turbulence and damping. Actually, when the results for the oxygen abundance from the same source of data were compared by Müller (Mü 68) using four basic solar model atmospheres, (i) Mutshlecner (Mu 64), (ii) Utrecht (Ut 64), (iii) Heinztze (He 65) and (iv) Holweger (Ho 67) which differ in temperature and turbulence distribution, it was found that there is less of a discrepancy in the oxygen abundance in using forbidden lines (15% between the two extreme models) than from using the permitted lines (35%).

---

†The equivalent width, $W_\nu$, of an absorption line is defined as the width of a perfectly black rectangular line that could remove exactly the same amount of energy from its continuum spectrum. It is obtained by dividing the total energy absorbed in this line by the energy per unit frequency emitted by the light source in the continuum spectrum at the frequency $\nu_o$:

$$W_\nu = \int \frac{I_\nu - I_o}{I_o}$$

The element abundance in the solar and other stellar atmospheres is derived from its "curve of growth" - the relationship between the equivalent width $W_\nu$ and the product of the abundance N and the oscillator strength or f-value (and the damping constant $\Gamma$, if the line is strong). The f-value of a line is directly related to its transition probability A, so that an accurate knowledge of the A-coefficient, together with a choice of forbidden lines which give the advantages discussed above, would be appropriate for use in the determination of element abundances. So far, only theoretical A-values of forbidden lines have been used for this purpose - Swings et al. (Sw 69), for the solar abundance of sulphur and Müller (Mü 68) and Malia (Ma 68), for that of oxygen could be singled out among many others.

(3) The excitation of metastable levels in $np^4$ elements was investigated by Bokhan (Bo 69) from the point of view of obtaining new efficient materials for gas lasers. Such elements possess very favourably situated energy levels for "population inversion"† (Be 65). The three near-degenerate levels of the ground state P can lead to rapid relaxation through collisions, while the absence of

---

†"Population Inversion" between two energy levels means that the upper level is more densely populated than the lower one and is one of the basic characteristics of a laser transition.

a dipole transition between the P and the D and S states, together with the relatively large energy difference of S-P and D-P transitions, leads to a long lifetime for the S and D levels. Furthermore, the excitation of transitions that are active in dipole radiation requires an energy which considerably exceeds that of the S and D states, so that the latter may be enhanced to a fairly high atomic density as compared to that of the P state. However, obtaining inversion between metastable states does not guarantee the possibility of obtaining a practical laser because of the low transition probability between them and of other factors such as those represented by equations (4) and (5) in Gould's paper (Go 65).

Selenium and tellurium were considered among the $np^4$ elements for laser production rather than oxygen and sulphur because to obtain a sufficient vapour pressure for the latter, a temperature would be required, at which the Boltzmann population of the P levels is very substantial. More specifically, the selenium forbidden line at 4887 Å, which is the transition between the metastable levels $^1S_0$ and $^3P_1$, was used by Bokhan (Bo 69) throughout his investigations.

Transition probabilities of forbidden lines have been theoretically calculated by several methods, all based on the atomic structure of the element involved. Until

recently there has not been an absolutely correct determination of the A-values, the main problems involved being associated with the relevant and correct interaction among the term configurations that are all essential in obtaining the correct choice of the wave functions used in the transition probability calculations. These problems become more complicated for heavier elements. Previous work on the subject are numerous; two excellent reviews are those of Garstang (Ga 51) and Sinanoğlu (Si 71).

Techniques for the experimental measurement of transition probabilities of allowed lines, such as those using stabilised arc and shock tube sources, were found to be quite complicated and laborious (Wi 61). As for the forbidden lines, further complications, such as production of a steady and measurable source of the normally faint lines, are involved. Until recently the only determination of the absolute transition probability of a forbidden line was the work carried out by McConkey and Kernahan (Mc 69). However, their results, obtained on the auroral green line, had an uncertainty of up to a factor of 2. In the present work the same technique was employed but improvements in the instrumentation (mainly the availability of more precise and modern equipment) and the use of recent theoretically calculated f-values have resulted in much more reliable data.

Basically, this technique involves simultaneous measurement of the forbidden line's absolute intensity and the population density of its upper energy level. The forbidden lines are produced in a discharge tube containing the element under investigation in a gaseous form and a "buffer" gas, all under some optimum conditions, and the absolute intensity is measured photoelectrically by comparison with a standard lamp. The population measurement is carried out by a line - absorption method applied to the vacuum ultraviolet line that is feeding the upper level of the forbidden line. Full experimental details and the advantages and disadvantages of the technique are discussed later.

Transition probabilities can be considered as the basic atomic parameter of the forbidden lines and their measurements justified solely on that basis. As mentioned previously, in addition to their application in calculating the element abundance of the photosphere, they are also used in the determination of the deactivation rates of the metastables in the upper atmosphere. The experimental technique used also enables measurements to be made on the atomic state population of the metastables which, in turn, would allow studies of possible population inversions that can lead to laser production (Bo 69). However, the main application of the experimental A-values

is to serve as a check on theoretical predictions based on atomic structure calculation (Ke 75a,b & c).

The above-mentioned reasons, then, provide the stimulus for the present work. Elements with an $np^4$ ground state configuration, i.e. oxygen (n = 2), sulphur (n = 3) and selenium (n = 4), have been chosen because of the relative ease by which these forbidden lines can be obtained. Moreover, the various types of processes in nature, for which studies related to astrophysics, upper atmospheric and atomic-molecular physics are important, involve $np^4$ elements.

# CHAPTER II

## THEORETICAL CONSIDERATIONS

As forbidden lines, arising from electric quadrupole and/or magnetic dipole radiation and allowed lines, arising from electric dipole radiation, are studied in this work, a concise description of the fundamental nature that characterizes these different types of radiation is first given here.

### 2.1 Electric Dipole (ED), Electric Quadrupole (EQ) and Magnetic Dipole (MD) Radiation

The "electric dipole" and the "electric quadrupole" are basically systems of charges ($\pm q$), separated by distances ($\ell_i$) of atomic dimensions and arranged with a resultant zero total charge (Figs. 2-1 and 2-2). Actually, a "dipole" is produced by displacing a "monopole" (a point charge) through a small distance $\ell_1$ and replacing the original monopole by another of the same magnitude but of opposite polarity. Likewise, a "quadrupole" is produced by displacing a dipole by a small distance $\ell_2$ and then replacing the original dipole by one of equal magnitude but of opposite sign. For the linear quadrupole $|\ell_2|=|\ell_1|=|\ell|$. This "multipole" concept can be continued indefinitely.

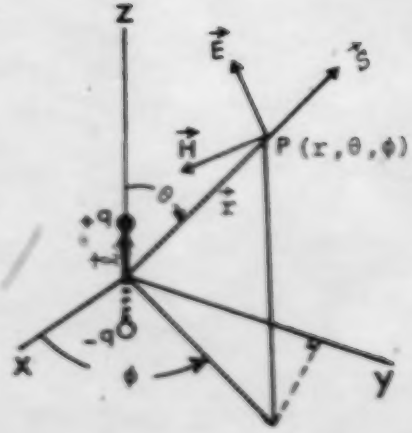


Fig. 2-1. The electric dipole, centered at the origin. The vector $\vec{l}$ and the current I are both oriented from -q to +q. The charges are assumed to oscillate with magnitude

$$q = q_0 \exp(i\omega t)$$

$\vec{E}$ is the electric field vector, $\vec{H}$ the magnetic field and $\vec{S}$ the Poynting vector at the point $P(r,\theta,\phi)$.

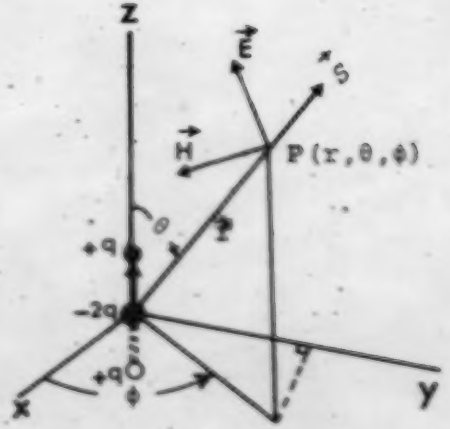


Fig. 2-2. The electric quadrupole, formed by two dipoles of opposite polarity one above the other and centered at the origin. The charges are assumed to oscillate with magnitude

$$q = q_0 \exp(i\omega t)$$

The vectors $\vec{E}$, $\vec{H}$ and $\vec{S}$ at point $P(r,\theta,\phi)$ are the same as for the electric dipole.

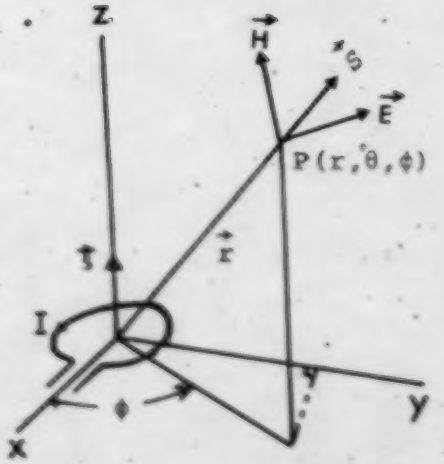


Fig. 2-3. The magnetic dipole, formed by a loop of area $S$ carrying a current I and centered at the origin. The current I is assumed to oscillate with magnitude

$$I = I_0 \exp(i\omega t)$$

The vectors $\vec{E}$, $\vec{H}$ and $\vec{S}$ are as shown.

The electric dipole has a moment given by

$$\vec{p} = q\vec{\ell}$$

or generally,

$$\vec{p} = \int \rho \vec{r}\, d\tau$$

where $\rho$ is a charge distribution in a volume $d\tau$.

The electric quadrupole has a zero dipole moment ($\Sigma qz = 0$) but its quadrupole moment is, in terms of magnitude,

$$P_{zz} = \Sigma qz^2 = 2q\ell^2$$

or generally,

$$P_{zz} = \int \rho z^2\, d\tau$$

for a charge distribution $\rho$ in a volume $d\tau$.

The "magnetic dipole" is formed by a circular loop of an area $\vec{s}$ of atomic dimension, carrying an alternating current I (see Fig. 2-3).

The magnetic dipole has a moment $\vec{m}$ given by

$$\vec{m} = I\vec{s}$$

and generally,

$$\vec{m} = 1/2 \oint \vec{r} \times I\, d\vec{\ell}$$
$$= 1/2 \int \vec{r} \times \vec{J}\, d\tau$$

for a current distribution $\vec{J}$ in a volume $d\tau$.

When the dipole or quadrupole moment for a charge or current distribution is a sinusoidal function of time,

electromagnetic waves are radiated into space. Thus ED radiation is produced when the electric dipole moment is given by

$$p = p_o e^{i\omega t}$$

where $p_o$ is the amplitude of the oscillation, $\omega$ the angular frequency and t the time.

Similarly, for EQ radiation, the quadrupole moment, is given by

$$P_{zz} = P_{zz_o} e^{i\omega t}$$

and, for MD radiation, the magnetic dipole moment by

$$m = m_o e^{i\omega t}$$

To calculate the power W emitted each of ED, EQ or MD radiation at a certain point $P(r,\theta,\phi)$, the Poynting vector $\vec{S}$ must first be determined, since W is obtained by integrating $\vec{S}$ over the surface of a sphere of radius r. The Poynting vector is given by

$$\vec{S} = 1/2 \ \mathrm{Re}(\vec{E} \times \vec{H}^*)$$

where $\vec{E}$ is the electric field vector and $\vec{H}$ the magnetic field vector. Also, the $\vec{H}$ vector is related to the electromagnetic vector potential $\vec{A}$ by

$$\vec{H} = \frac{1}{\mu_o}(\vec{\nabla} \times \vec{A})$$

where $\mu_o$ is the permeability of the medium. And, the $\vec{E}$ vector

is related to $\vec{A}$ and to the electromagnetic scalar potential V by

$$\vec{E} = - \left(\frac{1}{c}\right) \frac{\partial \vec{A}}{\partial t} - \nabla V$$

The values of V, $\vec{A}$, $\vec{H}$, $\vec{E}$, $\vec{S}$ and W at the point $P(r,\theta,\phi)$ can be derived in turn for ED, EQ or MD radiation (Co 62). Using the assumption $r >> \lambda >> \ell$, the results for the $\vec{H}$, $\vec{E}$ and $\vec{S}$ vectors are as given in Table II-1 and illustrated (not to scale) in Figs. 2-1, 2-2 and 2-3.

As shown in Table II-1, for all three cases, the Poynting vector decreases with $1/r^2$, a condition necessary for conservation of energy. There are two differences between the dipole and the quadrupole radiation: for the former, the field decreases with the square of the wavelength ($\propto 1/\lambda^2$) whereas for the latter it decreases with the cube of the wavelength ($\propto 1/\lambda^3$); the dipole field is zero along the polar axis ($\propto \sin\theta$), whereas the quadrupole field is zero both at the poles and at the equator ($\propto \sin\theta \cos\theta$).

## 2.2 Identification of Multipole Transitions

In theory, a spectral line can be identified with the type of radiation producing it (ED, EQ and/or MD) by observing the Zeeman effect on it, in a transverse magnetic field. This is possible due to the fact that the Zeeman

| | ED | EQ | MD |
|---|---|---|---|
| $\vec{H}$ | $\vec{H}$ is perpendicular to the plane containing the radius vector $\vec{r}$ and the z-axis and towards observer in Fig. 2-1. $H \propto (p_o, \frac{1}{r}, \frac{1}{\lambda^2}$ and $\sin\theta)$ | $\vec{H}$ has same orientation as for the ED case. $H \propto (p_{zz_o}, \frac{1}{r}, \frac{1}{\lambda^3}$ and $\sin\theta\cos\theta)$ | $\vec{H}$ is perpendicular and above the radius vector $\vec{r}$ and in the plane containing the z-axis and the radius vector. $H \propto (m_o, \frac{1}{r}, \frac{1}{\lambda^2}$ and $\sin\theta)$ |
| $\vec{E}$ | $\vec{E}$ is perpendicular and above the radius vector $\vec{r}$ and in the plane containing the z-axis and the radius vector. $E \propto (p_o, \frac{1}{r}, \frac{1}{\lambda^2}$ and $\sin\theta)$ | $\vec{E}$ has the same orientation as for the ED case. $E \propto (p_{zz_o}, \frac{1}{r}, \frac{1}{\lambda^3}$ and $\sin\theta\cos\theta)$ | $\vec{E}$ is perpendicular to the plane containing the radius vector $\vec{r}$ and the z-axis and away from observer in Fig. 2-3. $E \propto (m_o, \frac{1}{r}, \frac{1}{\lambda^2}$ and $\sin\theta)$ |
| $\vec{S}$ | $\vec{S}$ is along the radius vector $\vec{r}$. $S \propto (p_o^2, \frac{1}{r^2}, \frac{1}{\lambda^4}$ and $\sin^2\theta)$ | $\vec{S}$ is along the radius vector $\vec{r}$. $S \propto (p_{zz_o}^2, \frac{1}{r^2}, \frac{1}{\lambda^6}$ and $\sin^2\theta\cos^2\theta)$ | $\vec{S}$ is along $\vec{r}$. $S \propto (m_o^2, \frac{1}{r^2}, \frac{1}{\lambda^4}$ and $\sin^2\theta)$ |

Table II-1. The magnetic field vector $\vec{H}$, electric field vector $\vec{E}$ and the Poynting vector $\vec{S}$ for the ED, EQ and MD radiation with the assumption that $r \gg \lambda \gg \ell$.

patterns are characteristically different for each type of radiation. Table II-2 shows the various Zeeman patterns exhibited by the multipole transitions. Here, $\Delta m$ denotes the change in the magnetic quantum number, $\alpha$ the angle between the direction of observation and the magnetic field, $\pi$ and $\sigma$ the plane of polarisation parallel or perpendicular to the magnetic field respectively, and R.C. and L.C. right circular and left circular polarization respectively.

The longitudinal ($\alpha = 0$) effect is the same for all types of radiation whereas the transverse ($\alpha = \pi/2$) effect is different for each of them. It is therefore possible to distinguish among the different types of radiation by observations of the $\pi$ and $\sigma$ components in a transverse magnetic field. Such a method was used by Fredricks and Campbell (Fr 30) on the green auroral line of oxygen, when they established for the first time an experimental verification of the occurrence of electric quadrupole radiation. Similarly, Niewodniczanski (Ni 34) established the existence of magnetic dipole radiation through his investigation on the forbidden line of PbI 4618 Å. Also, Jenkins and Mrozowski (Je 41) identified the line in PbI at 7330 Å (which produces six $\pi$- components and seven $\sigma$- components in a transverse field) as being due to an admixture of EQ and

| ΔM | | 2 | 1 | 0 | -1 | -2 |
|---|---|---|---|---|---|---|
| Electric Dipole | α = π/2 | | σ | π | σ | |
| Magnetic Dipole | | | π | σ | π | |
| Electric Quadrupole | | σ | π | | π | σ |
| Electric Dipole | α = 0 | | RC | LC | RC | |
| Magnetic Dipole | | | RC | LC | RC | |
| Electric Quadrupole | | | RC | LC | RC | |

Table II-2. Zeeman patterns from ED, MD and EQ transitions in a longitudinal ($\alpha = 0$) and a transverse ($\alpha = \pi/2$) magnetic field.

MD radiation. Their investigation on the intensities of the individual Zeeman components of that line also confirmed an "interference effect" between those two types of radiation - the intensities of the individual Zeeman components are not found by simply summing the intensities for independent EQ and MD radiation, but must include a term dependent on the fact that both modes of radiation are possible (Ge 41, Sh 41). In contrast, the intensity of a line as a whole, which if it is isotropic and unpolarised in natural excitation, is the sum of the intensities of the quadrupole and magnetic dipole radiation separately computed, so that the EQ transition probability and the MD transition probability are to be directly added to obtain the total transition probability (Sh 41). It can be noted here that the red auroral lines of oxygen (OI 6300 Å and OI 6364 Å) are both due to an admixture of EQ and MD radiation.

## 2.3 Transition Probabilities for Stimulated Emission, Absorption and Spontaneous Emission

The interaction between a classically charged oscillator and a radiation field may be regarded as a perturbation which can cause transitions in the unperturbed system, with the result that atoms may jump from one stationary state to another, along with the emission or

absorption of light quanta. Such "stimulated" or "induced emission" and "absorption" effects take place according to the phase relation between the field and the oscillator. However, a classical oscillator can also emit radiation "spontaneously", whether or not an external radiation field is interacting. The probability per unit time of any of these three types of transitions between two stationary states is known as the "Einstein Probability Coefficient" or "Transition Probability". The relationships among the three types of transition probability can be derived from statistical considerations and from the "principle of detailed balancing" (Ei 17). They are:

$$B_{ji} = \left(\frac{g_i}{g_j}\right) B_{ij}$$

and (2-1)

$$A_{ij} = \left(\frac{8\pi h\nu^3}{c^2}\right) B_{ij}$$

where $A_{ij}$ is the spontaneous emission, $B_{ij}$ the induced or stimulated emission and $B_{ji}$ the absorption transition probability between the upper level i and the lower level j; the g's are the statistical weights, h is Planck's constant, c the velocity of light and $\nu$ the frequency of the isotropic and unpolarized light emitted in the transitions. Thus if one of the coefficients is known, the others may be found by substituting in equation (2-1).

It can also be shown that in the spectral region where $h\nu/kT >> 1$, for a system with T as its absolute temperature and k as Boltzmann's constant, the stimulated emission or absorption is negligible compared to the spontaneous emission - consider visible radiation at 5000 Å and at temperature of 500°K. Then for $h = 6.62 \times 10^{-27}$ erg sec and $k = 1.38 \times 10^{-16}$ cgs units, we will obtain, $h\nu/kT = 50$, i.e. >> 1. Under such conditions Planck's law (A1 53) is reduced to

$$I_\nu \approx \left(\frac{2h\nu^3}{c^2}\right) e^{-h\nu/kT}$$

and the number of stimulated emissions per $cm^3$ per sec will be, for a blackbody,

$$B_{ij} I_\nu = B_{ij} \left(\frac{2h\nu^3}{c^2}\right) e^{-h\nu/kT}$$

$$= A_{ij} e^{-h\nu/kT} << A_{ij}$$

since $h\nu/kT >> 1$.

## 2.4 Derivation of Transition Probabilities

### (a) For ED Radiation

A rigorous derivation of transition probabilities requires that quantum equations of motion of the electromagnetic field be found that are analogous to Maxwell's equations, whereby Planck's original quantum hypotheses can be fitted into a general theoretical framework. However,

the derivation can be achieved by treating the electromagnetic field classically and the particles with which the field interacts by quantum mechanics. Such a semi-classical treatment can yield an approximately correct value of the absorption or stimulated transition probability, and then by substituting into equation (2-1) one can obtain a value for the spontaneous transition probability.

Consider the motion of a charged mass point in a general external e.m. field and with an internal potential energy V. The classical Hamiltonian, expressed in terms of the canonical variables $\vec{r}$, $\vec{p}$ and the electromagnetic potentials $\vec{A}$, is

$$H = \frac{1}{2m}\left(\vec{p} - \frac{e}{c}\vec{A}\right)^2 + e\phi + V$$

$$= \frac{\vec{p}^2}{2m} - \frac{e}{mc}\left(\vec{A}.\vec{p} + \vec{p}.\vec{A}\right) + \frac{e^2}{2mc^2}A^2 + e\phi + V \qquad (2\text{-}2)$$

where e is the charge on the particle and c is the speed of light; the electric and magnetic field strengths are given in terms of the potentials by

$$\vec{E} = -\frac{1}{c}\frac{\partial \vec{A}}{\partial t} - \vec{\nabla}\phi \qquad \vec{H} = \vec{\nabla} \times \vec{A} \qquad (2\text{-}3)$$

Substituting for p with $-(ih/2\pi)\nabla$, as required by quantum mechanical theory, into equation (2-2), the corresponding time-dependent Schrödinger wave equation is obtained:

$$\frac{i\hbar\partial\psi}{\partial t} = \left[-\frac{\hbar^2}{2m}\nabla^2 + \frac{ie\hbar}{mc}(\vec{A}.\vec{\nabla}) + \frac{ie\hbar}{2mc}(\vec{\nabla}.\vec{A}) + \frac{e^2\vec{A}^2}{2mc^2} + e\phi + V\right]\psi \qquad (2\text{-}4)$$

V is the potential energy that binds the particle; $(A, \phi)$ represent an e.m. field that is weak enough so that those terms can be regarded as a perturbation.

The e.m. field is described by Maxwell's equations which, in Gaussian units, are:

$$\vec{\nabla} \times \vec{E} + \frac{1}{c}\frac{\partial\vec{H}}{\partial t} = 0 \qquad \vec{\nabla} \times \vec{H} - \frac{1}{c}\frac{\partial\vec{E}}{\partial t} = \frac{4\pi}{c}\vec{J}$$
$$\vec{\nabla}.\vec{E} = 4\pi\rho \qquad \vec{\nabla}.\vec{H} = 0 \qquad (2\text{-}5)$$

Substituting equations (2-3) and (2-4) into the third of equation (2-5), we obtain

$$\vec{\nabla} \times \vec{\nabla} \times \vec{A} + \frac{1}{c^2}\frac{\partial^2\vec{A}}{\partial t^2} = 0 \qquad (2\text{-}6)$$

where

$$\vec{\nabla} \times \vec{\nabla} \times \vec{A} = \vec{\nabla}(\vec{\nabla}.\vec{A}) - \nabla^2\vec{A} \qquad (2\text{-}7)$$

In a vacuum ($J = \rho = 0$) the general solution of Maxwell's equations is

$$\vec{\nabla}.\vec{A} = 0 \text{ and } \phi = 0 \qquad (2\text{-}8)$$

Substituting equations (2-7) and (2-8) into equation (2-6), we obtain

$$\nabla^2\vec{A} - \frac{1}{c^2}\frac{\partial\vec{A}}{\partial t^2} = 0 \qquad (2\text{-}9)$$

A typical plane wave solution of equation (2-9) is one that represents a real potential with the propagation

vector $\vec{k}$ and the polarization (complex) vector $\vec{A}_o$ which is perpendicular to $\vec{k}$:

$$\vec{A}(\vec{r},t) = \vec{A}_o \exp\,[i(\vec{k}.\vec{r} - \omega t)] \qquad (2\text{-}10)$$

where the frequency of the wave $\omega = kc$.

The vector potential from equation (2-10) is now used as a small perturbation in equation (2-4) to calculate the probability of the transition that it has caused between the stationary states. The third term $(\vec{\nabla}.\vec{A})$ and the fifth term $(\phi)$ on the R.H.S. of equation (2-4) are now zero and, to the first order of perturbation theory, the term $e^2\vec{A}^2/2mc^2$ can be neglected and equation (2-4) re-written as

$$i\hbar \frac{\partial \Psi}{\partial t} = (H_o + H')\Psi$$

where $$H_o = -\frac{\hbar^2}{2m}\nabla^2 + V(\vec{r}) \qquad H' = \frac{ie\hbar}{mc}(\vec{A}.\vec{\nabla}) \qquad (2\text{-}11)$$

Using $H_o$ as the unperturbed Hamiltonian and H' as the perturbation that causes the transitions it can then be shown (Sc 55) that the transition probability per unit time of the stimulated emission is given by

$$B_{ij} = \frac{e^2}{2\pi m^2 \nu^2} \left| \int \Psi_i^* \exp(i\vec{k}.\vec{r})\nabla_A \Psi_j \, d\tau \right|^2 \qquad (2\text{-}12)$$

where $\Psi_i$, $\Psi_j$ are the wavefunctions of the initial and final states and $\nabla_A$ is the component of the gradient vector along the polarization vector $\vec{A}_o$.

In most cases of practical interest, the wave-

length ($\lambda$) of the radiation is many times greater than the linear dimensions ($r = a$) of the wavefunctions that describe the motion of the particle, i.e. $\lambda >> a$, so that

$$\vec{k}.\vec{r} = \left(\frac{2\pi}{\lambda}\right) a \cos\theta << 1$$

Thus, whenever $\Psi_i$ and $\Psi_j$ are large enough to give an appreciable contribution to the integral of (2-12), $\vec{k}.\vec{r} << 1$ so that

$$\exp(i\vec{k}.\vec{r}) = 1$$

and equation (2-12) becomes

$$B_{ij} = \frac{e^2}{2\pi m^2 \nu^2} \left| \int \Psi_i^* \nabla_A \Psi_j \, d\tau \right|^2 \qquad (2\text{-}13)$$

Then, transforming the integral of equation (2-13) as a matrix element of the momentum and the position of the particle ($\nabla_A \rightarrow \frac{i}{\hbar} p_A \rightarrow \frac{im}{\hbar} \frac{dr_A}{dt}$) and considering an isotropic radiation, the <u>stimulated emission transition probability</u> becomes

$$B_{ij} = \frac{8\pi^3}{3h^2 c} \left| e \int \psi_i^* \vec{r} \, \psi_j \, d\tau \right|^2 \qquad (2\text{-}14)$$

And the <u>absorption transition probability</u> is obtained by substituting in equation (2-1), i.e.

$$B_{ji} = \left(\frac{g_i}{g_j}\right) \frac{8\pi^3}{3h^2 c} \left| e \int \psi_i^* \vec{r} \, \psi_j \, d\tau \right|^2 \qquad (2\text{-}14a)$$

The <u>spontaneous transition probability</u> is then obtained by substituting equation (2-14) into (2-1):

$$A_{ij} = \frac{64\pi^4\nu^3}{3hc^3} \left| e\int \psi_i^* \vec{r}\, \psi_j \, d\tau \right|^2 \qquad (2\text{-}15)$$

The quantity $e\int \psi_i^* \vec{r}\, \psi_j \, d\tau$ is referred to as the dipole moment, and transitions for which this matrix element is non-zero are the "electric dipole transitions".

(b) For MD and EQ Radiation

It may happen that the dipole matrix element is zero for particular states i and j, but yet transitions still occur between them. In that case, the replacement of $\exp(i\vec{k}.\vec{r})$ by 1 as an approximation in the integral of (2-12) is not justified. Expanding the exponential in a power series, we have:

$$\exp(i\vec{k}.\vec{r}) = 1 + i\vec{k}.\vec{r} + \frac{1}{2^1}(i\vec{k}.\vec{r})^2 + \ldots \qquad (2\text{-}16)$$

or in a series of spherical harmonics

$$\exp(i\vec{k}.\vec{r}) = j_0(kr) + 3ij_1(kr)\, P_1(\cos\theta) - 5j_2(kr)\, P_2(\cos\theta) + \ldots$$

where $\theta$ is the angle between $\vec{k}$ and $\vec{r}$.

Thus if the dipole matrix element which is provided by the first term of the series expansion vanishes, the second term of the expansion may provide a transition matrix element that does not vanish. This so-called "forbidden" transition has therefore a matrix element which is reduced by a factor of the order of $ka$, where

$r = a$ is of the linear dimension of the particle wave-function. The transition probability, which is proportional to the square of its matrix element, is therefore reduced by a factor $(ka)^2$ with respect to dipole or "allowed" transitions. Actually, for an atom of radius $a = 1$ Å and for a wavelength $\lambda = 5000$ Å, we have

$$(ka)^2 = \left(\frac{2\pi a}{\lambda}\right)^2 \approx 10^{-6}$$

Thus the transition probability for second order radiation is $\approx 10^{-6}$ times less strong than that of allowed radiation.

When the second order term in equation (2-16) is fully developed, it is found to consist of two parts:

(i) the magnetic dipole moment $\vec{M}$ and

(ii) the electric quadrupole moment $\overleftrightarrow{N}$.

(i) The theory for magnetic dipole radiation field is the same as that of electric dipole and the MD transition probability, $A_{m_{ij}}$ from state i to state j, is obtained by replacing the ED moment, $\int e\psi_i^* \vec{r}\, \psi_j \, d\tau$, in equation (2-15) by the MD moment, $\int \psi_i^* \vec{M} \psi_j \, d\tau$, so that

$$A_{m_{ij}} = \frac{64\pi^6 \nu^3}{3hc^3} \left| \int \psi_i^* \vec{M} \psi_j \, d\tau \right|^2 \qquad (2\text{-}17)$$

Whereas the ED moment is classically defined as $\vec{P} = \Sigma\, e\vec{r}$, the MD moment is

$$\vec{M} = \frac{e}{mc} \Sigma\, (\vec{L} + 2\vec{S}) \qquad (2\text{-}18)$$

where $\vec{L}$ and $\vec{S}$ are the resultant orbital and spin angular

momenta measured in Bohr units, $h/2\pi$.

The square of the matrix element in (2-17) is defined by Condon and Shortley (Co 35) in terms of the line strength $S_{m_{ij}}$ in such a way that the intensity is proportional to the number of atoms in any one of the initial levels instead of the total number of atoms in the initial level (as done traditionally for an ED line). Thus the strength of the MD line is

$$S_{m_{ij}} = \left| \int \psi_i^* \hat{M} \psi_j \, d\tau \right|^2 \qquad (2\text{-}19)$$

with the number of atoms N in any one of the initial levels i converted into $(2J_i + 1)N_i$, where $(2J_i + 1)$ is the statistical weight of the initial level, so that the transition probability

$$A \propto \frac{1}{N} \propto \frac{1}{(2J_i + 1)N_i}$$

Then substituting equation (2-19) into (2-17), we obtain for the Magnetic Dipole Transition Probability,

$$A_{m_{ij}} = \frac{64\pi^6\nu^3}{3hc^3} \frac{1}{2(J_i + 1)} S_{m_{ij}} \qquad (2\text{-}20)$$

(ii) Similarly, the Electric Quadrupole Transition Probability is obtained as

$$A_{q_{ij}} = \frac{32\pi^6\nu^5}{5hc^5(2J_i + 1)} S_{q_{ij}} \qquad (2\text{-}21)$$

where the strength of the EQ line,

$$S_{q_{ij}} = \left| \int \psi_i^* \vec{N} \psi_j \, d\tau \right|^2 \qquad (2\text{-}22)$$

Here, $\overleftrightarrow{N}$ is the EQ moment expressed as a symmetric tensor or dyadic which, in terms of the position vectors $\vec{r}_s$ of the electrons, is given by

$$\overleftrightarrow{N} = e \sum_s \vec{r}_s \vec{r}_s - \frac{1}{3} r_s^2 \overleftrightarrow{F} \qquad (2\text{-}23)$$

where

$$\overleftrightarrow{F} = \hat{i}\hat{i} + \hat{j}\hat{j} + \hat{k}\hat{k}$$

## 2.5 The Selection Rules

Selection Rules for ED, MD and EQ-types of transitions can be formulated by considering the non-disappearance of the integrand in each of the equations (2-15), (2-20) and (2-21). This will therefore depend on the parity sum of all the functions it contains. It is known that an ordinary function is even or odd according to whether it does or does not change sign, through reflection at the origin respectively; for a quantum mechanical wavefunction the parity depends on the number of nodal surfaces which go through the origin of co-ordinates, i.e. it is even or odd if the sum of the $\ell$-values ($\Sigma \ell_i$) for the electron configuration is even or odd respectively. For instance, the wavefunctions of the ground configuration states among the $np^4$ elements ($np^4$ $^1S_0$, $^1D_2$, $^3P_{0,1,2}$) are all even.

The results of all the above-mentioned considerations are as shown in Table II-3. Here L, S, J are the

Table II-3. Selection rules for atomic spectra.

| | Electric Dipole | Magnetic Dipole | Electric Quadrupole |
|---|---|---|---|
| (1) | $\Delta J = 0, \pm 1$ | $\Delta J = 0, \pm 1$ | $\Delta J = 0, \pm 1, \pm 2$ |
| | $0 \not\leftrightarrow 0$ | $0 \not\leftrightarrow 0$ | $0 \not\leftrightarrow 0, \frac{1}{2} \not\leftrightarrow \frac{1}{2}, 0 \not\leftrightarrow 1$ |
| (2) | $\Delta M = 0, \pm 1$ | $\Delta M = 0, \pm 1$ | $\Delta M = 0, \pm 1, \pm 2$ |
| (3) | Parity change | No parity change | No parity change |
| (4) | $\Delta S = 0$ | $\Delta S = 0$ | $\Delta S = 0$ |
| (5) | $\Delta L = 0, \pm 1$ | $\Delta L = 0$ | $\Delta L = 0, 1, 2$ |
| | $0 \not\leftrightarrow 0$ | | $0 \not\leftrightarrow 0, 0 \not\leftrightarrow 1$ |
| (6) | One electron jump | No electron jump | One or no electron jump |
| | $\Delta l = 1$ | $\Delta l = 0$ | $\Delta l = 0, 2$ |
| | | $\Delta n = 0$ | |

orbital, spin and total angular momenta of the atomic electrons respectively. M is the magnetic quantum number and n the principal quantum number.

Not all the rules listed are strictly adhered to. For instance, if the spin-orbit interaction in the atom becomes appreciable, i.e. if the interaction between the spin of each electron with its own orbit is appreciable compared to the interactions between the spins and orbits of the electrons, departures from LS-coupling will occur and the wavefunctions will be modified - they will become an admixture of the original wavefunction and others associated with different multiplicities and L-values, but with the same value of J (intercombination transitions). However, for light elements, the interaction is slight and the modified wavefunction for any term is not very different from the pure Russel-Saunders wavefunction for the same term. For the large spin-orbit interactions, i.e. jj-coupling, L and S are no longer "good quantum numbers" and the selection rules $\Delta S = 0$, $\Delta L = 0$ are meaningless.

## 2.6 Theoretical Calculations of the Spontaneous Transition Probabilities for the "Forbidden" Lines of $np^4$ Elements

We have seen previously how the spontaneous transition probabilities of forbidden lines can be derived by using the small electromagnetic potentials A and $\phi$ as a pertur-

bation to the Hamiltonian. The results as represented by equations (2-20) and (2-21) indicate that to compute the A-coefficient accurately the wavefunctions of the states involved must be as accurate as possible.

Basically, there have been two theoretical approaches towards this problem - in the first one a "perturbation theory" is used and in the second, a "non-closed shell many-electron theory" is applied.

(a) The "Perturbation Method"

In this method, the unperturbed Hamiltonian is that of a pure LS-coupling system. The interaction potential V, that binds the particles of the atom (equation 2-4) and that consists mainly of the electrostatic energies due to the Coulomb force between each electron and its nucleus and among themselves), is considered as part of the unperturbed Hamiltonian. The starting wavefunction is thus made self-consistent with the Coulomb field interactions, i.e.

$$H_0 = E + V$$

$$= E + \left( \sum_{i=1} - \frac{Ze^2}{r_i} + \sum_{i>j} \frac{e^2}{r_{ij}} \right) \qquad (2\text{-}24a)$$

where the first term in the parenthesis is the Coulomb attractive force between each electron and its nucleus, and the second

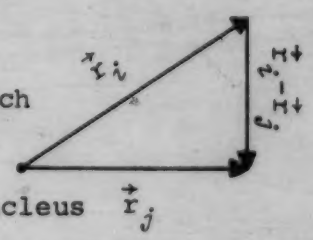

term is the Coulomb mutual repulsive force among the electrons.

However, practically all energy levels lie between LS- and jj-coupling, although mostly very close to LS-coupling. The interactions that cause the departure from LS-coupling are small and their net effect is here considered as the perturbation H'. Thus we ask the question: what are the relevant interactions that contribute to this perturbation? The accuracy of the transition probabilities depends on the correctness of the answer to this question.

The perturbations involved are usually classified into two main categories, namely,

(1) the coupling between the electron's spin and its own orbit ($\gamma$)

(2) the coupling between the electrons' spin-spin and spin-other orbit ($\eta$).

Perturbations of the first category alone have been used in the computations by such previous workers as Condon (Co 34), Pasternack (Pa 40) and Shortley et al. (Sh 41). Perturbations of the second category were added to those of the first category in the calculations by Araki (Ar 48), Aller et al. (Al 49), Yamanouchi and Horie (Ya 52), Czyzak and Krueger (Cz 63) and Garstang (Ga 51, 56, 64).

The A-coefficients from the results obtained by Garstang are more often used as a standard reference

nowadays. A brief survey of the theoretical calculations undertaken in this perturbation method, with emphasis on Garstang's analysis, can be described as follows:

Consider an element which has a $np^4$ ground state configuration. Suppose $E(^1S)$, $E(^1D)$ and $E(^3P)$ denote the energies of its unperturbed $^1S$, $^1D$ and $^3P$ terms respectively under pure LS-coupling. The matrix elements of the unperturbed Hamiltonian are then

$$\langle m|H_o|n\rangle = \begin{array}{c} \\ {}^1S_0 \\ {}^1D_2 \\ {}^3P_0 \\ {}^3P_1 \\ {}^3P_2 \end{array} \begin{array}{c} \begin{array}{ccccc} {}^1S_0 & {}^1D_2 & {}^3P_0 & {}^3P_1 & {}^3P_2 \end{array} \\ \begin{bmatrix} E(^1S) & 0 & 0 & 0 & 0 \\ 0 & E(^1D) & 0 & 0 & 0 \\ 0 & 0 & E(^3P) & 0 & 0 \\ 0 & 0 & 0 & E(^3P) & 0 \\ 0 & 0 & 0 & 0 & E(^3P) \end{bmatrix} \end{array} \qquad (2\text{-}24b)$$

The electron's spin and own-orbit interaction is given by (Sh 41):

$$H_1' = \frac{-2\mu^2}{e}\left(\frac{1}{r}\frac{dV}{dr}\right)\sum_{i=1} \vec{l}_i \cdot \vec{s}_i \qquad (2\text{-}25a)$$

where $\mu = \frac{eh}{4\pi mc}$ is the Bohr magneton,

$V = \mu^2 [Z - \sigma(r)] \times \frac{1}{\langle r^3 \rangle}$ is the Hartree central potential,

$\sigma(r) \equiv$ mean electronic charge, other than that of a

np electron interior to a radius r, which is due to the screening of the spin-orbit interactions between p-electrons and core-electrons,

$\frac{1}{\langle r^3 \rangle} = \int_0^\infty \frac{1}{r^3} R_{np}^2(r)\, dr \equiv$ radial part of the wavefunction of an np electron, normalised such that $\int_0^\infty R_{np}^2(r)\, dr = 1$.

The matrix elements of $H_1'$ in terms of $\gamma$ can be deduced from Condon and Shortley in "The Theory of Atomic Spectra", pp. 266-271 or from G. Araki (Ar 48). For the $np^4$ elements, they are

$$\langle m|H_1'|n\rangle = \begin{array}{c} \\ {}^1S_0 \\ {}^1D_2 \\ {}^3P_0 \\ {}^3P_1 \\ {}^3P_2 \end{array} \begin{array}{c} \begin{array}{ccccc} {}^1S_0 & {}^1D_2 & {}^3P_0 & {}^3P_1 & {}^3P_2 \end{array} \\ \begin{bmatrix} 0 & 0 & \sqrt{2}\gamma & 0 & 0 \\ 0 & 0 & 0 & 0 & \frac{-\gamma}{\sqrt{2}} \\ \sqrt{2}\gamma & 0 & & 0 & 0 \\ 0 & 0 & 0 & \frac{\gamma}{2} & 0 \\ 0 & \frac{-\gamma}{\sqrt{2}} & 0 & 0 & \frac{-\gamma}{2} \end{bmatrix} \end{array} \qquad (2\text{-}25b)$$

where $\gamma = 2\mu^2 \int_0^\infty \left(-\frac{1}{r}\frac{dV}{dr}\right) R_{np}^2(r)\, dr$ (2-26)

The electrons' spin-spin and spin-other orbit interactions are given by Aller et al. (Al 49):
For the spin-spin interaction

$$H'_{2a} = \sum_{j>i} \frac{4\mu^2}{r_{ij}^3}\left[\hat{s}_i \cdot \hat{s}_j - \frac{3}{r_{ij}^2}(\hat{s}_i \cdot \vec{r}_{ij})(\hat{s}_j \cdot \vec{r}_{ij})\right] \qquad (2\text{-}27a)$$

For the spin-other orbit interaction

$$H'_{2b} = \sum_{j=1} \frac{4\mu^2}{h r_{ij}^3} \left[ \vec{r}_{ij} \times (\hat{p}_j - \tfrac{1}{2}\hat{p}_i) . \hat{s}_i \right] \qquad (2\text{-}28a)$$

where $\vec{r}_i$, $\vec{r}_{ij}$ are the distance vectors of the electrons from the nucleus and from each other, $\hat{p} = (h/2\pi i)\nabla$ is the momentum operator and $\hat{s}$, in $h/2\pi$ units, is the electron spin whose components are proportional to Pauli matrices. The matrix elements of $H'_{2a}$ and $H'_{2b}$ in terms of $\eta$ can be deduced from Garstang (Ga 51) or from Yamamouchi and Horie (Ya 52):

$$\langle m|H'_{2a}|n\rangle = \begin{array}{c} \\ {}^1S_0 \\ {}^1D_2 \\ {}^3P_0 \\ {}^3P_1 \\ {}^3P_2 \end{array} \begin{array}{c} \begin{array}{ccccc} {}^1S_0 & {}^1D_2 & {}^3P_0 & {}^3P_1 & {}^3P_2 \end{array} \\ \begin{bmatrix} 0 & 0 & 0 & 0 & 0 \\ 0 & 0 & 0 & 0 & 0 \\ 0 & 0 & 6\eta & 0 & 0 \\ 0 & 0 & 0 & 3\eta & 0 \\ 0 & 0 & 0 & 0 & -3\eta \end{bmatrix} \end{array} \qquad (2\text{-}27b)$$

$$\langle m|H'_{2b}|n\rangle = \begin{array}{c} \\ {}^1S_0 \\ {}^1D_2 \\ {}^3P_0 \\ {}^3P_1 \\ {}^3P_2 \end{array} \begin{array}{c} \begin{array}{ccccc} {}^1S_0 & {}^1D_2 & {}^3P_0 & {}^3P_1 & {}^3P_2 \end{array} \\ \begin{bmatrix} 0 & 0 & 0 & 0 & 0 \\ 0 & 0 & 0 & 0 & 0 \\ 0 & 0 & -4\eta & 0 & 0 \\ 0 & 0 & 0 & 2\eta & 0 \\ 0 & 0 & 0 & 0 & \frac{-2}{5}\eta \end{bmatrix} \end{array} \qquad (2\text{-}28b)$$

where $\eta = \mu^2 \int_0^\infty \frac{1}{r_2} \frac{\partial a_0}{\partial r_2} R_{np}^2(r_1)\, R_{np}^2(r_2)\, dr_1\, dr_2$ (2-29)

with $a_0 = \begin{cases} \frac{1}{r_2} & (r_1 \leq r_2) \\ \frac{1}{r_1} & (r_1 > r_2) \end{cases}$

The net perturbation H' in matrix form is then obtained by adding up equations (2-25b), (2-27b) and (2-28b):

$\langle m|H'|n\rangle = \langle m|H_1'|n\rangle + \langle m|H_{2a}'|n\rangle + \langle m|H_{2b}'|n\rangle$

$$= \begin{array}{c} \\ {}^1S_0 \\ {}^1D_2 \\ {}^3P_0 \\ {}^3P_1 \\ {}^3P_2 \end{array} \begin{array}{c} \begin{array}{ccccc} {}^1S_0 & {}^1D_2 & {}^3P_0 & {}^3P_1 & {}^3P_2 \end{array} \\ \begin{bmatrix} 0 & 0 & \sqrt{2}\gamma & 0 & 0 \\ 0 & 0 & 0 & 0 & \frac{-\gamma}{\sqrt{2}} \\ \sqrt{2}\gamma & 0 & (\gamma+2\eta) & 0 & 0 \\ 0 & 0 & 0 & (\frac{\gamma}{2}+\sqrt{\eta}) & 0 \\ 0 & \frac{-\gamma}{\sqrt{2}} & 0 & 0 & -(\frac{\gamma}{2}+\frac{17}{5}\eta) \end{bmatrix} \end{array} \quad (2\text{-}30)$$

Now, since the ${}^3P$ states are "near-degenerate", the Perturbation Theory treatment for the degenerate case should be applied here. Also, it is known (Sc 55b) that "a necessary and sufficient condition that degeneracy is removed in any given order is either that the diagonal matrix elements of H' for the three degenerate unperturbed states are unequal or that the off-diagonal matrix elements of H' between these states is non-zero". These conditions are satisfied here by the matrix elements of

H' (see equation 2-30). The degeneracy can thus be removed as follows:

The Hamiltonian H, obtained by adding up equations (2-24b) and (2-30) is

$$H = H_0 + H' \qquad (2\text{-}31)$$
$$= H_{mn}, \text{ in matrix form.}$$

Then if $\psi_n$ is the unperturbed wavefunction of the level n

$$H_0 \psi_n = E_n^0 \psi_n \qquad (2\text{-}32)$$

and the perturbed wavefunction $\psi'$ can be represented mathematically as a linear combination of $\psi_n$:

$$\psi' = \sum_n a_n \psi_n \qquad (2\text{-}33)$$

Substitution of equation (2-33) into the Schrödinger equation,

$$(H - E)\ \psi' = 0$$

reduces to an infinite system of algebraic equations,

$$\sum_n (H_{mn} - E\ \delta_{mn})\ a_n = 0 \qquad (2\text{-}34)$$

where $$H_{mn} = \langle m|H|n\rangle = \begin{cases} E_n^0 + H'_{nn} & \text{if } m = n \\ H'_{mn} & \text{if } m \neq n \end{cases}$$

Equation (2-34) can be solved for the $a_n$'s if and only if the determinant of their coefficients vanishes, and the roots of the secular equation thus obtained are the exact energy eigenvalues of H. The secular solution is

$$|H_{mn} - E\ \delta_{mn}| = 0$$

i.e.

$$\begin{vmatrix} E(^1S)-E_1' & 0 & \sqrt{2}\gamma & 0 & 0 \\ 0 & E(^1D)-E_2' & 0 & 0 & -\frac{\gamma}{2} \\ \sqrt{2}\gamma & 0 & E(^3P)+\gamma+2\eta-E_3' & 0 & 0 \\ 0 & 0 & 0 & E(^3P)+\frac{\gamma}{2}+5\eta-E_4' & 0 \\ 0 & -\frac{\gamma}{2} & 0 & 0 & E(^3P)-\frac{\gamma}{2}-\frac{17\eta}{5}-E_5' \end{vmatrix} = 0 \quad (2\text{-}35)$$

and the solution (neglecting $\gamma\eta$ and $\eta^2$ and retaining powers of $\gamma$ up to the fourth) is

$$E_1' = E'(^1S_0) = E(^1S) + \frac{2\gamma^2}{(SP)} + \frac{2\gamma^3}{(SP)^2} + \frac{2\gamma^4}{(SP)^3} \quad (2\text{-}36a)$$

$$E_2' = E'(^1D_2) = E(^1D) + \frac{\gamma^2}{2(DP)} - \frac{\gamma^3}{4(DP)^2} - \frac{\gamma^4}{8(DP)^3} \quad (2\text{-}36b)$$

$$E_3' = E'(^3P_0) = E(^3P) + \gamma + 2\eta - \frac{2\gamma^2}{(SP)} - \frac{2\gamma^3}{(SP)^2} - \frac{2\gamma^4}{(SP)^3} \quad (2\text{-}36c)$$

$$E_4' = E'(^3P_1) = E(^3P) + \frac{1}{2}\gamma + 8\eta \quad (2\text{-}36d)$$

$$E_5' = E'(^3P_2) = E(^3P) - \frac{1}{2}\gamma - \frac{17}{5}\eta - \frac{\gamma^2}{2(DP)} + \frac{\gamma^3}{4(DP)^2} + \frac{\gamma^4}{8(DP)^3} \quad (2\text{-}36e)$$

where $(SP) = E(^1S) - E(^3P)$ and $(DP) = E(^1D) - E(^3P)$.

The next step taken by Garstang distinguished his results from others - he substituted the values of $E'(^1S_0)$, $E'(^1D_2)$ and $E'(^3P_{0,1,2})$ found by observation or from C. E. Moore's Tables (Mo 49) in the above five equations. In so doing, he claimed to have removed partially the effect of configuration interaction. The five unknowns $\gamma$, $\eta$, $E(^1S)$,

$E(^1D)$ and $E(^3P)$ are then solved and the following "semi-empirical" values are obtained (Ga 51, 63):

Table II-4. Semi-empirical Values of the Coupling Parameters and the Ground State Energies in $cm^{-1}$.

| | $\gamma$ | $\eta$ | $E(^1S)$ | $E(^1D)$ | $E(^3P)$ |
|---|---|---|---|---|---|
| $2p^4$ (OI) | 146.6 | 1.33 | 33791 | 15867 | 78.5 |
| $3p^4$ (SI) | 384.2 | 0.56 | 22168 | 9231 | 201.9 |
| $4p^4$ (SeI) | 1808 | $\approx 0$ | 22112 | 9402 | 1075 |

The values of $\gamma$ and $\eta$ can be calculated on a purely theoretical basis from equations (2-26) and (2-29). There is satisfactory agreement between the theoretical and the semi-empirical results of $\eta$, but not for $\gamma$. In both cases, it was found that the spin-spin and spin-other orbit coupling parameter $\eta$ decreases to a negligible quantity for heavier elements. The semi-empirical values of $\gamma$ and $\eta$ have been preferentially used by Garstang in the deduction of exact (intermediate coupling) wavefunctions $\psi'$. As previously mentioned, the latter can be mathematically represented as a linear combination of the unperturbed wavefunctions $\psi$. Thus,

$$\psi'(^1D_2) = a_1\,\psi(^1D_2) + a_2\,\psi(^3P_2) \qquad (2\text{-}37a)$$

$$\psi'(^3P_2) = -a_2\,\psi(^1D_2) + a_1\,\psi(^3P_2) \qquad (2\text{-}37b)$$

$$\psi'(^3P_0) = b_1\,\psi(^3P_0) + b_2\,\psi(^1S_0) \qquad (2\text{-}37c)$$

$$\psi'(^1S_0) = -b_2\,\psi(^3P_0) + b_1\,\psi(^1S_0) \qquad (2\text{-}37d)$$

such that $a_1^2 + a_2^2 = 1$ and $b_1^2 + b_2^2 = 1$ (2-38)

and since there is only one level with J = 1

$$\psi'(^3P_1) = (^3P_1)$$

The coefficients $a_1$, $a_2$, $b_1$ and $b_2$ are solved in a manner similar to equation (2-34), and the results for the $p^4$ elements are

$$a_1 = 1 - \frac{1}{4}\frac{\gamma^2}{(DP)^2} - \frac{1}{4}\frac{\gamma^3}{(DP)^3} + \ldots$$

$$a_2 = \sqrt{2}\left[-\frac{1}{2}\frac{\gamma}{(DP)} + \frac{1}{4}\frac{\gamma^2}{(DP)^2} + \frac{1}{4}\frac{\gamma^3}{(DP)^3} - \frac{7}{5}\frac{\eta}{(DP)} + \ldots\right] \qquad (2\text{-}39)$$

$$b_1 = 1 - \frac{\gamma^2}{(SP)^2} - \frac{2\gamma^3}{(SP)^3} + \ldots$$

$$b_2 = \sqrt{2}\left[-\frac{\gamma}{(SP)} - \frac{\gamma^2}{(SP)^2} + \frac{2\gamma^3}{(SP)^3} - \frac{\eta}{(SP)} + \ldots\right]$$

where terms in $\gamma\eta$ and $\eta^2$ are omitted.

Hence, the magnetic dipole and electric quadrupole line strengths $S_m$ and $S_q$ which can be expressed in terms of the mixing coefficients $a_1$, $a_2$, $b_1$, $b_2$, as shown in equations (7) and (8) of Shortely et al. (Sh 41), can then be determined. Finally, by substitution of $S_m$ and $S_q$ into equations (2-20) and (2-21) the corresponding MD or EQ transition probabilities are obtained. The results for the $np^4$ elements can be found in the tables of comparison from Chapter VI of this thesis.

It is also to be noted that in the calculation of the quadrupole strength $S_q$, estimates of the radial part of the wavefunctions

$$D_q = \frac{2}{5} \int_0^\infty r^2 \, R_{np}^2(r) \, dr \qquad (2\text{-}40)$$

are required; it is thus important that the correct wavefunctions be adopted. In the results shown in the tables of Chapter VI, Garstang used self-consistant field (SCF) wavefunctions from Hartree et al. (Ha 39) for OI and SI and from Watson and Freeman (Wa 61) for SeI whereas Yamonouchi used those from Hartree and Black (Ha 33) for OI.

Comments on the "Perturbation Method"

The various theoretical and semiempirical A-coefficients so far obtained by this method have been based on the perturbation effects from (1) the individual electron's spin-own orbit coupling ($\gamma$) and (2), the spin-spin and spin-other orbit of different electrons ($\eta$). The inclusion of the spin-spin effect can alter the result considerably. For instance, among the strongest and most frequently observed of the forbidden lines found in the planetary nebulae such as IC 418 or NGC 40, in diffuse nebulae such as Orion or Messier 8 and in the faint patches of the Milky Way, are the 3726.16 Å and

3728.91 Å lines of [OII] corresponding to the $^4S_{3/2} - {}^2D_{3/2}$ and $^4S_{3/2} - {}^2D_{5/2}$ transitions in the $2p^3$ ground configuration. The intensity ratio

$$r = \frac{I(^4S_{3/2} - {}^2D_{5/2})}{I(^4S_{3/2} - {}^2D_{3/2})}$$

was derived, using the spin-orbit coupling $\gamma$ only, by Pasternack (Pa 40) who found r = 1.9, and Shortley et al. (Sh 41) who obtained r = 1.64, whereas the value observed by Aller et al. (Al 49) is 0.49. However, by including the spin-spin coupling $\eta$, Aller et al. (Al 49) obtained a more satisfactory value of r = 0.58. Thus, although the interaction $\eta$ is small compared to $\gamma$, the result for r is significantly altered. This is because $\eta$ affects the intensity of the forbidden lines in the first order only whereas $\gamma$ does so in both the first and second order.

Furthermore, there may well be another source of perturbation due to the coupling between the orbits of different electrons - an effect which may be as important in magnitude as $\eta$. In treating the electrostatic energies $E(^1S)$, $E(^1D)$ and $E(^3P)$ as adjustable parameters, to be fitted to observations, rather than using the Slater integral theory whereby 6(SP) = 15(DP), Garstang (Private communication 1974) believed that the above-mentioned orbit-orbit effect has been taken account

of so far as it could be without more information. However, this effect which introduces a $\alpha\vec{\ell}_i.\vec{\ell}_k$ or $\alpha L(L+1)$ correction term was in fact taken into account separately for the ($^1S$) level of heavier atoms (Ga 64). This correction term was first found by Trees (Tr 52), to be considerable and appropriate for explaining the discrepancy between experimental and theoretical term values of the $d^n$ configuration. Also, Racah (Ra 52) pointed out that the $\alpha L(L+1)$ correction explains the constancy of the ratio $(^1S - {}^1D)/(^1D - {}^3P)$ in the $2p^4$ configuration. It may, therefore, be concluded that if the orbit-orbit effect has been fully considered among the $np^4$ elements, the values of $\eta$ will all be different from previously, and so will be the electrostatic energies $E(^1S)$, $E(^1D)$, and $E(^3P)$ as computed from the five equations (2-36a,b,c,d,e). Thus the resulting A-coefficients will not be the same although the deviations may be very slight as the values of $\eta$ are already small compared to those of $\gamma$.

Another possible inaccuracy from this perturbation method stems from the use of a constant central-field approximation, i.e. assuming a uniform radial wavefunction regardless of the actual states involved in a particular transition. Of course, say for [OI] 5577 Å $2p^4(^1D_2 - {}^1S_0)$, changes in the central field in going

from $^1S_0$ to $^1D_2$ should affect the value of $D_q = \int_0^\infty r^2 R_{np}(r)\, dr$ (see equation 2-40), on which the line strength depends. Garstang (Private communication 1974) felt that different wavefunctions for the different terms should be used but that lack of the pertinent wavefunctions and computer systems for deducing them have prevented him from doing so.

(b) The Non-Closed Shell Many-Electron Theory (NCMET) of Atomic Structure

This is a non-perturbative and non-relativistic theory developed by Sinanoğlu and co-workers Öksuz, Nicolaides and Skutnik (Si 68, Ok 69 and Ni 71), whereby the exact wavefunctions used in the calculation of the forbidden-line transition probabilities are obtained by correcting for the relevant electron correlation effects in both ground and excited states. Unlike the perturbation method from the previous section where a constant central-field is used regardless of the actual states of the transition involved, different central and non-central fields are considered here in the determination of the correlation effects. In finding the exact N-electron wavefunction, a Hartree-Fock (HF) function is used as a starting point, just as in the perturbation method. This HF component of the total wavefunction takes care of most of the long-range part of the Coulomb field, and then the correlation effects are deduced from the

shorter range "fluctuation potentials" between electrons, just as the perturbation effects are deduced from the "spin-orbit, spin-spin, spin-other orbit and orbit-orbit interactions" in the previous method. The correlation effects are classified into three types, each of which can be distinguished physically and determined mathematically through configuration interaction (CI).

In non-closed shells represented by Figs. 2-4(a), (b), (c), some of the orbitals in the "Hartree-Fock sea A"† are unoccupied. The vacancies in the HF sea cause new correlation effects which do not exist in closed shells: In (a), electrons correlate and shift in pairs $(k_a, k_b)$

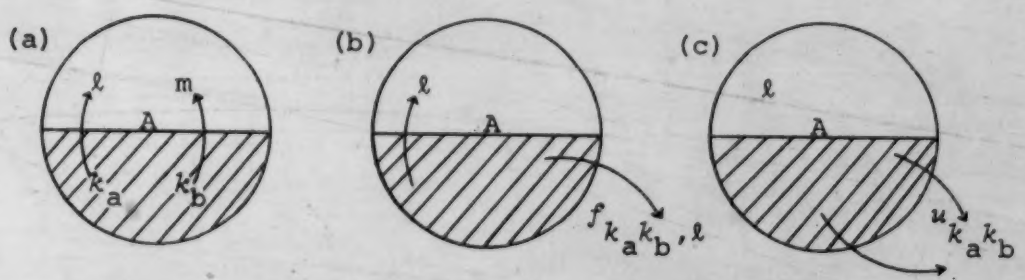


Fig. 2-4. Electron transitions in the non-closed shells.

from filled to unoccupied orbits in A and remain in the sea. Such virtual transitions of electrons within the HF sea

---

†The HF sea is defined as all the occupied orbitals plus all the vacant ones up to the next closed shell configuration. For the first row elements, all 1s, 2s, and 2p orbitals (= 10), occupied or unoccupied, define the HF sea.

produce the so-called "Internal Correlations". In (b), virtual excitations where one electron shifts within the HF sea while the other goes outside to a one electron correlation function $f_{k_a k_b}$ cause the so-called "Semi-internal Correlations". Some excitations due to symmetry polarizations are also considered with this effect. Finally in (c) a pair excitation analogous to those in closed shells occurs, and electrons in $k_a$ and $k_b$ end up in a pair - correlation function $u_{k_a k_b}$ outside the HF sea. Such effects are known as the "External Correlations". The first two correlations involve vacant orbitals lying close to the occupied ones and are dependent upon N, symmetry and Z, and are thus "non-dynamical" or "non-transferable" among systems of different N, symmetry and Z. The third or external correlations are dynamical just as for closed shells.

Thus in the NCMET approach, the exact N-electron wavefunction of an arbitary state can be written in the form

$$\Psi = \phi_{RHF} + \chi_{int} + \chi_{semi-p} + \chi_{ext} \qquad (2\text{-}41)$$

with all parts orthogonal to one another,

i.e. $\langle \phi_{RHF} | \chi_{int} \rangle = \langle \phi_{RHF} | \chi_{ext} \rangle = \langle \chi_{int} | \chi_{ext} \rangle = 0$ (2-42)

and $$\langle \phi_{RHF} | \phi_{RHF} \rangle = 1 \qquad (2\text{-}43)$$

$\chi_{int}$ and $\chi_{semi-p}$ can be calculated quite accurately by a

finite configuration - interaction (CI) expansion with no ambiguity as to which configurations to choose, whereas $\chi_{ext}$ can be calculated by the methods discussed by Silverstone and Sinanoğlu (Si 66). All three types are important in calculating energies, but in calculating transition probabilities, only the internal, the semi-internal and polarization correlation effects are taken into account because the external correlations due to their local, short range character, do not affect the Hartree-Fock charge distribution - a hypothesis borne out by results (Si 70, We 69). The wavefunctions to be used for calculating the transition probabilities are therefore the non-dynamical $\Psi_{Non-D}$ given by

$$\Psi_{Non-D} = \phi_{RHF} + \chi_{int} + \chi_{semi-p} \qquad (2-44)$$

$\phi_{RHF}$

Here $\phi_{RHF}$ is the starting wavefunction developed by Roothan (Ro 63) which, in general, has the form

$$\phi_{RHF} = \sum_{K=1}^{G} C_K \Delta_K \qquad (2-45)$$

where the $C_K$ are the vector coupling or CI coefficients (many of which may be zero because of symmetry); G is the number of antisymmetrized Slater determinants $\Delta_K$ in the ground configuration and

$$\Delta_K = A[k_1(\vec{x}_1)\ k_2(\vec{x}_2)\ \ldots\ k_N(\vec{x}_N)] \qquad (2-46)$$

where $A$ is the N-electron antisymmetrizer operator given by

$$A = \sum_P (-1)^P P$$

and $\{k_i\}$ is a set of N spin orbitals with $\vec{x}_i$ representing space and spin coordinates of particle $i$, so that

$$k_i(\vec{x}_i) = R_{\ell_i}(r)\ Y^{m}_{\ell_i}(\theta,\phi)\ X_{m_{s_i}}(\sigma_z) \qquad (2\text{-}47)$$

The radial functions $R_{\ell_i}(r)$ in equation (2-47) were obtained by using Slater-type orbitals whose exponents were optimized, i.e.

$$R_{\ell_i}(r) = \frac{\exp(-\alpha r)}{r^{n-1}}$$

<u>$\chi_{int}$</u>

$\chi_{int}$ is given in its CI form by

$$\chi_{int} = \sum_{K>G}^{\binom{M}{N}} C_K \Delta_K \qquad (2\text{-}48)$$

$$\binom{M}{N} = \frac{M!}{N!(M-N)!}$$

= number of possible different antisymmetrized Slater determinants $\Delta_K$ when the species considered has N-electrons out of a HF sea of M orbitals.

As indicated by equation (2-48), $\chi_{int}$ contains at most $\binom{M}{N}$ - G determinants, many of which, however, have $C_K = 0$ due to symmetry. Configurations arising from single-electron shifts between s and p orbitals are forbidden by parity considerations. Because of the large

energy gap between K and L shells, virtual transitions between them (i.e. $1s^2$–$2p^2$ or $1s^2$–$2s^2$) do not make appreciable contributions to $E_{int}$. These considerations restrict $\chi_{int}$ to, at most, three determinants for the first row - those from $2s^2$–$2p^2$ mixing (i.e. $1s^2\ 2s^2\ 2p^n$–$1s^2\ 2p^{n+2}$ CI) as shown by the internal pair excitations of Fig. 2-4(a). The internal correlations for the ground configuration of first row atoms were calculated and studied systematically by McKoy and Sinanoğlu (Mc 64) and by Öksuz and Sinanoğlu (Ok 69). In the calculations vacant 2s and 2p orbitals of the $1s^2\ 2s^2\ 2p^n$ configurations were taken to have the same radial part as their occupied counterparts and for $1s^2\ 2p^2$, the 2s orbital of $1s^2\ 2s^2$ was used after orthogonalizing it to 1s of $1s^2\ 2p^2$.

<u>$\chi_{semi\text{-}p}$</u>

$\chi_{semi\text{-}p}$ yields a finite CI because it is restricted to processes where only one electron is allowed to leave the HF sea. In its CI expansion, the semi-internal correlation-polarization function is given by

$$\chi_{semi\text{-}p} = \sum_{K=1}^{G} C_K \Delta_K^F$$

$$= \sum_{K=1}^{G} C_K \Big[ (k_c k_d \cdots k_N) \Big( \sum_{a=1}^{N} \frac{f^{K(p)}_{k_a}}{k_a} + \sum_{a>b}^{N} \sum_{\substack{\ell_i \geq 1 \\ \ell_i \neq k_c, k_d \cdots k_N}}^{M} \frac{\ell_i f^K_{k_a k_b; \ell_i}}{k_a k_b} \Big) \Big] \qquad (2\text{-}49)$$

where $\ell_i$ is an unoccupied HF sea spin orbital (not belonging to $\Delta_K$), which is given the same value as its occupied counterpart.

$f^{K(p)}_{k_a}$ is a one-electron correlation function describing the "polarization" effect due to the non-central field of electrons in non-spherically symmetric states, and $f^{K}_{k_a k_b;\ell_i}$ is a two-electron correlation function describing the "semi-internal" effect.

The above $f$ functions are calculated by a finite CI expansion due to vector coupling restrictions imposed by the symmetry of the state. For instance, in the first row atoms ($1s^2\ 2s^2\ 2p^m$) the $f$ functions can be shown to have only s, p, d, f symmetries as follows:

From equation (2-49), we have

$$\chi_{\text{semi-p}} = \chi_F = \sum_K C_K\ \Delta^F_K$$

so that, the semi-internal, polarization energy is given by

$$\begin{aligned} E_F &= \langle \phi_{RHF} | H | \chi_F \rangle \\ &= \sum_K C_K \langle \phi_{RHF} | H | \Delta^F_K \rangle \end{aligned} \qquad (2\text{-}50)$$

where $\Delta^F_K$ are determinants containing $f_{k_a}$- and $f_{k_a k_b}$-type virtual excitations represented by F. Equation (2-50) contains one-electron integrals of the type $\langle k | h_p | F \rangle$ and two-electron integrals $\langle k_a k_b | h_{pp} | k_c F \rangle$, where

$h_p$ and $h_{pp}$ are the one-electron and two-electron terms in the Hamiltonian and $k$ are the HF sea orbitals. In the first row ($1s^2\ 2s^2\ 2p^m$), the $k$ can be of s or p orbitals only.

$\therefore\ \langle k|h_p|F\rangle = 0$ if F has d or higher symmetries.

The bra in $\langle k_a k_b|h_{pp}|k_c F\rangle$, i.e. $\langle k_a k_b|$ can at most have p ⊗ p → s, p, and d components.

$\therefore\ \langle k_a k_b|h_{pp}|k_c F\rangle = 0$ if the ket $|k_c F\rangle$ has f or higher symmetries, which is true if F alone has a g or higher symmetries because, if $k_c$ is an s orbital and F has a g orbital, then $|k_c F\rangle$ has s ⊗ g → g symmetry and if $k_c$ is a p orbital and F has a g orbital, then $|k_c F\rangle$ p ⊗ g → f, g, h symmetry; but $\langle k_a k_b|$ has none of these symmetries, so that for $\langle k_a k_b|h_{pp}|k_c F\rangle \neq 0$, F has at most s, p, d, f symmetries. Through similar reasoning, it can be shown that in the second row F has s, p, d, f symmetries too, and in the third row, F has s, p, d, f, g, h symmetries.

The $f$ functions have the same form as the $k$ orbitals, i.e.

$$f(\vec{x}) = f(r)\ Y_m^{\ell}(\theta,\phi)\ X_{m_s}(\sigma_z)$$

The four radial functions of the first and second row atoms, i.e. $f(r)$, can be variationally approximated by 3s- like, 3p- like, 3d- like and 4f- like functions and can be expanded as a sum of Slater-type orbital (STO)

with an optimized exponent.

An automatic CI computer program (Ni 71) was prepared and used to calculate $\chi_{int}$ and $\chi_{semi-p}$. Thus the wavefunctions $\Psi_{Non-D}$ from equation (2-44) can be determined and when these are substituted into equation (2-19) or (2-22), strengths of the forbidden lines involved are obtained. Final substitution into equation (2-20) or (2-21) will yield the values of the transition probabilities.

Comments:

As mentioned previously, this non-perturbative method yields a more accurate value of the A-coefficient through consideration of all the electron correlation effects in central and non-central fields, and through the use of the appropriate radial wavefunction of the different states involved - made available by modern computer systems. It has since been successfully applied to transitions from such isoelectronic sequences as those of MgI (Be 72), BeI (Ni 72) and SiI (Si 73) and gives good agreement with reliable experimental results from the beam-foil technique. Moreover, it has been applied specifically to the forbidden line of the first $np^4$ element, i.e. [OI] 5577 Å $1s^2\ 2s^2\ 2p^4$ ($^1S_0$ - $^1D_2$) (Ni 70, 71). However, this

method has not yet been applied to the forbidden transitions of the other $np^4$ elements, which are the subjects of investigation in this work (Sinanoğlu, private communication 1975). The situation becomes more complex for transitions from these heavier elements because the number of HF sea orbitals increases accordingly and the selection of relevant CI becomes more involved.

# CHAPTER III

## EQUIPMENT

In this chapter, the main equipment used in the experiments (1) for the production and detection of the forbidden and allowed vacuum ultraviolet lines and (2) for the absolute intensity measurement of the spectral lines, through the photon-counting techniques, is described. A picture of the overall experimental set-up is illustrated in Fig. 3-1.

### The Discharge Tube (DT)

It consisted of pyrex tubing with three side arms which contained the electrodes. The overall dimensions are shown in Fig. 3-2. Each of the three vertical arms of the DT contained a tungsten rod which was sealed to its lower end and supporting a tantalum electrode (Ta). The latter was made with 1.0 mm thick tantalum foil shaped into a cylindrical form, 2.25 cm in length and with a spot-welded base of 2 cm diameter. The horizontal part was sealed at one end with a pyrex window and at the other end with a LiF window surrounded by a Pyrex B55/50 cone. (The latter was to be fitted to the entrance slit of a McPherson vacuum

Fig. 3-1. Photograph of the overall experimental set-up.

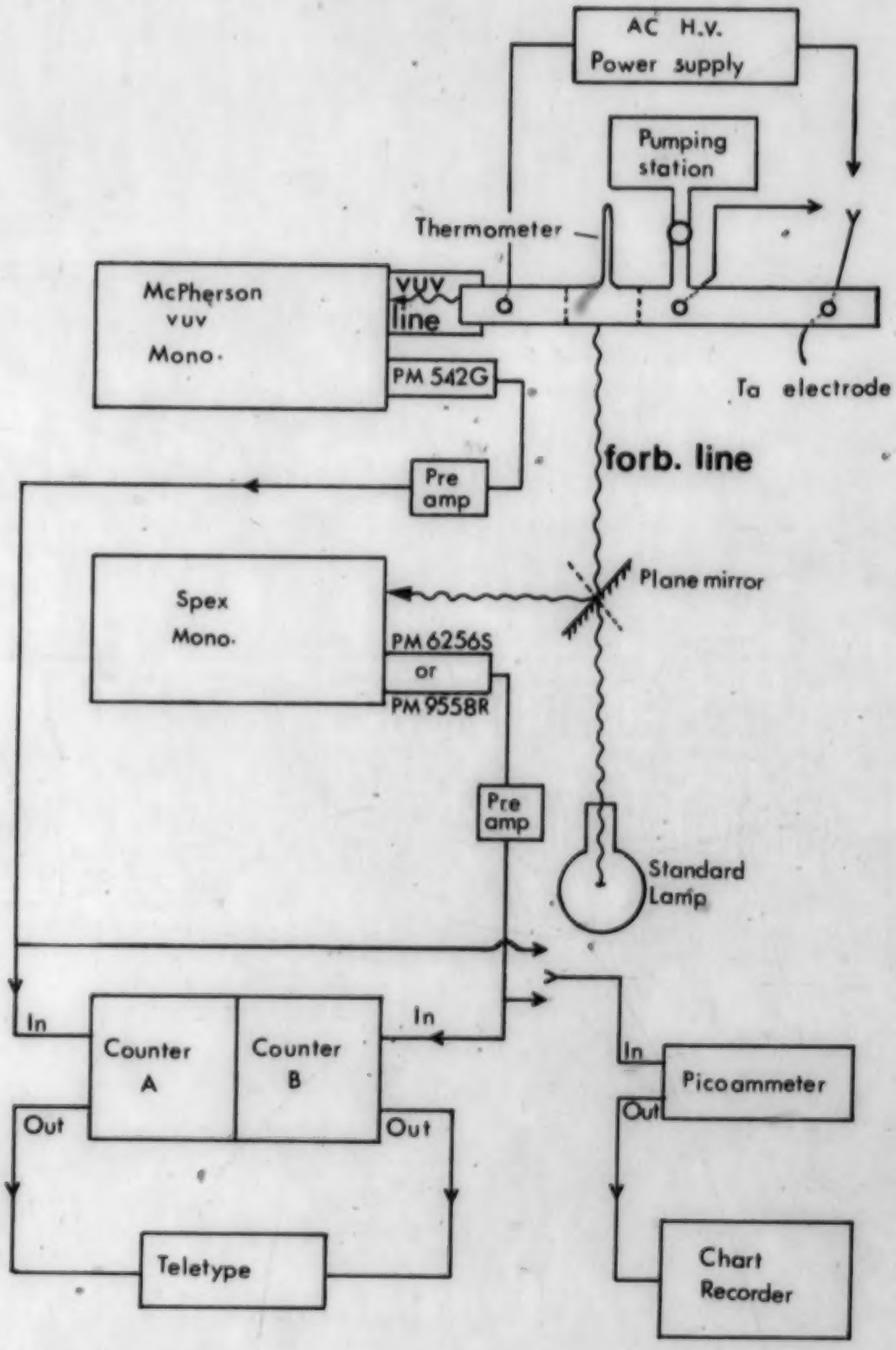


Fig. 3-1a. Diagrammatic sketch of the experimental set-up.

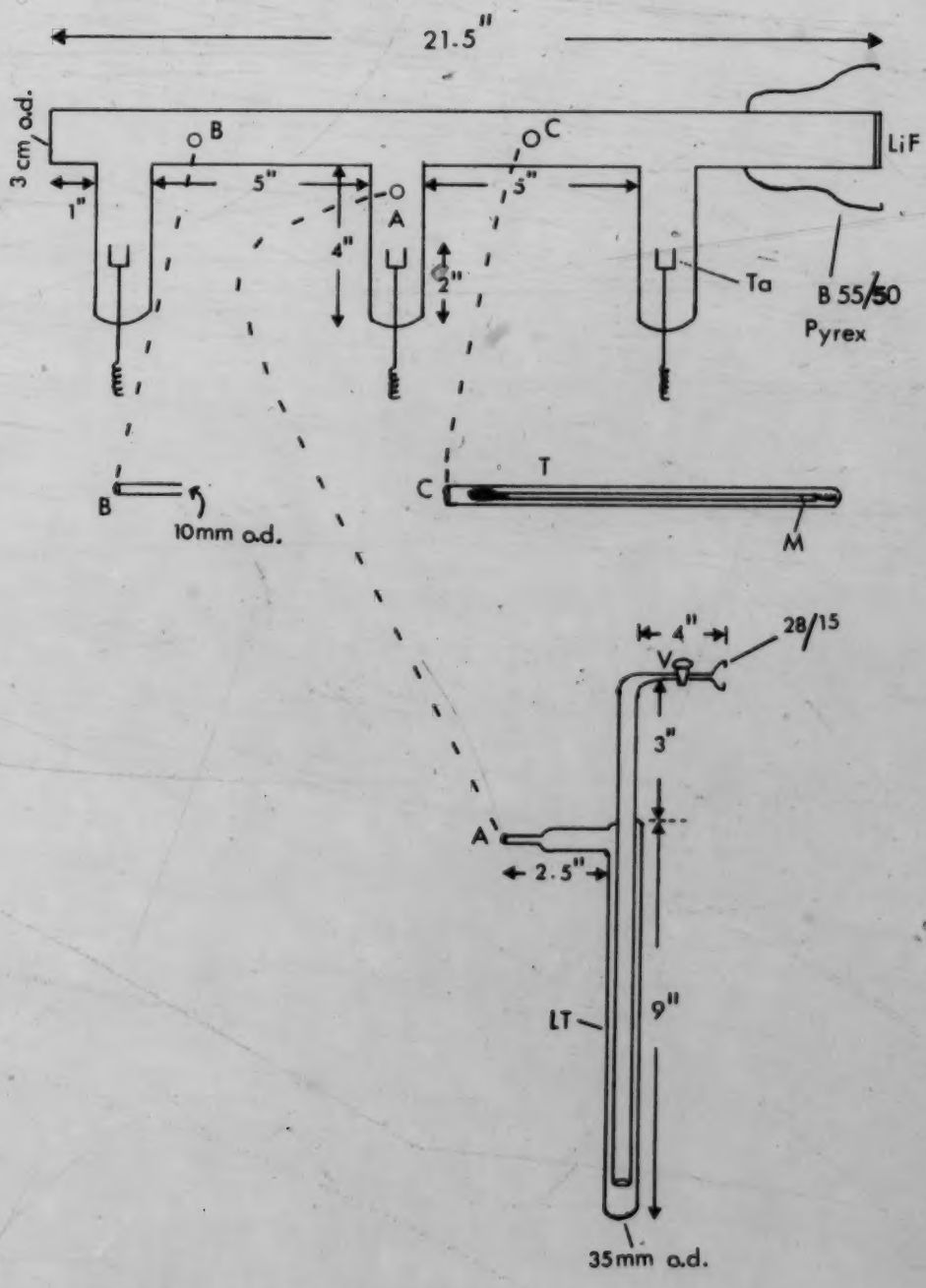


Fig. 3-2. The discharge tube (DT).

monochromator). Protruding from the horizontal part of the DT was an outlet which led to a thin arm for a 0-360°C mercury thermometer (T). The bulb could be moved in and out by means of a small metal slug (M) at the high-temperature end which was acted on by a small magnet as required. From the centre of the middle vertical leg of the DT another outlet led to a liquid-air trap (LT), then to a high-vacuum glass tap (V) and finally to a 28/15" 'female' end.

The DT was connected to a glass pumping system by means of a metal-bellow connector which had two 28/15" 'male' ends (Fig. 3-3). This flexible connector had the advantage of eliminating any strain that might have been otherwise placed on the DT or the glass pumping system.

Glass Vacuum System

The overall system is shown schematically in Fig. 3-3. The vacuum system was backed by a Welch duo-seal oil pump through a pentoxide water vapour trap. A single stage mercury diffusion pump (Hg-DP), cooled by tap water, was used with a liquid-air trap (LT). The latter prevented mercury from the diffusion pump entering the experimental tube as an impurity. The Edwards Speedivac Gauge (S) read directly the pressure in the range of 0 to 20 torr, while the Norton Ionization Gauge (IG) covered the range to 1.0 torr with a thermocouple (TC)

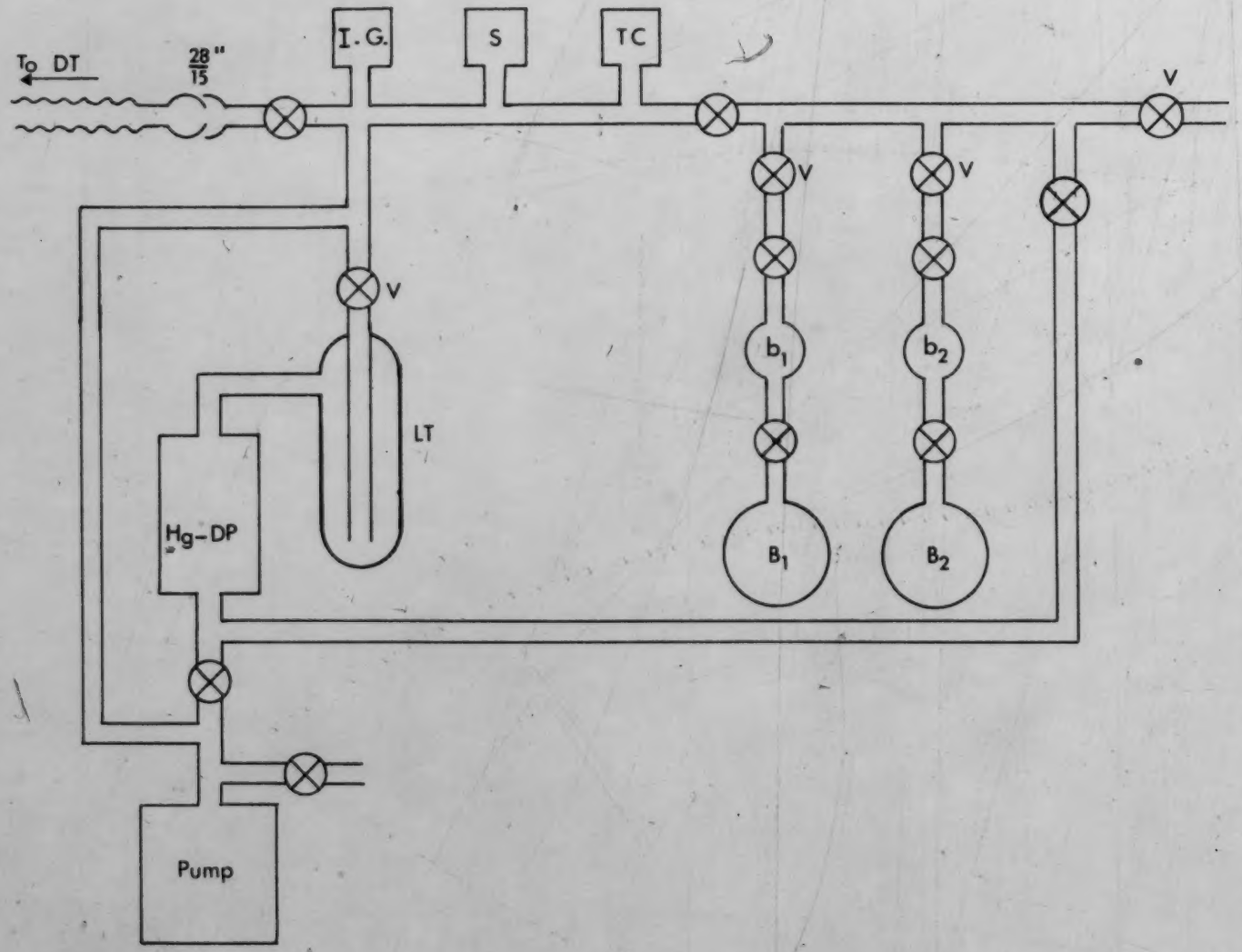


Fig. 3-3. The glass vacuum system.

and the range of $10^{-3}$ to $10^{-9}$ torr with a cold cathode (CC).

Various gases could be introduced into the discharge tube through expansion chambers ($b_1$ and $b_2$), the flow being regulated by high vacuum glass taps (V) which were lubricated with "Apiezon" vacuum grease. The gases used were "spectroscopically pure", supplied by Air Reduction Company (AIRCO) or Matheson, and were contained in 1.1 litre break-seal flasks ($B_1$ and $B_2$) which were attached to the pumping train.

The Spectrometers

Two scanning monochromators were used during the course of this project. Work in the visible and near-ultraviolet was carried out using a 0.75 meter Spex Model 1500 monochromator (f/6.8) while in the vacuum ultraviolet the radiation was analysed using a one-meter McPherson Model 225 vacuum monochromator (f/10.4, masked to f/5.5).

The Spex Model 1500 had a Czerny Turner mount with a plane grating ruled over an area of 120 mm x 120 mm at 1200 grooves/mm and blazed for 5000 Å. With this grating installed the first order reciprocal linear dispersion of the instrument was around 10 Å/mm.

The McPherson Model 225 had a normal incidence mounting with a one-meter radius of curvature concave grating ruled over an area of approximately 56 mm x 96 mm at 1200 grooves/mm and blazed at 1500 Å. It is to be noted that

with this grating installed, the first order reciprocal linear dispersion of the instrument was 16.6 Å/mm. The grating was overcoated with magnesium fluoride to improve the reflectance in the vacuum ultraviolet region.

The vacuum system for this McPherson monochromator included a freon refrigerant unit for cooling the Model 851 cold trap. The unit was a 1/4 horse power compressor charged with Freon 12 refrigerant, and the charge condition was indicated by a pressure-vacuum gauge. To operate the vacuum system the switches on the control unit for the components - forepump, diffusion pump, gate valve to the main chamber, foreline valve, roughing valve and main trap coolant - were activated in the correct sequence.

This vacuum system also had safety electrical interlocking devices which were automatically activated in the occurence of (1) a sudden rise of pressure in the main chamber, (2) a malfunction of the cooling system or (3) a power failure. During continuous pumping, if the foreline pressure rose to a level higher than that preset on a foreline monitor, the diffusion pump would be deactivated and the gate valve to the main chamber would close. (This would prevent back streaming of the diffusion pump oil and contamination of the main chamber and grating.) Also, if the diffusion pump water temperature

exceeded the maximum allowed, a "thermal switch" would open and this, in turn, would close the gate valve and de-energize the pump heater. Finally, a complete power failure would also automatically close the gate valve.

The Photon Detectors

Three different types of photomultipliers were used during the course of this experiment. For detecting the vacuum ultraviolet light an EMR 542-G was used, for the visible and near-ultraviolet an EMI 6256S and for the infrared and near-infrared an EMI 9658R.

The operating characteristics of these photomultipliers are shown in Table III-1. The "Quantum Efficiency $Q(\lambda)$" is the number of photoelectrons emitted from the cathode per incident photon and is usually expressed as a percentage. The "Radiant Cathode Sensitivity $E(\lambda)$" is related to the quantum efficiency as follows:

$$E(\lambda) = \frac{\lambda \times Q(\lambda) \times 10^9}{1.2395} \text{ mA/Watt}$$

where $\lambda$ is in meters and Q is in electrons per incident photon. The "Spectral Response" can then be given by a graphical plot between $Q(\lambda)$ and/or $E(\lambda)$ vs. the wavelength $\lambda$. The actual spectral responses of the EMI 9658R and 6256S or the EMR 542-G could thus be obtained from

| | EMR 542-G | EMI 5656S | EMI 9658R |
|---|---|---|---|
| Tube Diameter | 2" | 2" | 2" |
| Active Cathode Size | 28 mm | 10 mm | 44 mm |
| Cathode Type | CsI | $Cs_3Sb$ | $Na_2KSb$-Cs |
| Number of Dynodes | 18 | 13 | 11 |
| Secondary Emitting Surfaces of Dynodes | Ag-Mg | Cs-Sb | Cs-Sb |
| Range of Spectral Response | 1050 Å-2500 Å | 1650 Å-6800 Å | 3000 Å-9500 Å |
| Peak of Spectral Response | 1216 Å | 4000 Å | 4000 Å |
| Peak Quantum Efficiency | 8% | 16% | 30% |
| Peak Radiant Cathode Sensitivity | 7.8 mA/Watt | 51.6 mA/Watt | 96.3 mA/Watt |
| Window Material | LiF | Fused Silica | Borosilicate |
| Overall Typical Voltage | 2900 V | 1600 V | 1150 V |
| Typical Dark Current | $6 \times 10^{-3}$ nA | 0.3 nA | 2 nA |

Table III-1. Operating characteristics of EMR 542-G, EMI 6256S and 9658R.

the corresponding manufacturer's data.

One of the most important characteristics shown in Table III-1 was the "Dark Current" - i.e. the current produced by the photomultiplier even when it was operated in complete darkness, and which arises from electrons emitted from the cathode by agencies other than incident light (such as thermionic emission). This dark current introduces an equivalent "noise" which, however, can be neglected if it is about a factor of ten less than the signal current (EMI catalogue).

The Refrigerated Chamber for Photomultiplier Tube Operation

The signal-to-noise ratio referred to above usually presented the basic limitation to accuracy in photoelectric measurement. It was thus desirable that the dark current, which was mainly due to thermionic emission, should be minimized. A "RF shielded" thermoelectric refrigerated chamber Model RFI 2010 (see Fig. 3-5) was used to provide cooling for photomultiplier tubes, thus reducing the dark current. The RFI 2010 version did not require supplemental cooling materials such as dry ice, and would cool the tube cathode to at least -20°C in a 50°C ambient. The device also had a temperature regulation control which could hold the tube cathode temperature stable to ±0.5°C within the selected range of -20°C to

+20°C in a maximum ambient of +50°C. Heat losses from the thermoelectric device plus heat pumped from the chamber were expelled by a water-cooled heat exchanger.

The dark current noise in the EMI 9658R tube was relatively high compared to that in either the EMI 6256S or EMR 542-G tube (see Table III-1), so that its signal-to-noise ratio, especially when the signal was from weak forbidden lines, was usually unsatisfactory (<5:1) for the acquisition of reliable data. Consequently, only the EMI 9658R was found to require cooling. In fact, when the cooling process was undergone in the refrigerated chamber, it was found that the signal-to-noise ratio could be increased by a factor of about 20 in around 45 minutes when the chamber was preset at -10°C. Thus, the dark current in the photomultiplier tube could be maintained at a greatly reduced level for a preset tube temperature.

The Electronics for Simultaneous Photon-Countings

Fig. 3-4 illustrates the electronic components employed to monitor simultaneously the photon counts at two different wavelengths belonging to the same radiating source. The analog system represented by a chart-recorder and a micro-microammeter was used to locate the peaks of the spectral lines which were being investigated. The data

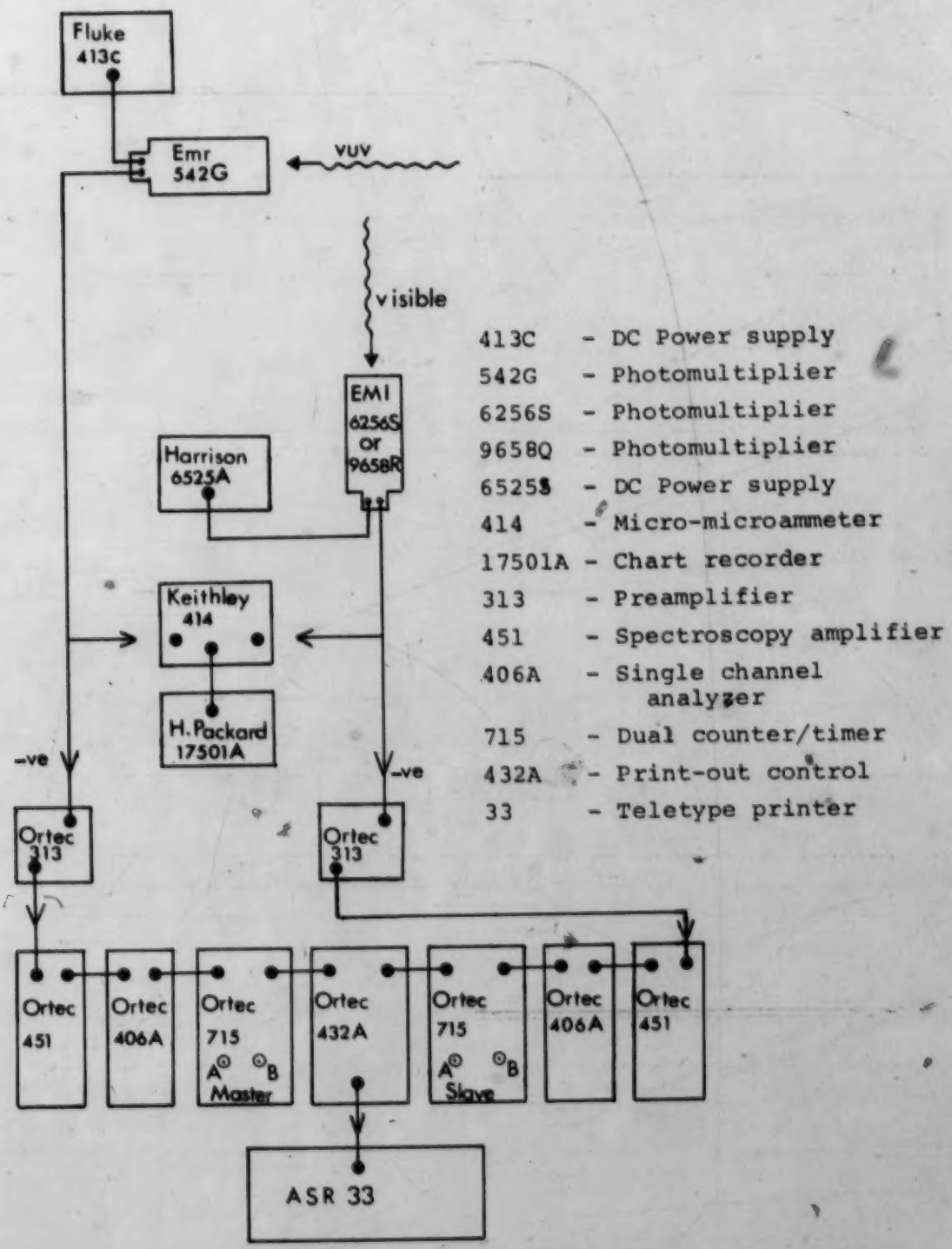


Fig. 3-4. Block diagram of electronics for simultaneous photon-countings.

acquisition was performed using a standard photon counting system consisting of, for each channel, a preamplifier, an amplifier, a single-channel analyzer and a dual counter-timer.

The dual counter-timer Ortec 715 was a flexible data accumulation module, built-in with two counters and a time base which could be used as the input to one of the counters when both counting and timing were desired. For simultaneous photon countings both Ortec 715's were linked with a common time base. One Ortec 715 was set as a "Master" and the other as a "Slave". Synchronized starting and stopping of both Ortec 715's was then obtained by using the control logic of the Master only. The latter could also be controlled manually, or automatically, single cycled with preset stop or recycled with preset stop. The accumulated data from both Ortec 715's could then be monitored visually and/or read to a teletype printer after passing through a print-out control unit.

The Standard Lamp

Absolute radiant intensities (of the forbidden lines) were measured by comparison with an Eppley standard lamp calibrated at the National Bureau of Standards. The lamp, shown in Fig. 3-5 was a commercial General Electric type 30A/T24/7 having a tungsten ribbon filament

(SR-8A type) centered about 8 to 10 cm behind a fused silica window, 3 cm in diameter. It could be used as a laboratory standard of spectral radiance for the wavelength region of 2500 to 26000 Å.

For the region of longer wavelength (above 7500 Å) the lamp was calibrated by comparison with a blackbody operated up to 1400°K[†]. Such a blackbody, made from a casting of an alloy of 20% chromium and 80% nickel, was so constructed as to yield an emissivity of 0.999 or higher. As for the shorter wavelengths or below 7500 Å, a comparison was made with a blackbody operated at above 1400°K. The latter was made of highly pure graphite and the enclosure so constructed as to yield an emissivity of 0.996. The spectral radiance of either blackbody was based upon the Planck Radiation Law. Values of spectral radiance supplied by Eppley for the lamp were tabulated as a function of wavelength in microwatts per (steradian-millimicron-square millimeter of filament).

An alternating current was used to operate the standard so as to prevent "filament-crystallizing effects" that would occur if the operation was on direct current. The filaments were massive and "ironed-out" all effects of the normal fluctuations present in a commercial AC supply. The standard lamp was provided with (1) a Sola constant voltage transformer Model 23-25-210 which was

---

[†]The calibration was carried out by the Eppley Laboratories.

used as a line voltage regulator, (2) an Eppley standard lamp power supply Model 501 which had a coarse and a fine current adjustment dials and (3) an Eppley irradiance power Model SN4403 which was connected to the lamp by an AC line cord.

An optical bench made of aluminium was built in this laboratory for positioning the standard lamp and its auxilliary plane mirror with respect to the spectrometer slit, as shown in Fig. 3-5.

Device Used to Excite the Discharges

An AC source, shown in Fig. 3-6, was used to excite the discharges in the tube. Two luminous tube transformers, one of 60 mA and the other of 120 mA capacity were interchangeably used in the circuit, depending on the range of current required for the different types of discharge. The line voltage from the mains was connected to a "Variac" which could control the input to the primary of the transformers, and the secondary was then placed in series with sets of resistors and an AC milliameter. The resistors used were either 1KΩ or 250KΩ, all rated at 50 watts, and arranged in series and/or in parallel according to the current and voltage range required. Essentially, one end of the discharge tube was connected to the ground potential of the transformer (i.e. the central

Fig. 3-5. (1) The standard lamp set up with an auxillary plane mirror on an aluminium optical bench.
(2) The refrigerated PM chamber attached to the exit end of the Spex 1500.

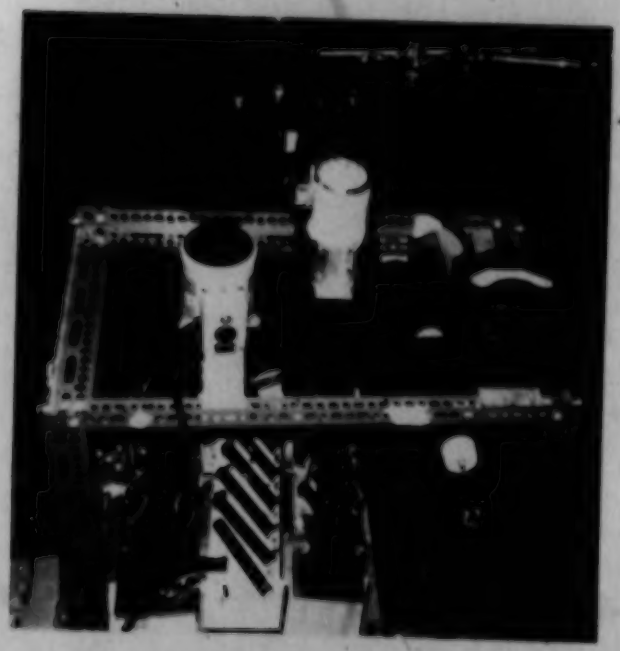

Fig. 3-6. The AC discharge circuit.

point of the windings) while the other end was made to oscillate about ground. Typical potential differences across the discharge tube were around 6,000 volts.

Spectroscopy Photography

The Spex 1500 was converted into a spectrograph of speed factor f/6.8 when a camera unit replaced the exit slit. The camera box supplied with the instrument, was replaced by a more versatile one built in our laboratory. Inside the camera box was a holder which could accommodate a plate or film strip of size 6 cm x 3 1/2 cm. A plate-cutter with a diamond edge was also built in our laboratory and the available 10" x 4" Kodak plates were cut into sizes to fit the holder in the camera box.

Spectrograms were taken with film strips or spectroscopic plates chosen according to the wavelength response or spectral sensitivity of their emulsion type. The sensitivity of different emulsions in different spectral regions is tabulated in "Kodak Scientific and Technical Data Handbook, No. P-9". In the present work, the following emulsion types were used:

(1) Spectroscopic plate type 103a-F, for the near-ultraviolet and visible.

(2) Spectroscopic plate type I-N, for the infrared.

(3) Colour film EH-135, for the visible.

The spectroscopic plates were processed by developing for 4-minutes in D-19B developer and then fixing and hardening in a universal fixing solution.

# CHAPTER IV

## THEORIES OF THE EXPERIMENTAL METHOD

The experimental method developed and employed in the determination of the absolute transition probabilities of forbidden lines in the $np^4$ elements and the theories which provide the basis of this method are discussed in this chapter. The most important of these theories are those related to the following: (1) the excitation and depopulation mechanisms of the metastable levels whereby we may establish the optimum conditions for producing the forbidden lines up to a steady and measurable level in intensity, (2) the absorption processes in the vacuum ultraviolet whereby we may determine the atomic density of the metastable levels and (3) the standard spectral radiance whereby we may obtain the absolute intensity of the forbidden lines.

### 4.1 Excitation Mechanisms

#### (a) Direct Electron-Atom Collisions

The excitation of the metastable levels ($^1S$) and ($^1D$) in the $np^4$ elements is accomplished to a large extent by electron-atom collisions of the second kind. For example, for an $np^4$ element M in the $^3P$ ground state,

$$M(^3P) + e(v') \rightarrow M(^1S) + e(v'') \qquad (4\text{-}1)$$

$$M(^3P) + e(v') \rightarrow M(^1D) + e(v'') \qquad (4\text{-}2)$$

where v' and v" are different velocities.

The number of atoms excited per sec from the ground state o to a metastable state j by electron collisions is given by

$$\left(\frac{dN_j}{dt}\right)_{e\text{-collision}} = N_o \, \alpha_{oj} \, n_e \qquad (4\text{-}3)$$

where $n_e$ is the electron density; $N_o$, $N_j$ are the atomic density of the ground and of the metastable state respectively, and $\alpha_{oj}$ is the excitation probability of the level j from ground state o given by

$$\alpha_{oj} = \int \sigma_{oj} \, n(E) \, v(E) \, dE \qquad (4\text{-}4)$$

where $\sigma_{oj}$ is the excitation cross section of level j from level o; n(E) is the normalized electron energy distribution function; and v(E) is the electron velocity. Equation (4-3) shows that for a given atomic density in the ground state, the populating process of the metastable level by electron collisions is directly proportional to the number of electrons $n_e$, i.e. to the discharge current.

(b) Excitation by "Cascade" Energy

A metastable level can also be populated by "cascades" from higher levels through allowed transitions.

This population rate is given by

$$\left(\frac{dN_j}{dt}\right)_{cascade} = \sum_i N_i A_{ij} \qquad (4\text{-}5)$$

where the $N_i$'s refer to the populations of the upper levels and $N_j$ is that of the lower metastable level for the cascade transitions; and the $A_{ij}$'s are the corresponding spontaneous transition probabilities.

(c) Molecular Dissociation

Excitation by molecular dissociation is one of the most important processes that contribute to the metastable populations of the $np^4$ elements. The dissociation processes generally take place through (1) absorption of light quanta in the continua of the molecules (photodissociation), and (2) collisions between the molecules and the excited foreign atoms or molecules, the latter being themselves previously excited by direct collisions with the energetic electrons.

The dissociating molecule and the dissociation products, i.e. the atoms (normal or excited), usually follow certain rules which correlate (1) the Λ-values of the molecular states with the L-values of the atomic states, (2) the spin-values or multiplicities of the molecular states with those of the atoms. These rules were originally derived on the basis of quantum mechanics

and group theory by Wigner and Witmer (Wi 28) and, using more elementary considerations, by Herzberg who collected the results of all cases of practical importance in Tables 26 to 28 of "Molecular Spectra and Structure, Volume I" (He 50). However, these rules are valid and complete for normal LS-coupling of the molecules and atoms; departures from such coupling will allow for cases that violate the rules.

Besides the Wigner-Witmer rules there is another important criterion that is more pertinent in the determination of the actual dissociation products - it is the "Energy Resonance" involved in the dissociative processes. However, to establish the resonant dissociative reaction, a quantitative knowledge of the following must be taken into account: (1) "the potential curves" or the "dissociation limits"† of the molecules under consideration; (2) the energy levels of the excited foreign atoms or molecules from which the dissociation energy is transferred.

---

†The "dissociation limits" of an excited molecular state correspond to the position of the convergence limit of bands or of the beginning of the continuum under consideration.

Examples for Oxygen:

(i) Photodissociation

Of all the possible photodissociation products of the oxygen states X $^3\Sigma_g^-$, B $^3\Sigma_u^-$ and D $^3\Pi_u$, the ones which are most likely, after considerations of the Wigner-Witmer Correlation Rules and Energy Resonance, are the following:

$$O_2(X\ ^3\Sigma_g^-) + h\nu \rightarrow O(^3P) + O(^3P) + K.E. \qquad (4\text{-}6)$$

(Dissociation Limit: 2440 Å ≡ 5.12 eV)

$$O_2(B\ ^3\Sigma_u^-) + h\nu \rightarrow O(^3P) + O(^1D) + K.E. \qquad (4\text{-}7)$$

(Dissociation Limit: 1759 Å ≡ 7.05 eV)

$$O_2(D\ ^3\Pi_u) + h\nu \rightarrow O(^3P) + O(^1S) + K.E. \qquad (4\text{-}8)$$

(Dissociation Limit: 1340 Å ≡ 9.27 eV)

(ii) Dissociation by Energy Transfer from Excited Foreign Atoms or Molecules:

(1) From excited foreign xenon atoms Xe* (Wa 72):

$$Xe + e(v') \rightarrow Xe^* + e(v'') \qquad (4\text{-}9)$$

$$Xe^* + O_2(X\ ^3\Sigma_g^-) \rightarrow Xe(^1S) + O(^3P) + O(^1S) \qquad (4\text{-}10)$$

Here Xe($^1$S) are the ground state atoms of xenon and the energy released from Xe* atoms is taken up by $O_2(X\ ^3\Sigma_g^-)$ for its dissociation.

(2) From excited nitrogen foreign molecules (Me 69):

$$N_2 + e(v') \rightarrow N_2(A\ ^3\Sigma_u^+) + e(v'') \qquad (4\text{-}11)$$

$$N_2(A\ ^3\Sigma_u^+) + O_2(X\ ^3\Sigma_g^-) \rightarrow N_2(X\ ^1\Sigma_g^+) + O(^1S) + O(^3P) \qquad (4\text{-}12)$$

Here $N_2(A\ ^3\Sigma_u^+)$ are the foreign excited molecules, and the energy released in the collision is used to dissociate the ground state oxygen molecules into the metastable atoms.

(iii) Excitation by Direct Atom-Foreign Molecule Collisions:

Foreign excited molecules can also directly excite the ground state atoms of the $np^4$ elements into the metastable ($^1S$). For example (Pa 70):

$$N_2(A\ ^3\Sigma_u^+) + O(^3P) \rightarrow N_2(X\ ^1\Sigma_g^+) + O(^1S). \quad (4\text{-}13)$$

(d) Depopulation Mechanisms and the Buffer Gas

The excitation mechanisms described above indicate two main criteria in the production of the forbidden lines, namely, (1) the presence of a foreign agent for the energy-transfer type of excitations, and (2) the presence of an electric current for the excitations by electron collisions. However, the above-mentioned considerations do not exhaust all possible factors which may be contributing to the intensity of the forbidden lines produced.

The metastable atoms can also be destroyed by collisions with other species or with the walls of the discharge tube. Consequently, an approximate treatment

of diffusion effects, involving the mean distance $\bar{\Lambda}$ that a metastable atom diffuses before radiating spontaneously and the mean free path $\bar{\rho}$ that it travels between two collisions, may be considered.

The mean free path of an atom is inversely proportional to the pressure of the medium in which it is moving (Ar 65a). A lower collision frequency and thus less deactivation would therefore be expected from the use of a low pressure medium in the discharge tube. An inert gas, usually introduced into the discharge medium to "buffer" the deactivating collisions between the metastable atoms of interest and the discharge tube's walls, would however increase the medium's pressure and enhance the chance for collisions. Fortunately there is no de-activation in a collision between a metastable atom and an inert gas atom, since the excitation potentials of their lowest energy levels vary from 8.3 eV for xenon to 19.8 eV for helium (Table IV-1) and these are all much above the energies of the metastable states (Figs. 6-1,12,17) being considered here.

Calculations based on the theory of probability show that the mean distance $\bar{\Lambda}$ is related to the diffusion coefficient D and to the mean life $\tau$ as follows (Ar 65b):

$$\bar{\Lambda} = \sqrt{D\tau} \qquad (4\text{-}14)$$

| He | Ground State $1S^2\ {}^1S_0$ | $1s2s\ {}^3S_1$ | $1s2s\ {}^1S_0$ | $1s2p\ {}^3P^o_{2,1,0}$ |
|---|---|---|---|---|
| | 0 | 19.814 | 20.610 | 20.958 |

| | Ground State $np^6\ {}^1S_0$ | $np^5({}^2P_{3/2})(n+1)s$ | | $np^5({}^2P_{1/2})(n+1)p$ | |
|---|---|---|---|---|---|
| | | $^3P^o_2$ | $^3P^o_1$ | $^3P^o_0$ | $^1P^o_1$ |
| Ne(n = 2) | 0 | 16.619 | 16.671 | 16.715 | 16.848 |
| Ar(n = 3) | 0 | 11.545 | 11.623 | 11.723 | 11.828 |
| Kr(n = 4) | 0 | 9.915 | 10.032 | 10.562 | 10.643 |
| Xe(n = 5) | 0 | 8.315 | 8.436 | 9.447 | 9.570 |

Table IV-1. The low-lying metastable levels of the inert gases in eV (from C. E. Moore's Tables on "Atomic Energy Levels").

It was also shown by McDaniel (Mc 64) that D is inversely proportional to the pressure of the medium, therefore $\bar{\lambda}$ is inversely proportional to the square root of the pressure. Thus, when the pressure of a discharge medium is increased (such as when a buffer gas is introduced), the path $\bar{\lambda}$ that the metastable atom would travel before radiating spontaneously will decrease.

The upper atmospheric pressure is very low ($\approx 10^{-4}$ torr at an altitude of 100 km), so that to simulate such conditions in the laboratory, for the studies of forbidden lines as observed in the aurorae, would require an extremely large discharge vessel. This is rather impractical for laboratory work, but from the above discussion we can see that the compromise solution is to use a buffer gas mixed with a small proportion of the element to be investigated in a gaseous or vaporized form.

## 4.2 Absorption-Line Theories

In the previous section the theories on the population and depopulation mechanisms of the low-lying

metastable levels in the $np^4$ elements were treated. Here we shall see how the optical-line absorption theories can be applied in the determination of the net population of such a metastable level.

(a) The Absorption Line

When light passes through a transparent medium, such as an element in a gaseous or vaporized form, it emerges diminished in intensity. Part of the light may be lost through scattering or reflection at the surfaces, but the rest is said to be lost through "absorption" by the medium. (The absorbed energy may be transformed into heat or into fluorescent or phosphorescent light of longer wavelengths.) The well-known "Lambert-Bouguer Law" gives the relationship between the intensities of the radiation incident on and transmitted by a layer of absorbing material. This law is expressed in the form that each successive layer of thickness dx of the medium absorbs the same fraction dI/I of the radiation of intensity I incident upon it, i.e.

$$\frac{dI}{I} = - k_\nu \, dl \qquad (4\text{-}16)$$

where $k_\nu$ is the constant rate of absorption at a frequency $\nu$ and is called the "Absorption Coefficient". Equation (4-16), on integration, becomes

$$I_\nu = I_0 \, e^{-k_\nu X} \qquad (4\text{-}17)$$

where $I_0$ is the (unattenuated) intensity of radiation just inside a layer of thickness x and $I_\nu$ is the emergent intensity.

If the absorbing medium has an "absorption line" at the frequency $\nu_0$, then part of the energy absorbed will be used to raise atoms from the lower energy level j to the upper level i of that line and the frequency distribution of the line intensity $I_0$ will be as shown in Fig. 4-1; the corresponding frequency distribution of the absorption coefficient $k_\nu$ will be as shown in Fig. 4-2. Maximum absorption corresponding to $k_0$ occurs at the centre of the line $\nu_0$. The width of the chord joining the two points of the curve where $k_\nu$ has fallen to half its maximum is called the "half width" of the absorption line and is denoted by $\Delta\nu$. The latter will differ according to the way the absorption line has been broadened.

(b) Absorption-Line Breadths

There are, in general, five types of processes that may contribute to the broadening of an absorption line of a gas. They are as follows:

(1) Natural broadening

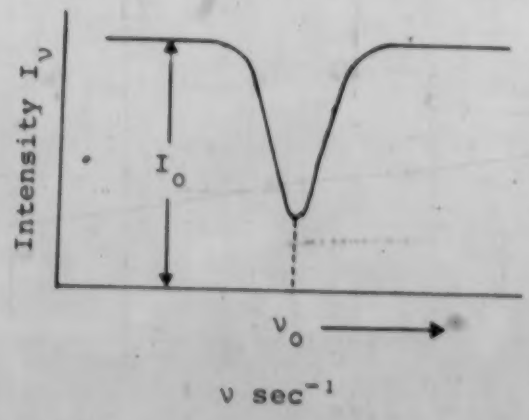


Fig. 4-1. An absorption line.

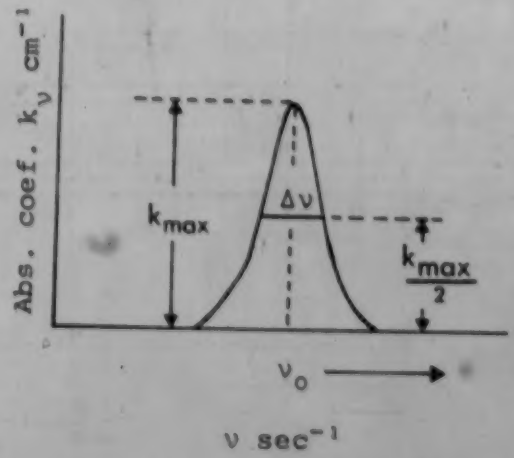


Fig. 4-2. The frequency distribution of the absorption coefficient in an absorption line.

(2) Doppler broadening

(3) Collision broadening

(4) Pressure broadening

(5) Stark broadening.

In many cases it is possible to choose experimental conditions such that all but one or two broadening processes are completely absent or negligible. The present experiments, leading to the A-values of forbidden lines, were performed under conditions in which only the Doppler (and natural) broadening prevailed. To see how this is possible, a brief comparison of the different half widths is treated here.

The Doppler Effect is due to the random motions of the atoms or molecules in a gas and the half width (Wh 34a) of a spectrum line broadened by such effect is given by

$$\Delta\nu_D = \frac{2\sqrt{2R \ln 2}}{c} \nu_o \sqrt{\frac{T}{M}} \qquad (4\text{-}18)$$

where T is the absolute temperature of the moving atoms or molecules, M the molecular weight, $\nu_o$ the frequency at the line centre, R the universal gas constant and c the velocity of light. For, say, a sodium D line at $\lambda$5893 Å at 500°K, equation (4-18) gives a $\Delta\lambda_D$ of 0.02 Å, a value which is about 200 times as large as the natural half width (see the next page).

The Natural width, $(\Delta\nu_N)_{ih}$, of a line is equal to the sum of the widths of the two levels,

$$(\Delta\nu_N)_{ih} = (\Delta\nu_N)_i + (\Delta\nu_N)_h \qquad (4\text{-}18)$$

where, by the principle of indeterminacy,

$$(\Delta\nu_N)_i = \Delta E_i/h = 1/2\pi\tau_i \quad (\tau_i \equiv \text{lifetime of level } i)$$

Thus, for the absorption lines used in this work, it can be shown that $(\Delta\nu_N)_{ih} \approx 1 \times 10^{-4}$ Å, i.e., the natural width is negligible compared to that of the Doppler effect.

The Collision and Pressure effects are characterized by the following: If, during the time an atom is emitting or absorbing radiation, it collides elastically with another atom, the phase and amplitude of the radiation have a chance of undergoing a considerable change. The Collision effect is categorized as that occurring when the mean time between collisions is long compared with the collision time whereas if the mean time between collisions is short compared with the collision time, the Pressure effect will occur. However, the conditions for the latter exist in a gas only when the pressure is relatively high (≈ 10 atmospheres); thus this type of broadening is seen to be negligible under the pressure conditions chosen in the present experiments.

The Collision half width (Wh 34c) is given by

$$\Delta\nu_c = \frac{4N_A D^2 p}{\sqrt{RT\mu\pi}} \qquad (4\text{-}20)$$

where $N_A$ is the Avogadro's Number or $6.06 \times 10^{23}$ $mole^{-1}$,

D the effective collision diameter, p the pressure and μ the reduced molecular weight of the two colliding species (one of which may be foreign). For visible light at 273°K and p = 760 torr, $\Delta\nu_C = \Delta\nu_D$ (Wh 34d). For typical experimental conditions in this project, i.e. 1200 Å light with T about 500°K and 20 torr pressure we have

$$\Delta\nu_D = \left(\frac{5000}{1200} \times \frac{500}{273} \times \frac{760}{20}\right) \Delta\nu_C$$

$$= 300\ \Delta\nu_C$$

Thus, collision broadening is negligible compared to Doppler broadening for the conditions employed in the present work.

Stark broadening is due to the strong electric field produced by the collisions between ions and atoms or to "ion" fields. However, under the chosen conditions of the present experiments, the current ($\leq$ 100 mA) would be too low to produce sufficient energy to dissociate the molecules in question and ionize the resulting atoms afterwards. Also, the only region in the discharge where a Stark effect might occur would be that around the electrodes, where the potential gradient might be around 30,000 volts/cm. However, the electrodes are situated at the bottom of the vertical arms of the discharge tube; consequently, the lines viewed would be practically free from Stark broadening, under the conditions of the present experiment.

(c) The Absorption Coefficient $k_o$ and the Population Density N

Having ascertained that the Doppler effect is the only important factor that contributes to the broadening of the absorption lines involved under the chosen conditions of the present experiments, we can now consider the population N of the metastable levels and their relation to the absorption coefficient $k_\nu$ due to the Doppler effect only:

It is well-known (Mi 34a) that for Doppler broadened lines, the absorption coefficient is given by

$$k_\nu = k_o \exp -\left[\frac{2(\nu-\nu_o)}{\Delta\nu_D}\sqrt{\ln 2}\right]^2 \qquad (4\text{-}21)$$

Integrating equation (4-21) we obtain

$$\int_0^\infty k_\nu \, d\nu = \frac{1}{2}\sqrt{\frac{\pi}{\ln 2}}\, k_o \, \Delta\nu_D \qquad (4\text{-}22)$$

Mitchell and Zeemansky (Mi 34b) have shown that

$$\int_0^\infty k_\nu \, d\nu = \frac{\pi e^2}{mc} Nf \qquad (4\text{-}23)$$

where f is the absorption oscillator strength of the line involved. Equating (4-22) and (4-23) we obtain

$$k_o = \frac{2}{\Delta\nu_D}\sqrt{\frac{\ln 2}{\pi}}\,\frac{\pi e^2}{mc} Nf \qquad (4\text{-}24a)$$

or, more specifically, for an absorption line $\nu_{ih}$ where h refers to an upper level, we have

$$k_{o_{ih}} = \frac{2}{\Delta\nu_D}\sqrt{\frac{\ln 2}{\pi}}\,\frac{\pi e^2}{mc} N_i f_{ih} \qquad (4\text{-}24b)$$

Hence, if the f-value of the line is known and also $\Delta\nu_D$ which can be derived from the temperature T of the gas atoms or molecules in question (see equation 4-18), then the population density N of the lower level i can be deduced from equation (4-24), provided that the absorption coefficient $k_0$ at the centre of the line has been first determined independently.

(d) Theory of the Experimental Determination of the Absorption Coefficient

To deduce the population density N of a metastable state in a $np^5$ element from equation (4-24) the absorption coefficient $k_0$ of an allowed line whose lower level is this metastable state must be first determined separately. This allowed line, in general, falls in the vacuum ultraviolet region of the spectrum. Consequently, part of the experimental procedures will be concerned with vacuum ultraviolet techniques and instrumentation.

The determination of $k_0$ is based on a theory which is a slight variation of that used by Harrison (Ha 59) in his studies on self-absorption within a plasma. The discharge medium can be regarded as being uniform and cylindrical in shape and the theory which follows is valid provided that the optical arrangement shown in Fig. 4-3 is such that, for all measurements,

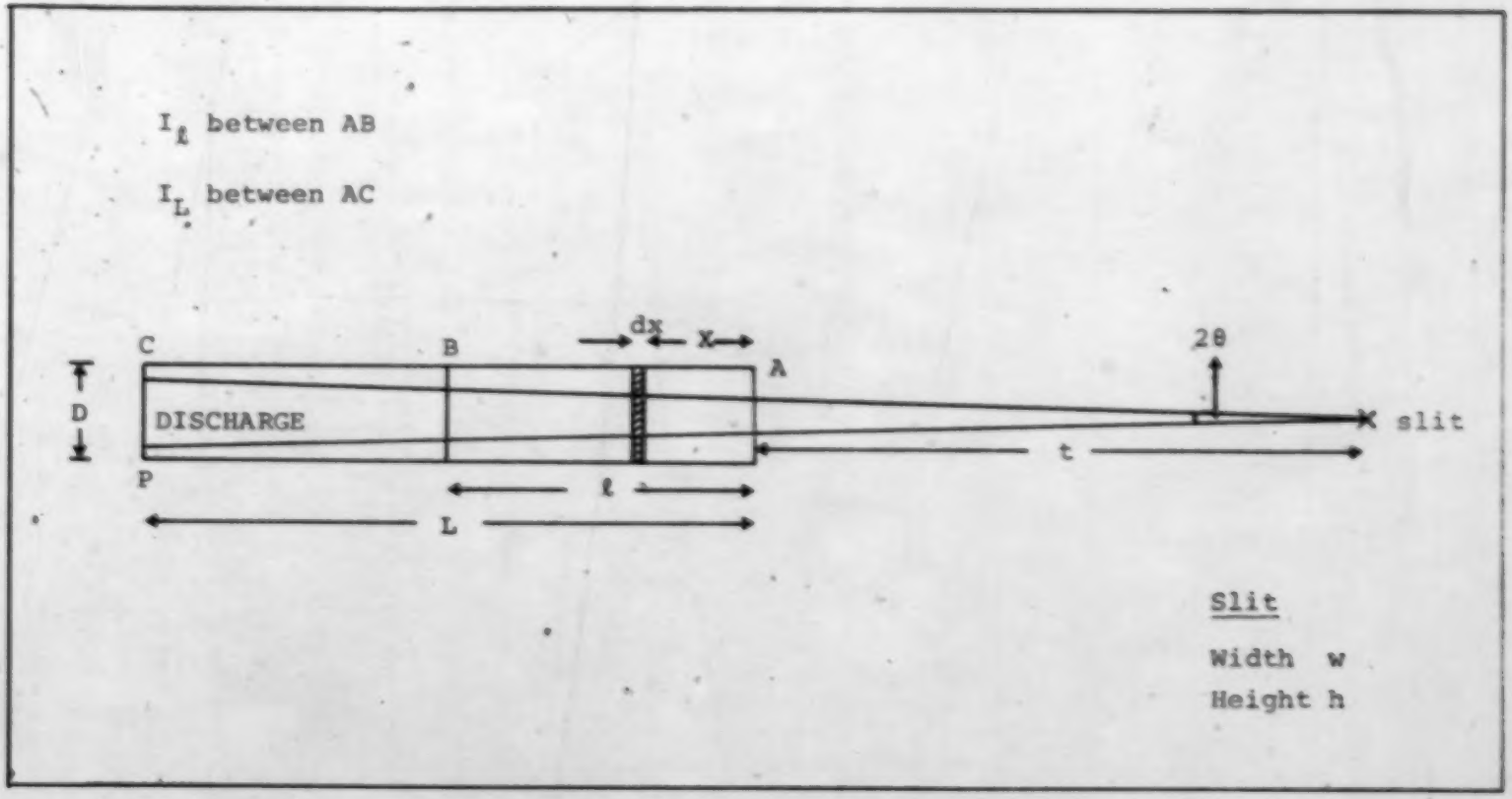


Fig. 4-3. Diagram of the optical arrangement with $(t + L)2\theta < D$.

$$(t + L)2\theta < D \qquad (4\text{-}25)$$

Let T be the transmission coefficient of the window material of the discharge tube and let the monochromator slit have width w and height h. Then for an element dx of the discharge medium, the corresponding volume element that radiates isotropically and that is bounded by the conic sections whose apex points form the slit area and whose bases are always on the left end (CP) of the discharge medium (the diameter of each of these bases $\leq$ D), can be shown to be

$$[w + (t + x)2\theta][h + (t + x)2\theta]\, dx$$

Also, only a faction $Thw/4\pi(t + x)^2$ of the radiant flux from the above volume enters the spectrograph slit. Therefore, the "effective" volume element that enters the spectrograph slit is

$$dV = \frac{Thw}{4\pi(t+x)^2}\,[w + (t + x)2\theta][h + (t + x)2\theta]\, dx \qquad (4\text{-}26)$$

And, since $w << h << (t+x)2\theta$, the effective volume becomes

$$dV = \frac{Thw\theta^2}{\pi}\, dx$$

$$= C\, dx \qquad (4\text{-}27)$$

where C is a constant.†

Suppose the intensity emitted in the frequency interval dν is $E_\nu\, d\nu$ per unit volume of the discharge, then the intensity of the whole emitted line per unit

†Through rigorous consideration, it can be shown that C is in fact a "weak" function of x, which, like a constant, would cancel out in the ratio $I_L/I_\ell$ expressed in equation 4-37.

volume of discharge is

$$I = \int E_\nu \, d\nu \qquad (4\text{-}28)$$

where the integration is across the whole line.

Also, suppose that light from the element dx is partly absorbed according to Lambert-Bouguer law, i.e.

$$E_{\nu x} = E_{\nu 0} \exp(-k_\nu x) \qquad (4\text{-}29)$$

where $k_\nu$ is the absorption coefficient per unit length for light of frequency $\nu$; then the total intensity of the emitted line entering the monochromator and from the whole volume of the discharge (which is then of length L as shown in Fig. 4-3) is

$$I_{AC} = I_L = \int_0^{\nu V} E_{\nu 0} \exp(-k_\nu x) \, dV \, d\nu \qquad (4\text{-}30)$$

Substituting equation (4-27) into (4-30) we have

$$I_{AC} = I_L = \int_0^{\nu L} C \, E_{\nu 0} \exp(-k_\nu x) \, dx \, d\nu \qquad (4\text{-}31)$$

Similarly, under the same discharge conditions, the total intensity of the emitted line from a smaller volume corresponding to a length $\ell$ of the discharge and which is on the right hand section of the discharge (see Fig. 4-3) is

$$I_{AB} = I_\ell = \int_0^{\nu \ell} C \, E_{\nu 0} \exp(-k_\nu x) \, dx \, d\nu \qquad (4\text{-}32)$$

Again, for the volume of the discharge from the left hand section of the discharge, the intensity is

$$I_{BC} = I_{(L-\ell)} = \int_\ell^{\nu L} C \, E_{\nu 0} \exp(-k_\nu x) \, dx \, d\nu \qquad (4\text{-}33)$$

However, this intensity will be further attenuated by the absorbing path 0 → ℓ, so that $I_{BC}$ is actually given by

$$I_{BC} = I_{(L-\ell)} = \left[ \int_{\ell}^{\nu L} C\, E_{\nu 0} \exp(-k_\nu x)\, dx\, d\nu \right] \exp(-k_\nu \ell) \qquad (4\text{-}34)$$

Now, if the line has a Doppler profile, then we may write as in equation (4-21) (Mi 34a)

$$k_\nu = k_0 \exp(-\omega^2) \qquad E_{\nu_0} = E_{00} \exp(-\omega^2) \qquad (4\text{-}35)$$

where
$$\omega = \frac{2(\nu - \nu_0)}{\Delta\nu_D} \ln 2 \qquad (4\text{-}36)$$

and $\Delta\nu_D$ is given as in equation (4-18).

Taking the ratio of equation (4-31) to (4-32) and then substituting (4-35) into the resulting ratio, we obtain

$$\frac{I_{AC}}{I_{AB}} = \frac{I_L}{I_\ell} = \frac{\int_{|\omega|} [1 - \exp\{-k_0 L \exp(-\omega^2)\}]\, d\omega}{\int_{|\omega|} [1 - \exp\{-k_0 \ell \exp(-\omega^2)\}]\, d\omega} \qquad (4\text{-}37)$$

Similarly, taking the ratio of equations (4-31) and (4-34) and then substituting equation (4-35) into the resulting ratio, we obtain

$$\frac{I_{AC}}{I_{BC}} = \frac{I_L}{I_{(L-\ell)}} = \frac{\int_{|\omega|} [1 - e^{-k_0 L \exp(-\omega^2)}\, e^{k_0 \ell \exp(-\omega^2)}]\, d\omega}{\int_{|\omega|} [e^{-k_0 \ell \exp(-\omega^2)} - e^{-k_0 L \exp(-\omega^2)}]\, d\omega} \qquad (4\text{-}38)$$

The intensity ratios from equations (4-37) and (4-38) can be evaluated on a computer for different values of $k_0 \ell$,

with the upper limit $|\omega|$ of the integrations set by the bandwidth of the line beyond which absorption is absent or negligible. Figs. 4-4a & b show the result corresponding to equation (4-37), in which $L = 2.031\ell$ and $|\omega| = 3.0$. The value of $k_0$ for a certain line can then be determined in the following way: The intensities are measured for the two lengths $\ell$ and L of the discharge, both measurements being made under the same conditions, and the intensity ratio $I_L/I_\ell$ is then deduced. This ratio is then located on the ordinate of one of the graphs in Figs. 4-4a & b and the corresponding value of $k_0\ell$ is interpolated. Since $\ell$, the discharge length corresponding to AB in Fig. 4-3, is known, the value of $k_0$ can therefore be deduced.

## 4.3 Spontaneous Transition Probabilities of "Forbidden" Lines

We have seen how the absorption coefficient $k_0$ of an allowed ultraviolet line of frequency $\nu_{ih}$ can be determined and consequently, how the population density N of its lower state i can be calculated from equation (4-24), after having assumed the f-value of the line. Now we shall use this value of N in the determination of the A-coefficient of a line of frequency $\nu_{ij}$ as follows:

From Einstein's relation we know that the intensity

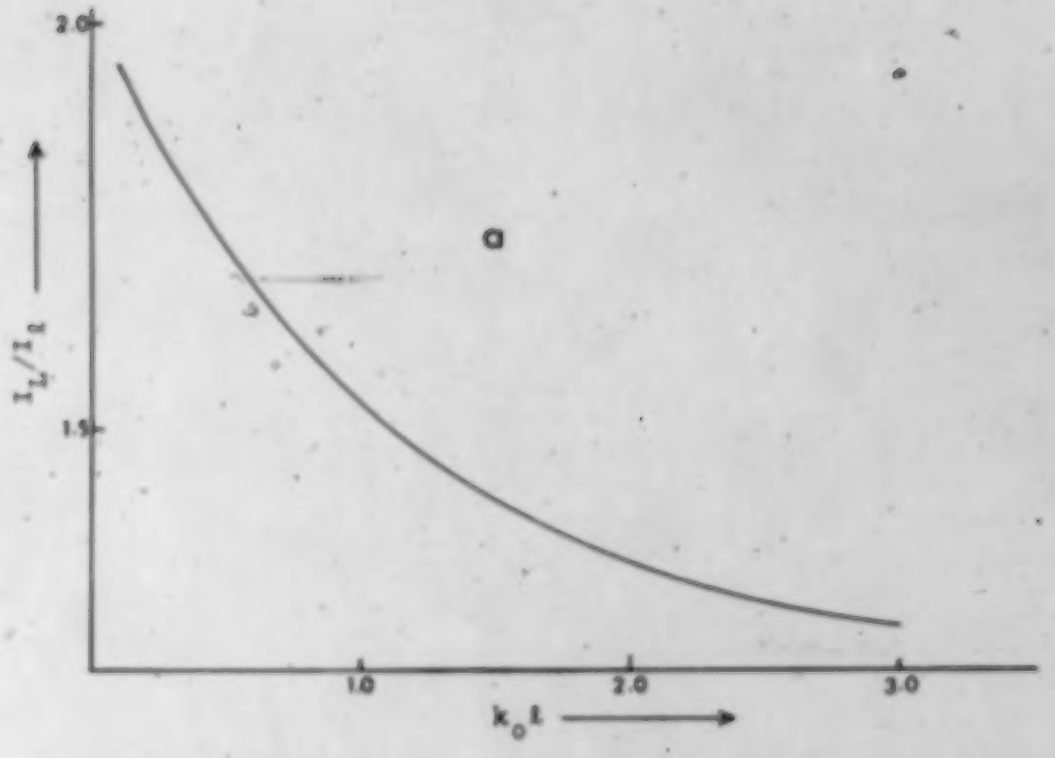


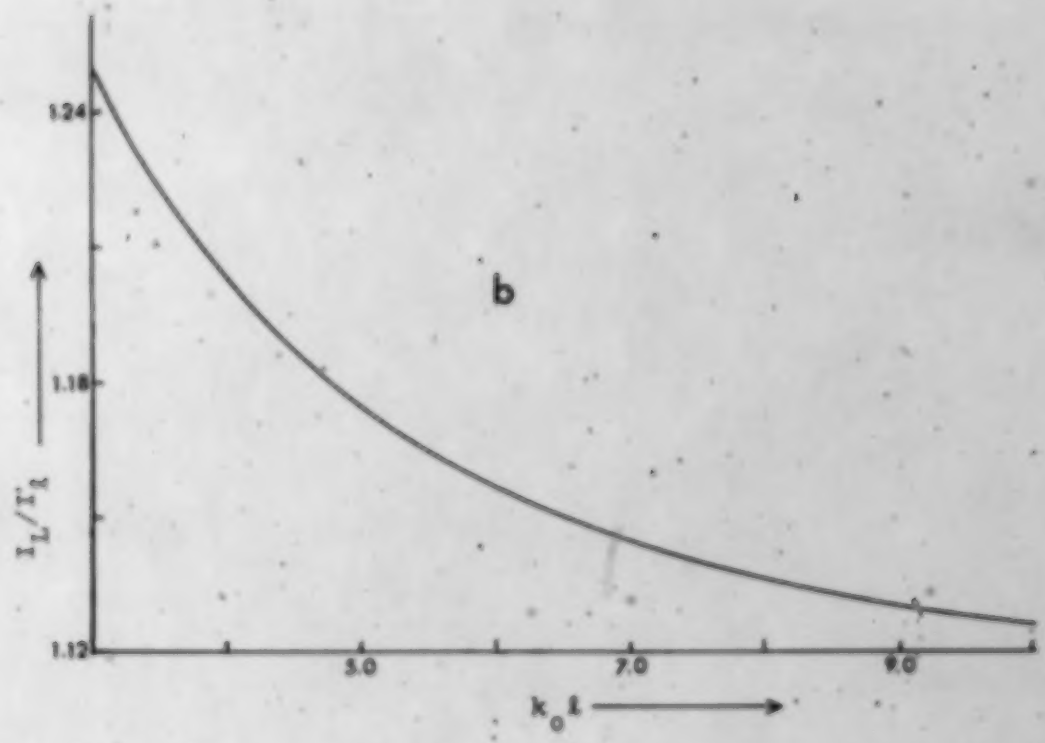


Figs. 4-3a & b. $I_L/I_\ell$ vs. $k_0\ell$ for Oxygen ($L = 2.031\ell$).

I of any spectral line of frequency ν is proportional to the spontaneous transition probability of that line and the population density N of its upper state, i.e.

$$I = NA\,h\nu \qquad (4\text{-}39)$$

where h is Planck's constant.

In the present cases where forbidden transitions between metastable states i and j in the $np^4$ elements are involved, equation (4-39) may be written more specifically as

$$I_{ij} = G\,N_i\,A_{ij}\,h\nu_{ij} \qquad (4\text{-}40)$$

where $I_{ij}$ and $A_{ij}$ are the absolute intensity and the spontaneous transition probability respectively, of the forbidden line of frequency $\nu_{ij}$ (see Fig. 4-5); G is a geometrical factor and $N_i$ is the population density of the state i.

$N_i$, from the net result of the populating and depopulation processes of the state i, should have a steady value for a given condition of the discharge. As mentioned before, this value is obtained by first determining the $k_0$-value of an allowed ultraviolet line of frequency $\nu_{ih}$ and then substituting in equation (4-24). Thus, a measurement of the absolute intensity $I_{ij}$ and of the steady state population $N_i$ should, as indicated by equation (4-40), yield a value for $A_{ij}$.

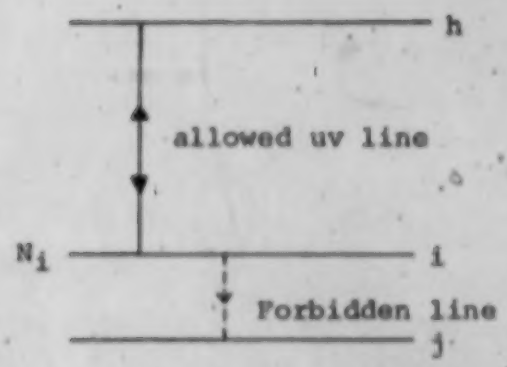


Fig. 4-5. The allowed and the forbidden lines with a common state i.

One important aspect that should be pointed out here is that the measurement of $I_{ij}$ and $N_i$ should be made simultaneously. This is made possible by employing a correct instrumentation arrangement (described in the next chapter).

## 4.4 The Absolute Intensity Measurement

To obtain the absolute A-coefficient of a forbidden line we have to measure, among other quantities (equation 4-40), the absolute intensity of that line. To do this, a calibrated standard of spectral radiance† in the form of a tungsten strip lamp may be used.

---

†The "Spectral Radiance" is the Radiant Power per unit solid angle per unit area of source per unit wavelength interval.

(a) The Standard of Spectral Radiance

Much research has been carried out on tungsten lamps, in particular regarding the spectral emissivity of tungsten (Or 36, De 54, Sc 68). Although all the results are not in perfect agreement, it is generally acknowledged that with reasonable caution the emmissivity of pure clean tungsten ribbon remains fairly constant throughout the life of the lamp. The determination of the spectral distribution of radiant energy from a tungsten filament lamp has then been obtained by making use of the published values of the emissivity of tungsten (St 43, Co 57, Ba 59). However, in these calculations, no account was taken of the effects of impurities present or of the size, shape and crystalline structure of the filament. All these properties affect markedly the true spectral and total emmissivity (De 54). Furthermore, De Vos (De 54) found that interreflections within the lamp affect the total spectral radiation from a particular tungsten strip. In order to obtain the correct spectral radiance of a lamp, it became necessary that the particular lamp be calibrated against a blackbody. The types of blackbody and the standard tungsten lamp used in this work are described by Stair et al. (St 60), working at N.B.S.

It has been well established that the spectral radiation characteristics of a blackbody may be defined

in terms of certain physical laws. Thus, from Planck's radiation law, the radiant intensity of a blackbody at an absolute temperature T in the wavelength interval $(\lambda, \lambda+d\ )$ is given by

$$I^B(\lambda,T)\ d\lambda = \frac{C_1\ d\lambda}{\lambda^5 \exp\left(\frac{C_2}{\lambda T} - 1\right)} \qquad (4\text{-}41)$$

where the radiation constants $C_1$ and $C_2$ are given as follows:

$$C_1 = 1.1908 \times 10^{-12} \text{ watt-cm}^2 \text{ - ster}^{-1}$$

$$C_2 = 1.4380 \text{ cm°K}$$

and $I^B(\lambda,T)$ is in watt-$\text{cm}^{-2}$ $\text{ster}^{-1}$/cm wavelength interval.

The radiant intensity at the surface of the tungsten strip at a temperature T in the wavelength interval $(\lambda, \lambda+d\ )$, in a direction normal to the surface, is defined by

$$I(\lambda,T)\ d\lambda = e(\lambda,T)\ I^B(\lambda,T)\ . \qquad (4\text{-}42)$$

where $I^B(\lambda,T)$ is given by equation (4-39), and $e(\lambda,T)$ is the "normal spectral emissivity"† of the tungsten ribbon surface with a value varying between 0 and 1.

---

†The normal spectral emissivity is the ratio of the spectral radiant intensity in a direction normal to the surface of the strip at a temperature T in the wavelength interval $(\lambda, \lambda+d\lambda)$ to that of a blackbody at the same temperature and in the same wavelength interval.

$e(\lambda,T)$ was determined for a tungsten ribbon surface by De Vos (De 54) as a function of wavelength at temperatures ranging from 1600 to 2800°K. The temperature T was derived from the brightness temperature of the ribbon surface with the aid of a disappearing filament pyrometer (Ru 54). Thus, knowing the wavelength $\lambda$, the temperature T and the corresponding emissivity e, the absolute radiance of the tungsten strip lamp for a certain geometry can be deduced from equation (4-41) and (4-42). The EPT-1182 tungsten ribbon filament lamp used in this work was calibrated at a temperature T corresponding to a current supply of 35 amperes and a table of results on the absolute spectral radiance $E(\lambda,T)$ in microwatt/steradian-nanometer wavelength interval - $mm^2$ source area, is given for a wavelength region ranging from 0.25 to 2.6 microns (Table IV-2).

(b) Absolute Intensity of the Forbidden Lines

The absolute radiant intensity of a forbidden line from a particular volume of the discharge and through a given slit width can be determined by comparing it with the known spectral radiance of a standard ribbon lamp as follows:

The forbidden line observed from a particular volume of discharge and the radiation from the ribbon surface of

Table IV-2. Spectral radiance $E(\lambda,T)$ in microwatts per (steradian-nanometer-mm$^2$ of source) of lamp No. EPT-1182 operated at 35 Amperes, supplied by Eppley Laboratory.

| $\lambda$ (nm ≡ mμ) | Spectral Radiance |
|---|---|
| 250 | $1.39 \times 10^{-2}$ |
| 260 | $3.09 \times 10^{-2}$ |
| 270 | $5.56 \times 10^{-2}$ |
| 280 | $9.68 \times 10^{-2}$ |
| 290 | $1.60 \times 10^{-1}$ |
| 300 | $2.55 \times 10^{-1}$ |
| 320 | $5.82 \times 10^{-1}$ |
| 350 | 1.56 |
| 370 | 2.78 |
| 400 | 5.48 |
| 450 | 13.4 |
| 500 | 26.9 |
| 550 | 44.2 |
| 600 | 64.8 |
| 650 | 86.5 |
| 700 | 107 |
| 750 | 124 |
| 800 | 137 |
| 900 | 150 |
| 1000 | 154 |
| 1100 | 150 |
| 1200 | 141 |
| 1300 | 129 |
| 1400 | 116 |
| 1500 | 103 |
| 1600 | 90.7 |
| 1700 | 79.2 |
| 1800 | 68.6 |
| 1900 | 59.6 |
| 2000 | 51.5 |
| 2100 | 44.7 |
| 2200 | 39.1 |
| 2300 | 35.0 |
| 2400 | 31.6 |
| 2500 | 28.2 |
| 2600 | 24.4 |

the lamp (run at the calibrated temperature) are, in turn, directed normally to the entrance slit of a monochromator, after having been totally reflected from an adjustable mirror (see Fig. 3-1a). The photomultiplier signals from both sources are recorded for a certain time interval.

In the present experimental set-up, suppose $a_s$, $a_L$ are the monochromator slit and the ribbon surface areas respectively; $d_P$, $d_L$ are the distances from the slit to the forbidden line source and the ribbon surface respectively; and $\Delta\lambda$ is the waveband obtained from the grating dispersion $d\lambda/dx$ of a particular slit width w, i.e. $\Delta\lambda = (d\lambda/dx)w$. Then the radiant energy/sec incident on the photomultiplier from the lamp at the calibrated temperature is

$$R(\lambda,T) = E(\lambda,T) \cdot \frac{a_s}{d_L^2} \cdot \frac{d\lambda}{dx} \cdot w \cdot a_L$$

where $(a_s/d_L^2)$ is the solid angle subtended by the slit on every point of the ribbon surface and $E(\lambda,T)$ is the spectral radiance of the standard lamp. The above rate of radiant energy expressed in photons/sec is

$$\frac{R(\lambda,T)}{h\nu} = E(\lambda,T) \frac{a_s}{d_L^2} \cdot \frac{d\lambda}{dx} \cdot w \cdot a_L \cdot \frac{\lambda}{hc} = N_L$$

Now, let $C_L$ be the photomultiplier signal rate (counts/sec) corresponding to $N_L$ and $C_P/T_P$ be that from the

particular source of the forbidden line after having been corrected for the transmittance $T_F$ of the glass tube wall. (It should be noted here that $C_L$ need not be corrected for the transmittance of the lamp window material since it was already corrected during its calibration.) Then, since the photomultiplier signal is proportional to the number of incident photons, the radiant energy of the forbidden line, expressed in photons/sec is

$$N_F = \frac{N_L}{C_L} \times \frac{C_F}{T_F}$$

$$= E(\lambda,T) \frac{a_s}{d_L^2} \cdot \frac{d\lambda}{dx} \cdot w \cdot \frac{\lambda}{hc} \cdot \frac{C_F}{C_L} \cdot \frac{1}{T_F}$$

Also, the solid angle subtended by the slit area on every point of the discharge volume seen from the side of the tube is $(a_s/d_F^2)$ whereas the total solid angle subtended on the whole volume of the discharge seen is $4\pi$. Thus, assuming that the radiation from the discharge seen is isotropic, the total radiant intensity of the forbidden line ($\nu_{ij}$) from the whole discharge volume seen, expressed in photons/sec is

$$I_{ij} = N_F \cdot 4\pi \left(\frac{d_F^2}{a_s}\right)$$

$$= 4\pi\, E(\lambda,T) \cdot a_L \cdot \frac{d\lambda}{dx} \cdot w \cdot \frac{\lambda}{hc} \cdot \frac{1}{T_F} \left(\frac{d_F}{d_L}\right)^2 \left(\frac{C_F}{C_L}\right) \quad (4\text{-}43)$$

Note that in equation (4-43), the slit area $a_s$ cancelled

out (as long as the same area was used during the comparison of the radiation sources).

## 4.5 Obtaining the Absolute Transition Probability $A_{ij}$ from its Implicit Relationship with the Measured Quantities in this Project

The absolute intensity $I_{ij}$ of a forbidden line is obtained by using equation (4-43). This value is related to the absolute transition probability $A_{ij}$ through equation (4-40) in which the geometrical factor G is given by the volume of the cylindrical-shaped discharge, i.e.

$$G = \pi r^2 L'$$

where r, L' are the radius and the length of the cylindrical discharge respectively.

Thus, substituting equation (4-43) into (4-40) (the latter is in photons/sec), we have

$$4\pi\, E(\lambda,T) \cdot a_L \cdot \frac{d\lambda}{dx} \cdot w \cdot \frac{\lambda}{hc} \cdot \frac{1}{T_F} \left(\frac{d_F}{d_L}\right)^2 \left(\frac{C_F}{C_L}\right) = \pi r^2 L' \cdot N_i A_{ij}$$

i.e.,

$$A_{ij} = \frac{1}{N_i}\left[\frac{4}{r^2 L'} \cdot E(\lambda,T) \cdot a_L \cdot \frac{d\lambda}{dx} \cdot w \cdot \frac{\lambda}{hc\, T_F} \left(\frac{d_F}{d_L}\right)^2 \left(\frac{C_F}{C_L}\right)\right] \qquad (4\text{-}44)$$

where $N_i$ is given by equations (4-24) and (4-18) as follows:

$$\frac{1}{N_i} = \frac{e^2}{mc}\sqrt{\frac{M}{2\pi RT}} \cdot \frac{f_{ih}}{k_{o_{ih}}} \qquad (4\text{-}45)$$

where the other quantities are as mentioned previously.

# CHAPTER V

## EXPERIMENTAL TECHNIQUES

In this project it is useful to consider some of the experimental techniques which yield the most favourable conditions for the acquisition of experimental results. The availability of modern equipment and facilities in our laboratory has led to several improvements over the only other experiment using this technique (Mc 69), thus resulting in more reliable A-values for forbidden lines. Some of these techniques are discussed in this chapter.

### 5.1 Techniques in the Production of Forbidden Lines

From the various theories described in the previous chapter on the excitation and depopulation of the metastable states in the $np^4$ elements we could infer that, to produce the forbidden lines (which represent the transition between those metastable states) in the laboratory, we would have to resort to special techniques, some of which are described as follows:

(a) Method of Excitation

An ordinary AC circuit, which characteristically transmits at high voltages and low currents (thus with a

small power loss $I^2R$), was found to be the most appropriate for the excitation of forbidden lines that were practically free from blending by molecular bands (Ke 69). However, the circuit employed had to be properly arranged. For instance, for a particular discharge it was necessary to choose the ballast resistance carefully so that a steady source of forbidden lines was maintained. Otherwise, either the "striking" potential would not be attained or a fluctuating, non-uniform discharge would be produced. The circuit diagram is illustrated in Fig. 5-1.

In general, after the striking potential was reached, the current or voltage range maintained in the discharge would depend on the nature of the element that was being investigated. For an element that exists naturally in a gaseous state, such as oxygen, an AC current of about 90 mA (with five 1 kΩ, 50 watt resistors connected in series) was found to be appropriate, and for an element that had to be vaporized, such as sulphur or selenium, a current of about 8 mA or less (obtained by arranging two sets of resistors in series, each set being made up of three 250 kΩ, 50 watt resistors in parallel) would be most suitable. In any case, it was important that a low current be used for the vaporized elements, since at higher currents the vaporization produced from the correspondingly higher temperature would be of such an extent that (1) the vapour

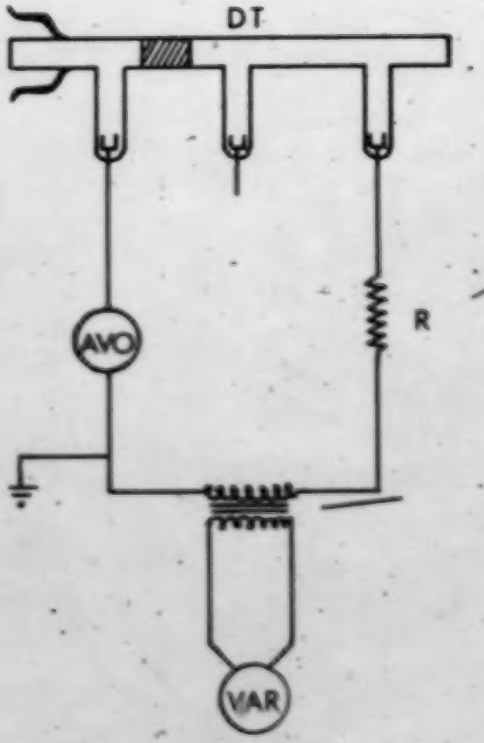


Ballast Resistance R

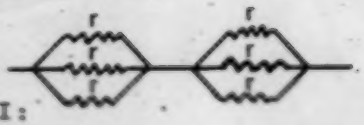


For SI & SeI:

r = 250 KΩ-50 Watts

For OI:

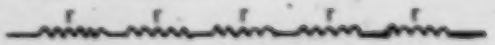


r = 1 KΩ-50 Watts

Transformers

For SI & SeI: $I_{max}$ = 60 mA

For OI: $I_{max}$ = 120 mA

Fig. 5-1. The AC circuit diagram used for exciting forbidden lines of the $np^4$ elements.

would readily reach and smear the LiF window of the discharge tube, (2) molecular excitation would prevail, as there would then be a high molecular concentration of the vaporized element.

Another important aspect related to the excitation of the non-gaseous elements was the means by which these elements were obtained in a vaporized form. To achieve this, the discharge tube, which already had deposited on its interior wall the distilled-in element, was heated from outside by means of a Nichrome resistance wire that was coiled around the discharge tube and electrically supplied through a Variac. The latter was set to a certain voltage until the temperature of the discharge tube had reached a steady level. After this stage the discharge between the electrodes of the tube was started; and if an "optimum"[†] discharge was still not obtained, the voltage supply across the electrodes would be switched off and that across the heating coil increased, until a steady temperature was reached again. This process was repeated until an optimum discharge was obtained. A graph relating the temperature on the outside of the discharge tube wall to the time and voltage supplied to a 225 cm length of heating coil is shown in Fig. 5-2.

---

[†]The "optimum" discharge is as defined in part (b) of this section.

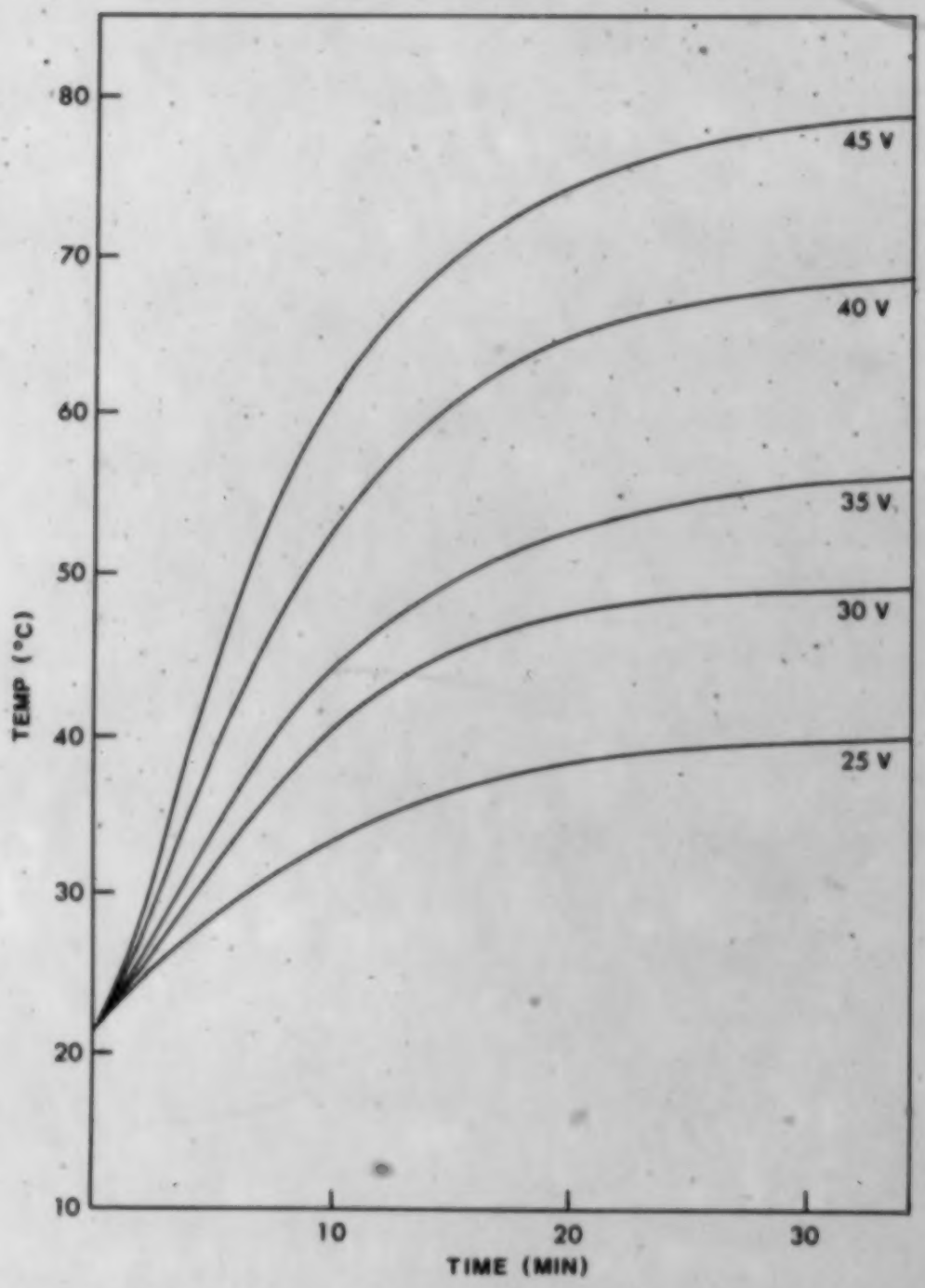


Fig. 5-2. Temperature-time curves on the external wall of the discharge tube. (The nichrome heating wire through which the different voltages were supplied was 2.25 m long.)

(b) Obtaining the Optimum Discharge

In the context of this work the "optimum" discharge represents a discharge (1) from which a relatively strong source of forbidden lines could be observed free from blending by impurity lines, and (2) which satisfied all the conditions on which the theories described in Chapter IV were based. Such a discharge should always possess a uniform, diffused appearance.

The inhibiting effect which some impurities had on the production of forbidden lines was one of the most important factors thatwere considered during the procedure aimed at obtaining the optimum discharge. Impurities, usually due to traces of hydrocarbon introduced by the vacuum grease applied to the glass stopcocks and by the roughing pump oil, and to mercury vapour excited by the electrical discharge, would interfere with the normal dissociation process of the sample molecules or collide with the sample or buffer gas atoms. In the case of collisions with the buffer gas the impurities would compete with the sample gas and vice versa. Thus transferred energy that was normally used for the excitation of the metastable sample atoms would instead excite the impurity atoms or molecules; the lines of interest, if still formed, would then be much reduced in intensity or would probably be blended by lines or bands from the impurity

spectra. Blending would, in turn, affect the resolution of the lines of interest, and yield inaccuracy in their intensity measurements.

However, the impurities could be systematically eliminated as follows:

The discharge tube, which has a section cooled by liquid air, was first of all evacuated to the lowest possible pressure. It was then filled up with about 25 torr of pure helium and run at a high current density (≃ 90 mA) for about one hour. The helium content was then flushed out of the tube and the whole system was then brought to a RF eddy-current heater. There, the tantalum electrodes were outgassed by heating them to red-hot temperatures with a RF induction coil. After having outgassed the electrodes, the tube was again filled up with helium mixed with a little oxygen, run at a high current density for another hour or so and flushed out. The process - filling, burning and flushing with helium - was repeated until the helium discharge showed the salmon color characteristic to pure helium, which was indicative of a clean discharge.

It should be noted that mere burning with a helium-oxygen mixture of high current density was insufficient to produce a clean discharge; cleaning the electrodes by RF induction heating must be undertaken as well.

Fig. 5-3 shows spectral scans of some selenium lines in the vacuum ultraviolet region from (a) a contaminated and (b) a clean discharge. In Fig. 5-3a the Se lines λ1994 Å and λ2063 Å are blended by CO bands whereas in Fig. 5-3b these lines appear sharp and free from blending.

Among the other conditions that an optimum discharge must satisfy were (1) equation (4-25), i.e. $(t + L)2\theta \leq D$ and (2) the homogeneity of the discharge medium; both of these conditions would not be satisfied if the discharge medium were "cored" at its centre. To obtain these conditions it was necessary to make delicate adjustments in the proportions and pressures of the gases used and in the current density or the ballast resistor of the AC circuit.

## 5.2 Temperature Measurement

A quantity that was to be measured for substitution into equation (4-45) was the (square root of the) Doppler temperature ($\sqrt{T}$) for the vacuum ultraviolet line that was feeding the upper level of the forbidden line of interest. This temperature was in fact that due to the average kinetic motion of the emitting atoms from the discharge medium. However, if there was a discrepancy of as high as ±50 degrees in the measurement of T (which, by interferometric measurement in a similar experiment (Mc 69),

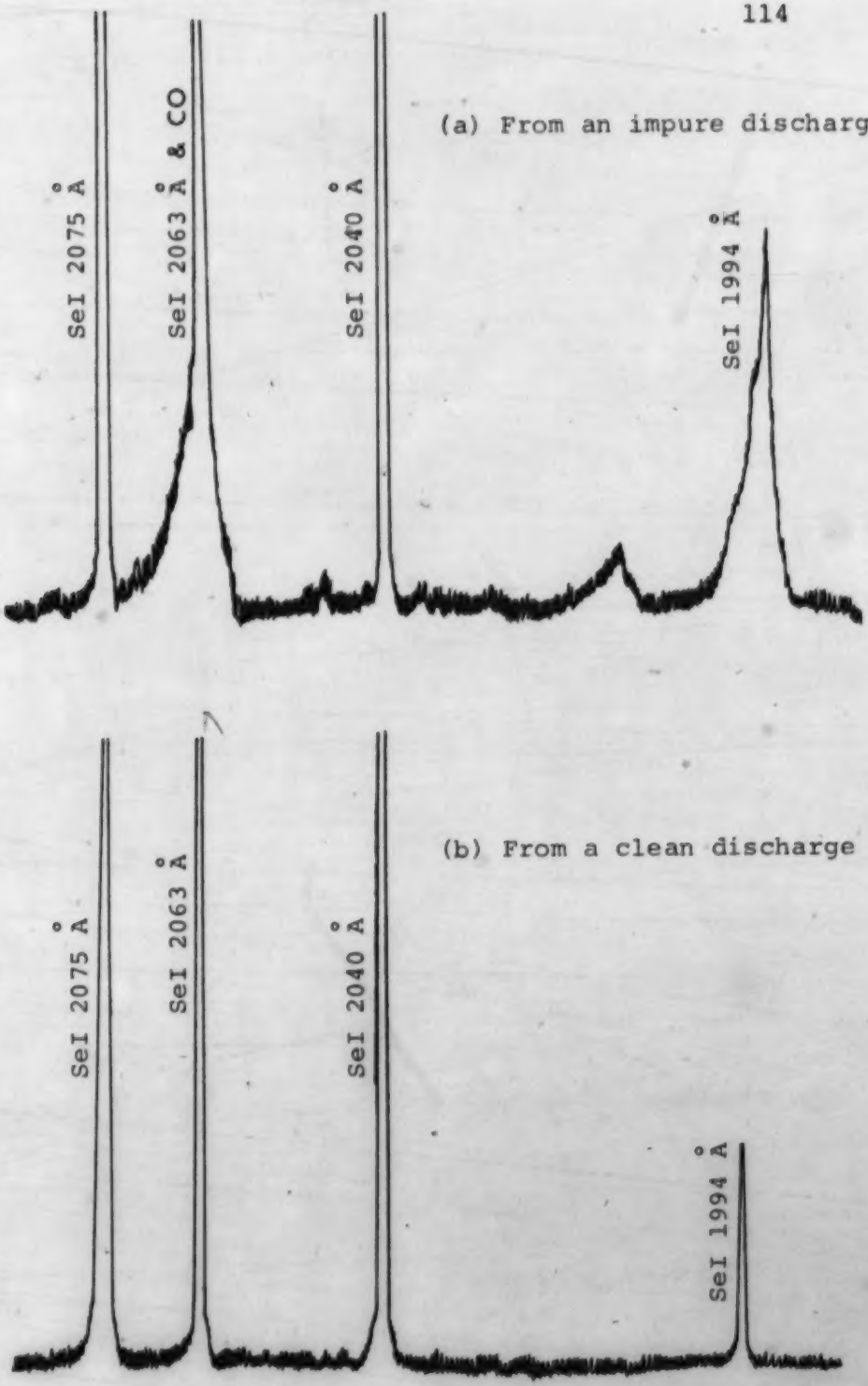


Fig. 5-3. Spectra of SeI from an impure and a clean discharge.
(a) SeI 1994 Å and SeI 2063 Å blended by CO.
(b) SeI 1994 Å and SeI 2063 Å.

yielded an approximate value of 500°K for a typical line in a similar discharge), the approximate percentage error involved would then be

$$\Delta(\sqrt{T}) = \left[\frac{\sqrt{500} - \sqrt{450}}{\sqrt{500}} \times 100\right] = \pm 5\%$$

In the present work, the temperature T was measured by means of a 0-360°C mercury thermometer that was lodged in a horizontal outlet from the side of the discharge tube. The thermometer bulb could be gradually slid into the discharge region by means of a magnet which acted on a small metal slug fitted to the top of the thermometer. For each optimum discharge used, several temperature measurements were taken, each being from a particular radial position inside the discharge and the average value of T determined. It was found that the maximum difference between the temperatures taken at two extreme radial positions, for the pressure range employed, was always much less than the upper limit of ±50 degrees set in the above example, so that the mean deviation in the temperature measurement was always < 5%.

In view of the fact that there was only a small temperature difference at the different radial position in the discharge, the previous assumption of an homogeneous discharge medium was taken as justified.

## 5.3 Photon-Counting Technique

Measurements of spectral line intensities could be performed either by a photographic or a photoelectric method.

In the photographic method the systematic errors involved from the equipment used and the accidental errors from observations could amount to a relatively large extent. These systematic errors could arise from such causes as the zero drift or sensitivity change in the measuring system, plate background due to chemical fog, stray light, reciprocity effects in the emulsion and faulty standards in the calibration patterns. On the other hand, accidental errors could arise from fluctuations in the light source, non-uniformity of emulsion thickness or sensitivity, temperature, solution concentration, processing techniques and uncertainity in the measuring scale. However, the photographic technique was undertaken in this project for (1) the preliminary identifications of the spectral lines of interest and (2) determining the reciprocal linear dispersion $d\lambda/dx$ of the grating in the Spex at the different wavelengths of interest.

In the photoelectric method, either an analog or a digital system could be used. In the analog system the output data were read out from a pen-chart recorder whereas in the digital system the output was read out from

a photon counter-timer.

The photon-counting technique has been employed advantageously in this work. For instance, the response in such a system was almost instantaneous, i.e. the actual quantities from the measured source were being read out - a fact that was very important especially when the measured source was not steady (e.g. the oxygen gradually burns out of the discharge over a period of several hours). This technique could also, among other things, yield a higher wavelength resolution - a fact borne out by comparing the photoelectric profiles obtained through the pen-chart and the photon-counter recordings (see Fig. 5-4).

(a) Preliminary Procedures

In the photon-counting technique, the preliminary procedures were undertaken systematically as follows:

First, the components of the spectrophotometric system - light sources, auxilliary optics and spectrometers - were aligned by means of a He-Ne laser so as to ascertain normal incidence of light on the spectrometer. Then after the photomultiplier voltage had stabilized, the lower window limit in the Ortec discriminator was adjusted until the dark current noise level recorded was around 5 to 10 counts/sec. The signal from the forbidden line of interest and through a particular spectrometer slit was next recorded,

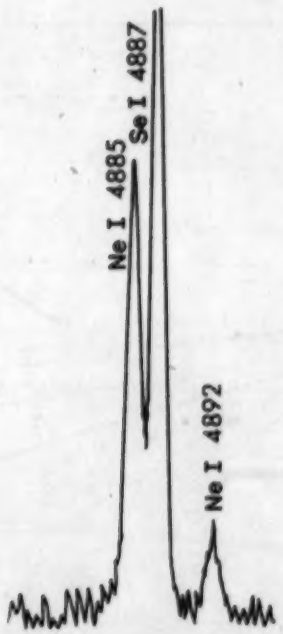


Fig. 5-4. Photoelectric profiles of NeI 4885Å and SeI 4887 Å:
(a) From chart-recording.
(b) From photon-counting.

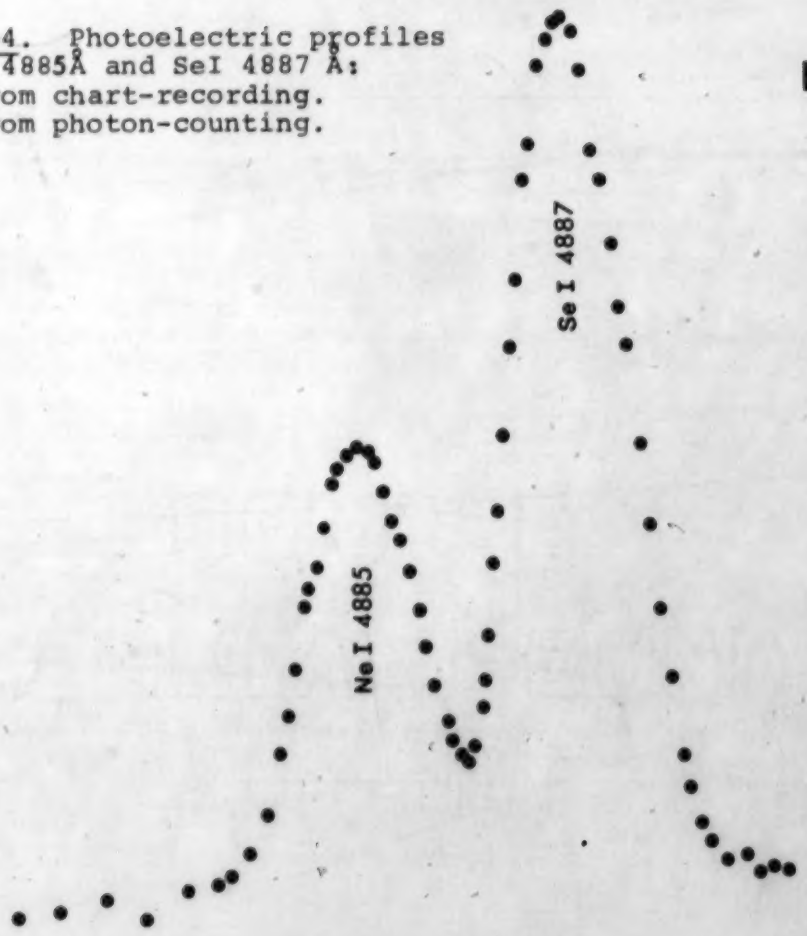

and the signal-to-noise ratio was determined. If that ratio was less than that recommended for the photomultiplier (usually around 10:1), the dark current would have to be reduced by cooling the photomultiplier in the refrigerated RFI chamber. In general, the data were each recorded repeatedly about ten times and were then averaged out. The statistical fluctuations in such data were usually within 0 to 5% - any abrupt fluctuation would indicate a major change in the discharge conditions and the corresponding data were discarded.

(b) Relative Intensity Measurements

The photon-counting technique was also employed in the measurement of relative line intensities. In such measurements the line profiles were first obtained by plotting the intensity values recorded through the same slit width at different positions from $(\lambda - d\lambda/2)$ to $(\lambda + d\lambda/2)$ where $(d\lambda/2)$ is the separation between the peak wavelength $\lambda$ and either of the line wing-ends (the positions of the line peak and wings were approximately located beforehand by the pen-chart recording). The different wavelength positions in the profile were made possible by driving the wavelength manually through steps of 0.1 to 0.3 Å on the Spex 1500 (for the McPherson - a stepping motor, that could automatically drive the wavelength at

uniform intervals, was available). The line peaks could then be read from the profiles and the ratio of the peak counts determined. As long as the same spectrophotometric components and slit width were used, the relative intensity ratio need not be corrected for reflectance, transmission on absorption characteristics. However, it must be corrected for (1) the second-order radiation, if present - eliminated by means of appropriate filters placed inside the spectrometer, and (2) the detector sensitivity response at the different wavelength regions involved - done by comparing the response from the standard lamp at those wavelengths. Fig. 5-5 illustrates the photon-counting profiles of the green auroral line OI 5577 Å and the transauroral line OI 2972 Å, whose relative intensity ratio is the same as that of their transition probability corrected for the wavelength difference.

(c) Simultaneous Photon-Counting

We have previously discussed in section 4.3 the importance of obtaining simultaneous measurements of the intensity I of a line and the population density N of its upper level, in the determination of the transition probability A. The photon-counting technique with its characteristic fast response in detecting and recording radiation was therefore utilized to advantage for this purpose.

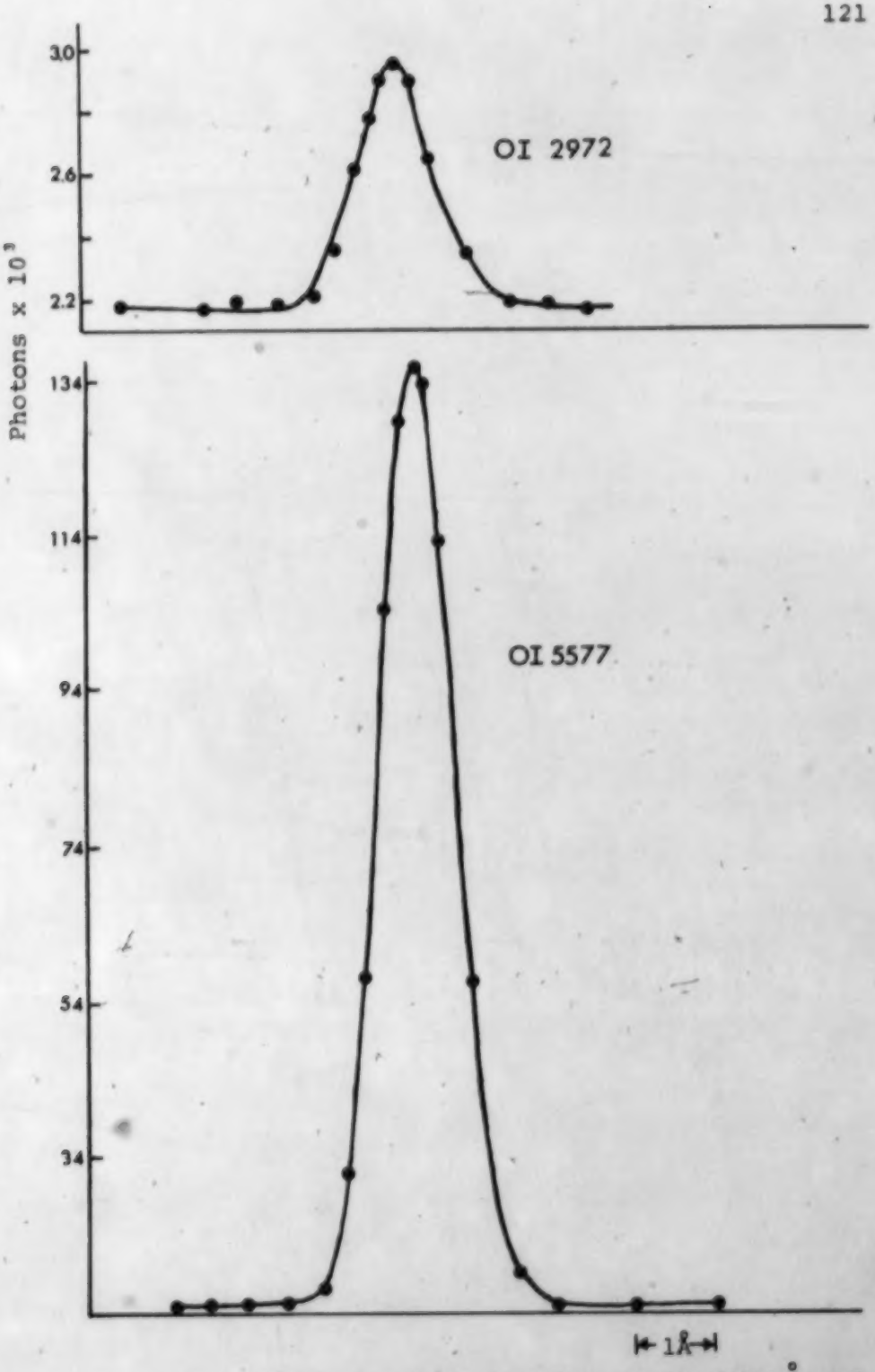


Fig. 5-5. Photoelectric profiles of OI 2972 Å and 5577 Å under the same discharge and slit conditions.

The electronics and optical set up for simultaneous photon-counting were illustrated in Figs. 3-4 and 3-1a respectively. Measuring N was shown in the theoretical discussion to be "equivalent" to measuring the intensity ratio $I_L/I_\ell$ of a vacuum ultraviolet line cascading into that level, where L and $\ell$ were the different lengths of the discharge column viewed end-on. Actually, during the experiment, $I_L$ (the intensity from a discharge length L viewed end-on) and I (the intensity from an area A viewed side-on) were first measured simultaneously for a certain optimum discharge at a particular current and voltage; then, under the same current, $I_\ell$ (the intensity from a discharge length $\ell$ viewed end-on) and I (the intensity from the same area viewed side-on) were measured simultaneously. However, when the pressure in the discharge tube was relatively too low, the voltage across the discharge length $\ell$ might not be the same as that across L, although the current through either of those lengths were equal. Thus, the second value of I might be different from the first one. If that were the case the value of $I_\ell$ must then be normalised to what it would have been had the second value of I been unaltered, i.e. $I_\ell$ must then be multiplied by the ratio: first value of I divided by second value of I. This normalisation was necessary (in some cases) because the intensity I

and the metastable population N measured from a constant discharge volume, viewed side-on and assumed to be under the same conditions of excitation, should be equal. In this way, the true extent of self-absorption through the lengths L and ℓ of the discharge, when measured from end-on ($I_L$ and I ), were being compared, as they would have been under simultaneous observation. However, as may be noted here, this normalisation made possible by the simultaneous photon-counting procedure was only valid if the line with side-on intensity I and the other line with end-on intensity $I_L$ or $I_\ell$ had the common level whose density N was being measured.

(d) Wavelength Resolution

A frequent spectrophotometric problem involved in this work was that of resolving the line of interest adequately enough for an accurate measurement of its intensity. To improve the resolution the slits were narrowed; but when the slit widths were reduced, the incident radiation on the detector was also reduced in proportion to the square of the slit opening, resulting in a lower signal-to-noise ratio. To compensate for this loss in signal power the gain in the system was increased which, in turn, raised the noise level proportionately. A longer counting time (or photomultiplier-cooling) was

then required to maintain photometric accuracy.

However, even under optimum resolution, the line of interest could be found to overlap the wing of a neighbouring line or band, as illustrated by the sulphur line λ1782 Å and the CO band λ1776 Å in Fig. 5-6.

When the wavelength drive was at the position P in this figure, the intensity measured through the spectrometer slit would be that due to the sum of the peak intensity of SI 1782 Å and part of the CO 1776 Å band that was overlapped in that waveband. To deduce the contribution from the CO band, a computer technique using the Lagrangian interpolation method, was applied. In this method, several points at uniformly spaced intervals on the slope AB of the CO band were first obtained by photon-counting while the wavelength of the spectrometer was being driven by a stepping motor or manually. A best-fit polynomial function was then computed and the point 0 on the slope AB, i.e. the intensity-value contributed by the CO band at that position, was interpolated. The true peak intensity of SI 1782 Å was thus obtained by subtraction.

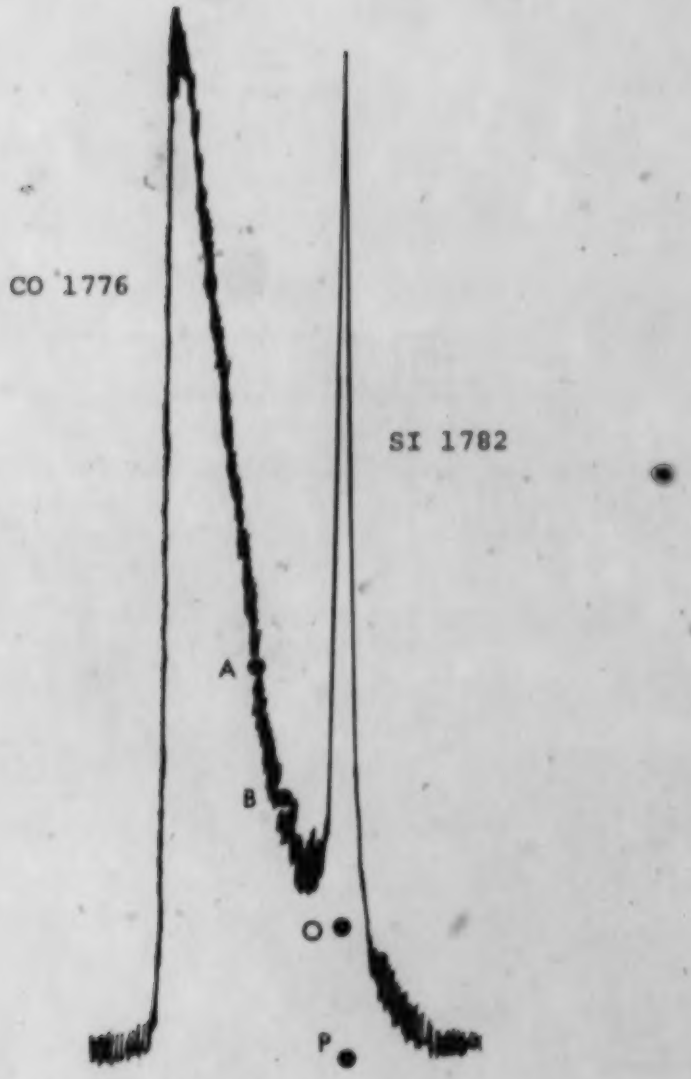


Fig. 5-6. The pen-chart profiles of SI 1782 Å and CO 1776 Å from an optimum krypton-sulphur discharge mixture. The intensity contribution from the CO band at the point O was computed by using the Lagrange Interpolation Method.

## 5.4 Geometrical Limitations

Unlike the case for allowed lines, forbidden A-coefficients cannot be measured by the beam-foil technique since the mean lifetime of a metastable level is about $10^8$ times that of a level in the allowed case; atoms would have to travel in a tube $10^8$ cm (i.e. 1000 km) before showing a decreasing intensity of light! On the other hand, time-resolution and other problems associated with the beam-foil technique need not be taken into account here. Nevertheless, the paths followed by the forbidden radiation in this experiment were under certain geometrical limitations which are described as follows: since the solid angle subtended by the Spex slit area on every point of the observed source was included in the absolute intensity calculation, then, during the intensity measurements, not only should the slit be completely illuminated over its surface area, but all the light passing through it must also be recorded. To verify this, let us consider the illumination condition illustrated in Fig. 5-7, which shows the Spex collimator mirror (a) in section and (b) in elevation. Of the light which entered the spectrometer through the slit, only that part intercepted by the collimating mirror would reflect into the plane grating and the camera mirror (not shown in Fig. 5-7). Any light beams which were outside the cone whose base was

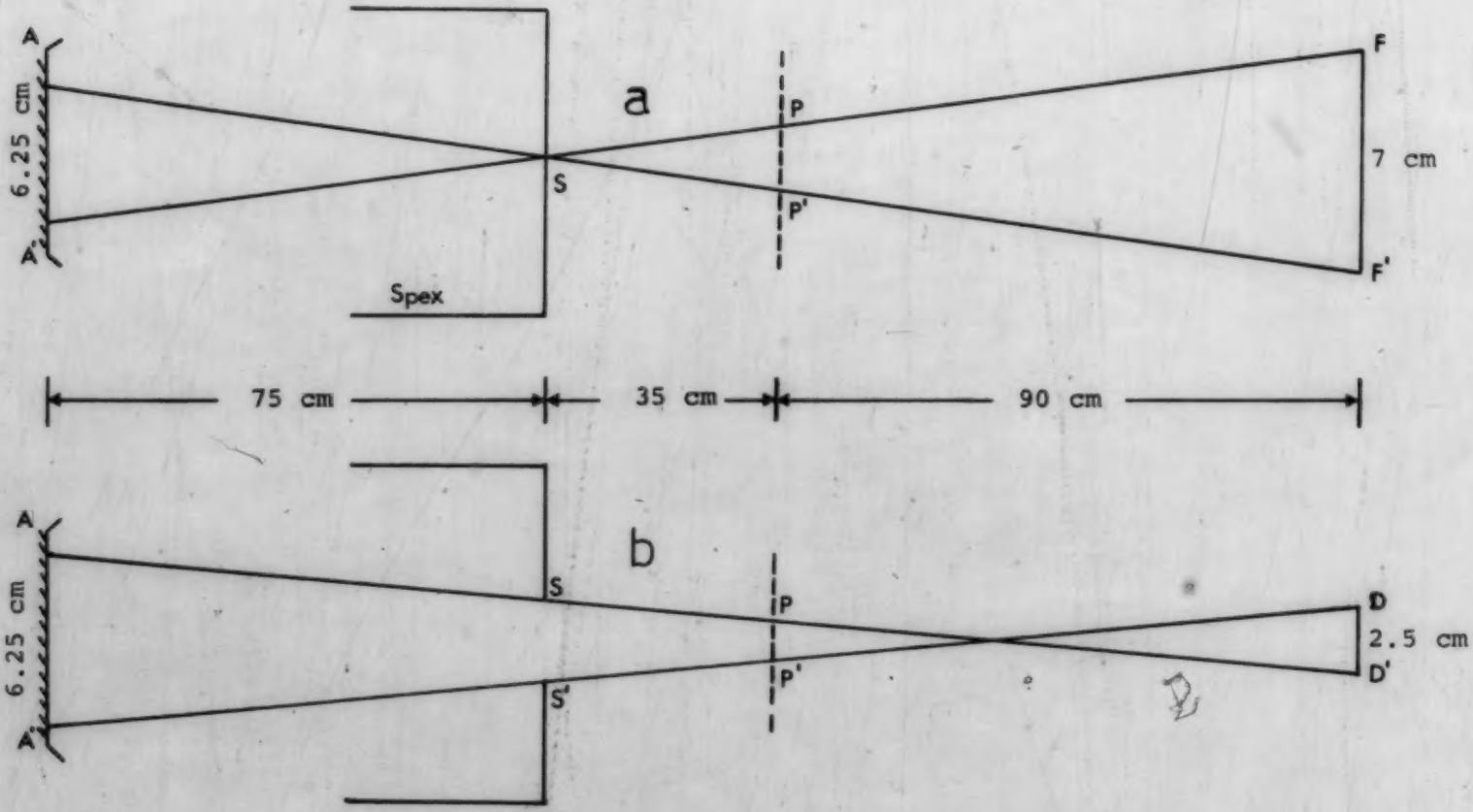


Fig. 5-7. Illumination of the collimator by a cylindrical discharge through a rectangular slit in (a) section and (b) elevation.
AA': collimator aperture; S: slit; PP': plane mirror; FF', DD': horizontal and vertical section of discharge viewed side-on, respectively.

the collimator mirror aperture AA' would not be recorded.

In case (a), the slit (≈ 100 μ) was narrow in comparison with the collimator aperture (≈ 6.25 cm) or the discharge width (≈ 7 cm); the slit width was therefore neglected. The projected aperture on the collimator from the discharge source could then be shown to be about 4.2 cm. i.e. smaller than the collimator aperture AA'. Thus, no loss of light would occur in case (a).

In the vertical case (b) it should be again ascertained that the projected aperture on the collimator was less than AA'. By applying the theorem on the geometrically similar triangles involved, the following results were obtained:

| Slit Height SS' in cm | Projected Aperture on the Plane Mirror PP'in cm | Projected Aperture on the collimating mirror CC' in cm |
|---|---|---|
| 2.5 | 2.50 | 5.0 |
| 3.0 | 2.86 | 6.0 |
| 4.0 | 3.58 | 8.0 |
| 4.5 | 3.94 | 9.0 |
| 5.0 | 4.30 | 10.0 |

Table V-1. Geometrical limitations for the "Spex" system.

A slit height of 2.5 cm and an auxilliary plane mirror which was larger than 2.5 cm were used so as to ensure that all the light from the observed source were indeed collected.

The geometrical limitations described above were

also applied to the illumination conditions through the McPherson slit. However, here it was not only necessary to ascertain that all the light coming end-on from the discharge and through the slit was recorded, but that the condition satisfying equation (4-25) was also taken into account. With the collimator (i.e. the concave grating) masked to 5.5 cm in width, a slit height of 2 mm and a slit width of 50 microns were then found appropriate in satisfying these requirements.

# CHAPTER VI

## RESULTS AND DISCUSSION

### 6.1 General Remarks:

To date the status of our knowledge of allowed or forbidden transition probabilities is considered as being far from ideal. The only transition probabilities known with a high degree of accuracy are those available for allowed lines of hydrogen and hydrogen-like ions and for some helium lines. Even for the allowed A-coefficient the measurement techniques are quite complicated and laborious, and it has proved to be very difficult to obtain accuracies of 10 percent or better.

Most of the allowed A- and f-values have been obtained from measurements of the intensities of spectral lines which are emitted from a source under known conditions. The sources are usually high-current stabilized arcs and, to a lesser extent, shock-tubes. Many uncertainties are involved in these methods, the main ones being from the condition of local thermal equilibrium (LTE) in the light source, which should be satisfied in the determination of the state population, and from the demixing effect of the arc. There exists also in these methods the usual discrepancies caused by the calibration of stan-

dard light sources, the intensity contributions in the line wings and self-absorption. Errors of 20 to 50 percent are not unexpected from these experiments.

The A-value of some allowed lines may also be derived by a direct measurement of the lifetime of its upper state. Lifetime measurements involve the delayed coincidence and phase shift techniques, the Hanle effect and the beam-foil technique. The sources of error are fewer in these methods, the main ones being attributed to radiative cascading, and insufficient spectral resolution for the detection of the radiation. Radiation trapping and collisional depopulation of a level may also introduce some discrepancies. Errors involved in these experiments can be much lower than those of the line emission experiments.

As for forbidden lines, which are generally not easy to produce in the laboratory, previous experimental work on them dealt mainly with techniques for their production and their wavelength measurements. Thus, the energy levels of ground states $^1S_0$, $^1D_2$ and $P_{0,1,2}$ for the first three $np^4$ elements (Oxygen I, Sulphur I and Selenium I) and consequently the wavelengths of the corresponding forbidden lines are well established; the most recent data obtained by Eriksson for OI (Er 65), SI (Er 72) and SeI (Er 73) could be singled out, although

several previous data were also obtained - (Mc 27, Ve 34 and Ca 56) for OI, (To 60 and Mc 68) for SI and (Ru 34) for SeI. However, to date one of the most important characteristics of these forbidden lines - their absolute transition probability - has received little experimental attention, although in some cases relative A-values have been measured (Mc 66, 68). In fact, until recently, the absolute A-value of the green auroral line [OI] 5577 Å has been the sole one measured (Mc 69). Corney and Williams (Co 72) measured the lifetime of the oxygen metastable (ground) state $2p^4\ {}^1S_0$ which, in turn, yields the sum of the A-values of [OI] 5577 Å and [OI] 2972 Å. Omholt also measured the lifetime of the metastable states $2p^4\ {}^1S_0$ and $2p^4\ {}^1D_2$ of oxygen from his experiments on the green and red auroral lines respectively. Yet, as mentioned at the introduction of this thesis, a knowledge of the absolute A-coefficients and the production mechanisms of forbidden lines are of much practical importance for certain studies in astrophysics, upper atmospheric and other aspects of atomic and molecular physics.

On the other hand, sophisticated theoretical calculations of forbidden A-coefficients, based on atomic structure, have been quite successful (for the lighter elements), but the theoretical methods have the shortcoming that they do not permit the estimates of the size of

the errors as do the experiments.

The aforementioned facts represent on the whole a great challenge for the experimentalists, which, it is hoped, has been at least partially answered. In this chapter, the data and analyses for each of the three $np^4$ elements studied and the final results derived are reported. (The block diagram for the overall experimental set-up is as shown in Fig. 3-1a.)

## OXYGEN RESULTS

### 6.2 The Spectra

The forbidden and allowed lines of atomic oxygen, that were investigated in this project, are illustrated in the simplified term scheme shown in Fig. 6-1. The procedures discussed in the previous chapter were applied to these lines accordingly; thus the A-value of OI 5577 Å was determined by measuring its absolute intensity and simultaneously carrying out the optical absorption experiment on an ultraviolet line which was feeding its upper level, in this case at λ1218 Å, to determine the $2p^4\ {}^1S_0$ population. Analogously, the A-value of the forbidden OI line at 6300 Å was obtained by applying the absorption method on the OI ultraviolet line at 1152 Å. Here the OI lines at λλ936 and 999 Å, which are strong and end on the $2p^4\ {}^1D_2$

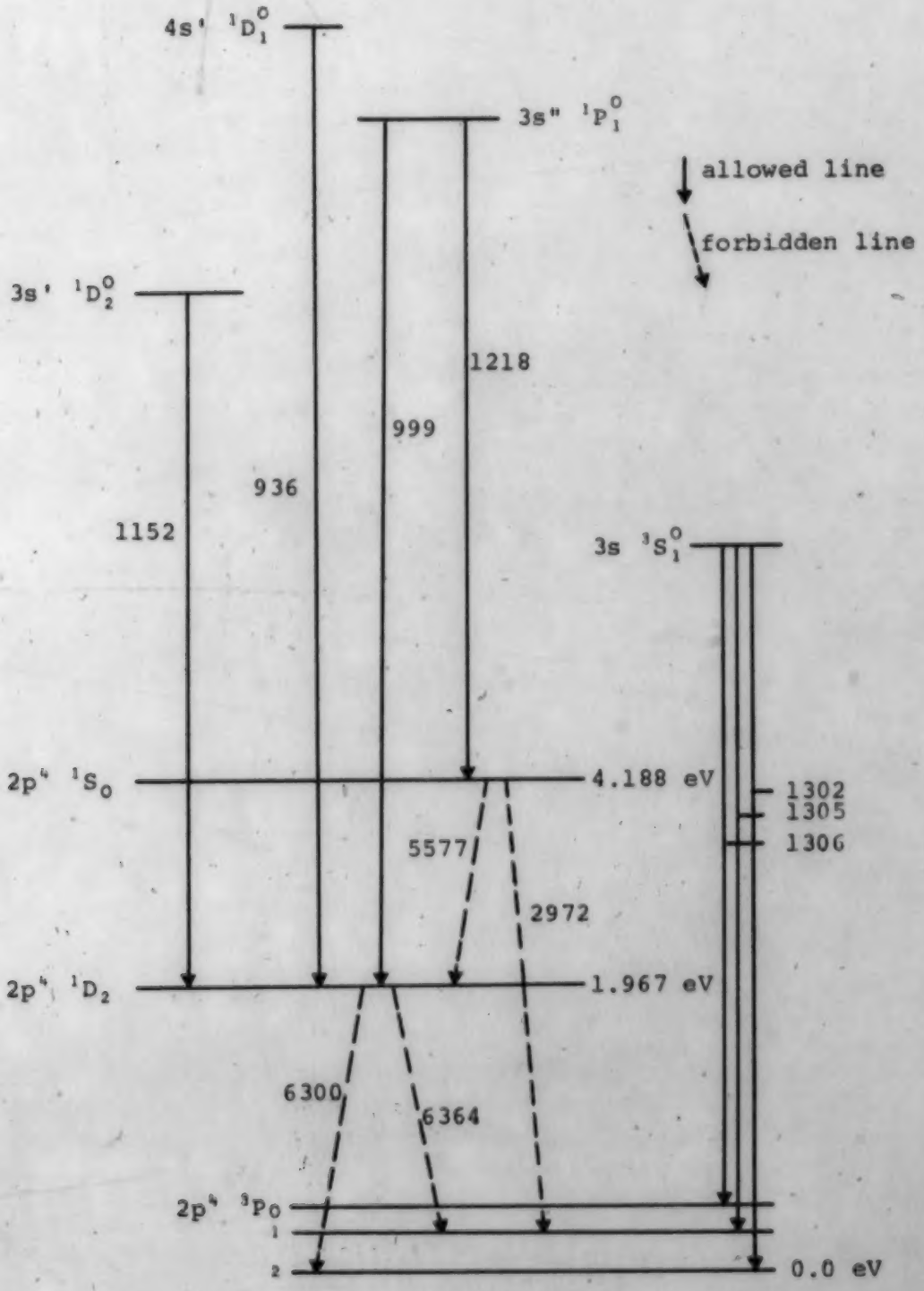


Fig. 6-1. Partial term scheme of OI (not to scale).

level have not been employed because the LiF window on the discharge tube cuts off at 1050 Å. The absorption experiment was also carried out on the OI resonance lines at λλ1302, 1305 and 1306 Å to determine the atomic densities of the $2p^4\ ^3P_{0,1,2}$ states respectively. As for the forbidden OI lines at λλ2972 and 6364 Å, their A-values were obtained by simply measuring their intensities relative to those at λλ5577 and OI 6300 Å respectively, since these pairs of lines have common upper (parent) levels $2p^4\ ^1S_0$ and $2p^4\ ^1D_2$ respectively.

## 6.3 Results and Analysis on the Forbidden OI Lines at λλ5577 Å and 2972 Å

### (a) Laboratory Production of [OI] 5577 Å

This forbidden line was first of all obtained steadily to an extent that was photoelectrically measurable when viewed side-on from a particular discharge volume and situated at about 80 cm away from the spectrometer slit. To achieve it, all the procedural steps which were described in section 5.1 on the "Techniques in the Production of Forbidden Lines" were followed rigorously. The green forbidden line of oxygen was, in fact, readily produced over a fairly large range of pressures and/or currents.

Using a discharge tube whose dimensions were as specified in Fig. 3-2, a current of 90 mA and a correspond-

ing voltage of about 6000 volts were used throughout all the experiments in the excitation of the green forbidden line. The pressure ranges used in the mixture were 0.020 torr to 0.100 torr for oxygen and 15 to 25 torr for helium.

An upper limit of 0.100 torr on the partial pressure of oxygen and a lower limit of 15 torr on that of helium were chosen because outside these limits the discharge became cored, whereby the intensities of the forbidden line viewed side-on and the ultraviolet line viewed end-on would be affected - a result which is in agreement to previous experiments (Ke 68) made on the intensity measurements of the ultraviolet OI lines at λλ1152, 1218 and 1302,4,6 Å; in a similar type of discharge these lines were found to peak in intensity when the partial pressure of oxygen used was 0.100 torr. Fig. 6-2a shows the spectral scan of the region around the green auroral line from a clean, "cored" discharge with 3 torr of oxygen and 25 torr of helium at 90 mA.

On the other hand, a lower limit of 0.020 torr on the partial pressure of oxygen and an upper limit of 25 torr on that of helium were chosen because beyond these limits molecular bands of oxygen and carbon monoxide were formed, which partially masked the green auroral line, as shown in Fig. 6-2b. Thus, when the ratio of the partial

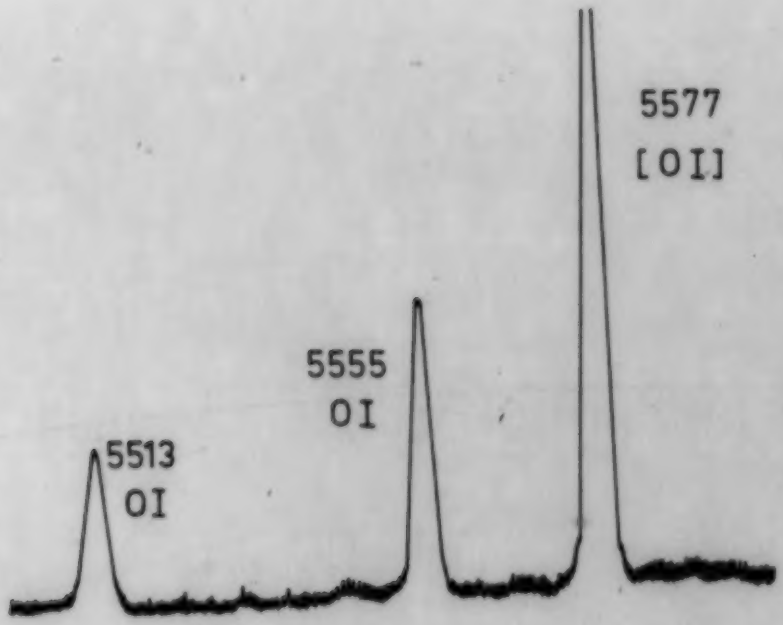


Fig. 6-2a. The green auroral line in a clean "cored" discharge containing 3 torr of oxygen and 25 torr of helium at 90 mA.

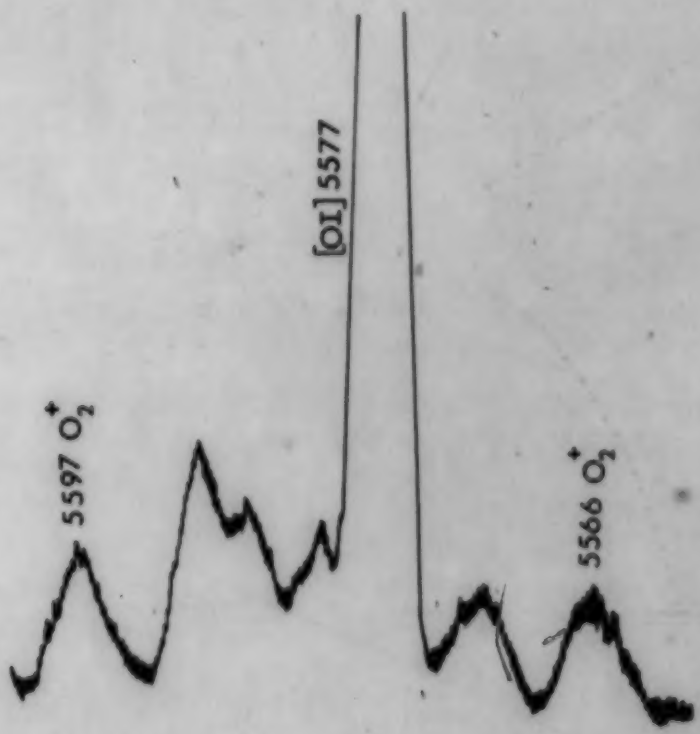


Fig. 6-2b. The green line blended by molecular bands in a discharge containing 0.01 torr of oxygen and 20 torr of helium at 90 mA.

pressure of helium to that of oxygen is > 250:1, the oxygen and impurity molecules would compete with the metastable $^1S$ oxygen atoms for excitation by energetic electrons. However, this degree of excitation was found to be less for the molecules than for the metastable $^1S$ atoms because, when the current through the discharge was decreased from 90 to 60 mA, the intensity of the green auroral line was found to diminish by a larger factor (> 2) than that (≈ 1.5) of the $O_2^+$ band λ5577 Å.

(b) Atomic Processes Involved in the Production of the Metastable $O(^1S)$ Atoms

Due to the fact that the chemical composition of the upper atmosphere can alter significantly or even radically by a number of processes such as photochemical reactions, recombination processes, mixing, diffusion and intrusion of extraterrestrial particles, research efforts in these areas have increased and considerable advances have since been made in our knowledge of the various properties of the upper atmosphere. Laboratory experiments on the chemical processes such as the dissociation and ionization of $O_2$, $N_2$ and NO and the corresponding theoretical calculations, pioneered by Chapman (Ch 30), have been invaluable in the pursuit of such knowledge.

(i) Previous Work

So far, no standard methodology exists in the investigation of the chemical processes that are assumed to be taking place in the production of the metastable $O(^1S)$ atoms and the corresponding forbidden lines [OI] 5577 Å and [OI] 2972 Å. However, the analysis used by Watadani (Wa 72) and Emeleus (Em 39) on the laboratory emission of OI 5577 Å are worthy of mention. Watadani claimed that the following processes took place in the production of the green line:

At first, ground state xenon atoms, $Xe(^1S_0)$, were excited by collisions with electrons:

$$Xe(^1S) + e(v') \rightarrow Xe'' + e(v'') \qquad (6\text{-}1)$$

The excited state Xe" would, in turn, excite ground state $O_2(X\ ^3\Sigma_g^-)$:

$$Xe'' + O_2(X\ ^3\Sigma_g^-) \rightarrow Xe' + O_2'(a\ ^1\Delta_g) \qquad (6\text{-}2)$$

where $Xe'' > Xe' > Xe^*(^3P_2) \equiv$ Xe metastable state (=8.31 eV). Then the excited molecular state $O_2'(a\ ^1\Delta_g)$, shown in Fig. 6-3, would take up the energy transferred from metastable Xe atoms (already present) for its dissociation:

$$Xe^*(^3P_2) + O_2(a\ ^1\Delta_g) \rightarrow Xe(^1S) + O(^3P) + O(^1S) \qquad (6\text{-}3)$$

8.31 eV + 0.97 eV  0.0 eV + 0.0 eV + 4.19 eV + D.E. (=5.12 eV)

Finally, $O(^1S) \rightarrow O(^1D) + h\nu$ ($\lambda$5577 Å) (6-4a)

$O(^1S) \rightarrow O(^3P) + h\nu$ ($\lambda$2972 Å) (6-4b)

With the dissociation energy (D.E.) of $O_2$ being 5.12 eV, equation (6-3) is thus satisfied energetically, i.e. quantal resonance exists here. However, Watadani did not point out two violations in this equation, which are the following: (1) $O(^1\Delta_g)$, being a singlet, cannot be formed by the combination of a singlet and a triplet ($^1S + {}^3P$), the Wigner-Witmer spin-conservation rule (section 4.1) disallows this. (2) S and P states can combine to yield at most a $\Sigma$ or a $\Pi$ molecular state but not a $\Delta$ state.

As for the mechanism put forward by Emeleus, it is as follows, in the case where argon was used as the buffer gas:

Metastable argon atoms, first of all, transferred energy to the ground state $O_2(X\ {}^3\Sigma_g^-)$:

$$Ar^*(^3P_2) + O_2(X\ {}^3\Sigma_g^-) \rightarrow Ar(^1S) + O_2'(?) \qquad (6\text{-}5)$$

$$=11.55 \text{ eV} \qquad 0 \text{ eV} \qquad 0 \text{ eV} \qquad \text{excited unknown}$$

The unknown excited molecular state $O_2'(?)$ would then dissociate spontaneously as follows:

$O_2'(?) \rightarrow O(^1S) + O(^3P) + 2.2$ eV (6-6a)

$O_2'(?) \rightarrow O(^1S) + O(^1D) + 0.3$ eV (6-6b)

And through spontaneous radiation,

$$O(^1S) \rightarrow O(^1D) + h\nu\ (\lambda 5577\ \text{Å}) \qquad (6\text{-}7a)$$

$$O(^1S) \rightarrow O(^3P) + h\nu\ (\lambda 2972\ \text{Å}) \qquad (6\text{-}7b)$$

Then Emeleus claimed that the choice of the excited state $O_2(?)$ must be such that, energetically,

$$9.30\ \text{eV} < O_2'(?) < Ar^*(^3P_2) \qquad (6\text{-}8)$$

However, it can be noted here that for quantal resonance in equation (6-5) and as implied in equations (6-6a & b), the energy of $O_2'(?)$ must be 11.55 eV, which contradicts equation (6-8). So again here, as in Watadani's procedure, there are some doubts cast on whether the correct production mechanisms of the green forbidden line have been put forward.

(ii) Present Proposition for the Production Mechanism of $O(^1S)$ Atoms and the Corresponding Forbidden Lines

For the present case, in which helium was used as the buffer gas, the proposed mechanism is as follows:

First of all ground state helium atoms, $He(^1S)$, were excited by some energetic electrons:

$$He(^1S) + e(v') \rightarrow He'' + e(v'') \qquad (6\text{-}9)$$

The excited He" would then excite the ground state oxygen molecule:

$$He'' + O_2(X\ ^3\Sigma_g^-) \rightarrow He' + O_2'(x?) \qquad (6\text{-}10)$$

where He" > He' > He*($^3S_1$) ≡ metastable state (= 19.81 eV)
Then, through spontaneous radiation,

$$He' \rightarrow He^*(^3S_1) + h\nu \text{ (He lines)} \qquad (6\text{-}11)$$

and, through photodissociation,

$$O_2'(x?) + h\nu \rightarrow O(^1S) + O(^3P) + K.E. \qquad (6\text{-}12a)$$
$$\rightarrow O(^1S) + O(^1D) + K.E. \qquad (6\text{-}12b)$$

Thus, from equations (6-12a) and (6-12b), it can be deduced that the potential curve(s) of the unknown molecular state(s) $O_2'(x)$ would have an asymptotic level (dissociation limit) at 9.30 eV for ($^1S + {}^3P$) or 11.27 eV for ($^1S + {}^1D$).

To find the unknown state(s) x' whose dissociation products are ($^1S + {}^1D$), the Wigner-Witmer and the ordinary Selection rules were first considered. After such considerations it was found that only the transitions to the $^1\Delta_u$ and $^1\Pi_u$ would be allowed from the a $^1\Delta_u$ ground state. In fact, in 1968, Alberti et al. (Al 68) identified the ($^1\Pi_u$ - a $^1\Delta_u$) and the ($^1\Delta_u$ - a $^1\Delta_u$) transitions, with strong band heads at 1229 Å (≃ 11.06 eV) and 1243.8 Å (≃ 10.89 eV) respectively, both lying energetically very near and above the dissociation limit (11.27 eV) for ($^1S + {}^1D$). The energy difference is only 0.77 eV for the continuum maximum at λ1229 Å and 0.60 eV for that at 1244 Å. Both upper states ($^1\Delta_u$ and $^1\Pi_u$) were also found to be

perturbed, i.e. unstable. From the aforementioned facts and applying Franck-Condon principle[†] (Ga 68), it can be seen that the potential curves of these two states would each have a shallow minimum which is asymptotic at 11.27 eV ($^1S + {}^1D$). These states ($^1\Delta_u$ and $^1\Pi_u$) are illustrated at the top of Fig. 6-3. Equation (6-12b) can then be filled up as follows:

Through photodissociation of the unstable states $^1\Delta_u$ and $^1\Pi_u$,

$$O_2'(^1\Delta_u) + h\nu \rightarrow O(^1S) + O(^1D) + K.E. \qquad (6\text{-}13a)$$

$$O_2'(^1\Pi_u) + h\nu \rightarrow O(^1S) + O(^1D) + K.E. \qquad (6\text{-}13b)$$

Now, to find the unknown state(s) whose dissociation products are ($^1S + {}^3P$), the Wigner-Witmer and the ordinary Selection rules should again be considered. After such considerations, it was found that only the transition to the $^3\Pi_u$ would be allowed from the $^3\Sigma_g^-$ ground state. In fact, Tanaka (Ta 52) identified three distinct continuum maxima in the absorption bands of $O_2$ in the far ultraviolet at $\lambda$1290 Å, $\lambda$1334 Å and $\lambda$1349 Å. Of these three absorption maxima the longest one (1349 Å ≈ 9.19 eV) lay situated

---

[†]According to the Franck-Condon principle, the most probable transition is that going up vertically from the minimum of the lower potential curve (here for a $^1\Delta_u$ the minimum is at r = 1.2 Å).

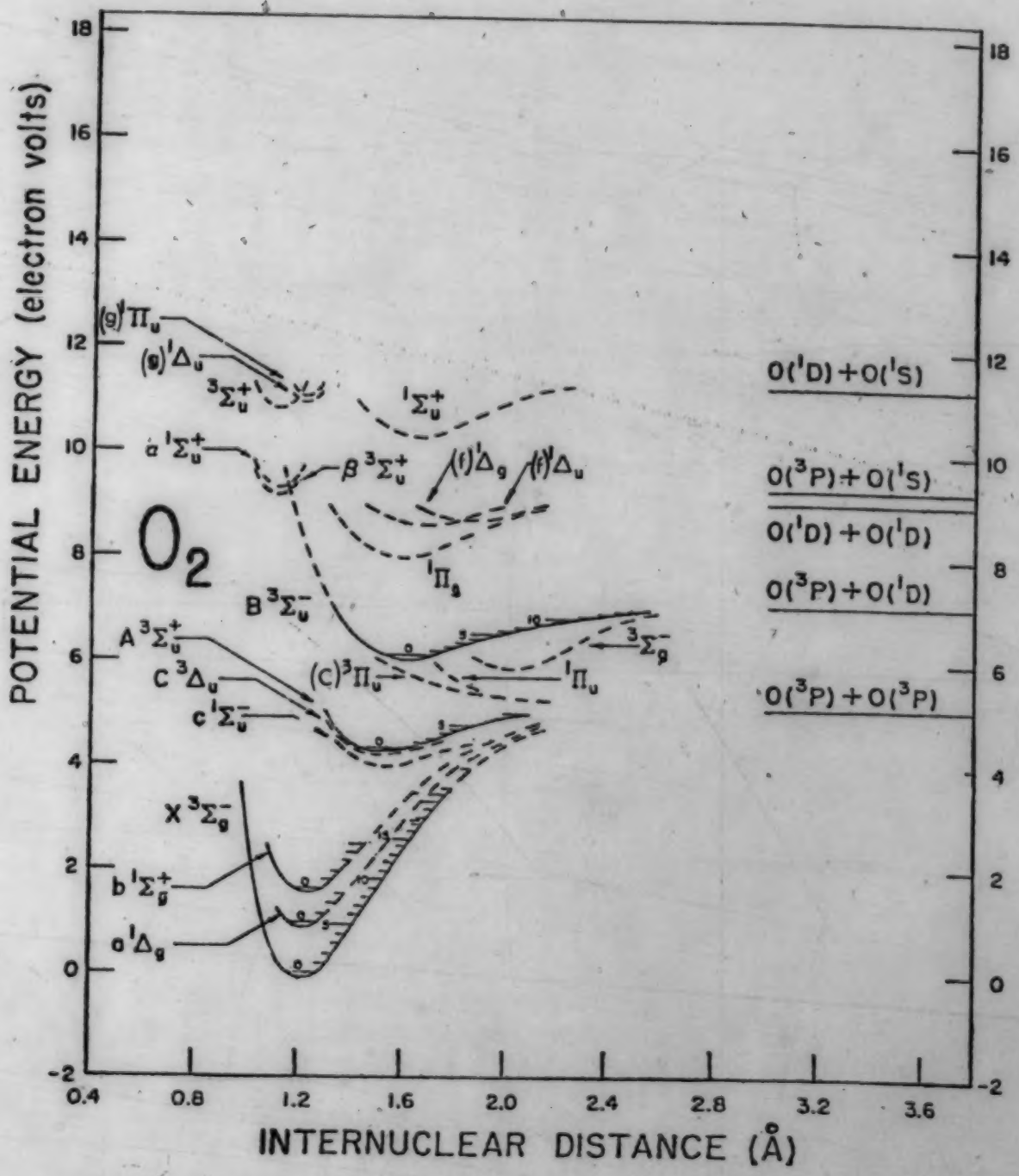


Fig. 6-3. Potential energy curves for $O_2$ (Kr 72). The notations inside the parentheses were added in the present work.

energetically very near the dissociation limit 9.00 eV ($^1D + {}^1D$), and the remaining two (1334 Å ≈ 9.29 eV and 1290 Å ≈ 9.61 eV) are very near the dissociation limit 9.30 eV ($^1S + {}^3P$). Thus the latter differs from the energy of the maximum intensity of the 1334 Å continuum by (- 0.01 eV), to that of 1290 Å by 0.31 eV and to that of 1349 Å by (- 0.11 eV).

The uppermost 1290 Å continuum maximum was also found to merge into the tail of the so-called "longest band" (1244 Å) at a certain pressure obtained during the experiment carried out by Tanaka; the state related to this maximum was henceforth considered as the most unstable of the three and was tentatively assigned by Tanaka to $^3\Pi_u$.

Thus, the unstable nature of the $^3\Pi_u$ state and the small energy difference between the dissociation limit ($^1S + {}^3P$) and the continuum maximum at 1290 Å would indicate, through the application of the Franck-Condon principle, that the potential curve for $^3\Pi_u$ has a shallow minimum which is asymptotic at 9.30 eV ($^1S + {}^3P$). (The other continuum at 1349 Å and 1334 Å are probably due to transitions forbidden by the ordinary Selection rules from the ground state to some excited unstable states expected from the same products.) This $^3\Pi_u$ state is not shown in Fig. 6-3, which was taken from the reference

data published by Krupenic (Kr 72); in fact, from the above analysis, it can be deduced that $^3\Pi_u$ would lie between $^1\Sigma_u^+$ and $^1\Delta_g$. It is assigned a type D here, so as to distinguish it from the other $^3\Pi_u$ (which is probably of type C) shown at the centre of Fig. 6-3. Equation (6-12a) can then be filled up as follows:

Through photodissociation of the unstable D $^3\Pi_u$ state,

$$O_2'(^3\Pi_u) + h\nu \rightarrow O(^1S) + O(^3P) + K.E. \qquad (6\text{-}14)$$

Finally, the forbidden lines at $\lambda\lambda$5577 and 2972 Å are produced through spontaneous radiation of the metastable $O(^1S)$ atoms, as described in equations (6-7a) and (6-7b).

(iii) Other Possible Mechanisms

It should be noted here that the mechanisms described above gave the "best-fit" among many others that were tried. Some unsuccessful mechanisms (that were also based on energy transfer) are the following:

(1) $$\underset{19.81\ eV}{He^*(^3S_1)} + \underset{0\ eV}{O(^3P)} \rightarrow \underset{0\ eV}{He(^1S)} + \underset{4.18\ eV}{O(^1S)} \qquad (6\text{-}15)$$

Since the energy difference obtained from equation (6-15) is about 15.63 eV, it was therefore not conceivable that $O(^1S)$ atoms could have been produced by exciting the ground state $O(^3P)$ with metastable helium atoms.

(2) $$He(^1S) + e(v') \rightarrow He' + e(v'') \quad (6\text{-}16)$$

$$He' + O_2(X\,^3\Sigma_g^-) \rightarrow He(^1S) + O(^3P) + O(^1S) \quad (6\text{-}17)$$

Here, for energy resonance in equations (6-16) and (6-17), the excited He' atoms must be of the order of the dissociation limit ($^1S + {}^1D$), i.e. 9.27 eV. This is not possible since the lowest excited level of He is that of $He^*(^3S_1)$ which is 19.81 eV.

(3) $$He(^1S) + e(v') \rightarrow He'' + e(v'') \quad (6\text{-}18)$$

$$He'' + O_2(X\,^3\Sigma_g^-) \rightarrow He' + O_2'(a\,^1\Delta_g) \quad (6\text{-}19)$$

where $$He'' > He' > He^*(^3S_1)$$

$$He' \rightarrow He^*(^3S_1) + h\nu \text{ (He lines)} \quad (6\text{-}20)$$

$$He^*(^3S_1) + O_2'(a\,^1\Delta_g) \rightarrow He(^1S) + O(^3P) + O(^1S) \quad (6\text{-}21)$$

19.8 eV  0.97 eV  0 eV  9.27 eV

As can be seen here, equation (6-21) is not satisfied energetically.

(4) $$He^*(^3S_1) + O_2(X\,^3\Sigma_g^-) \rightarrow He' + O_2'(^3\Pi_u) \quad (6\text{-}22)$$

11.55 eV  0 eV  ? eV  5.0 eV

$$O_2'(^3\Pi_u) \rightarrow O(^1S) + O(^3P) + h\nu \quad (6\text{-}23)$$

For energy resonance in equation (6-22), the excited He' atoms must be of the order of 6.55 eV, but the lowest excited helium atoms are of the order of 19.81 eV.

(5) $He^*(^3S_1) + O_2(X\ ^3\Sigma_g^-) \rightarrow He' + O_2'(^1\Delta_u)$ (6-24)

11.55 eV 0 eV ? eV 11.06 eV

$O_2'(^1\Delta_u) + h\nu \rightarrow O(^1S) + O(^1D)$ (6-25)

Here, equation (6-24) cannot be satisfied energetically.

(6) $He^*(^3S_1) + O_2(X\ ^3\Sigma_g^-) \rightarrow He' + O_2'(^1\Pi_u)$ (6-26)

11.55 eV 0 eV ? eV 10.89 eV

$O_2'(^1\Pi_u) + h\nu \rightarrow O(^1S) + O(^1D)$ (6-27)

Again here, equation (6-26) cannot be satisfied energetically.

(iv) Production Through Direct Collisions with Electrons

Among the possible production mechanisms of the $O(^1S)$ atoms, it was found that the most probable one would be through direct collisions between energetic electrons and ground state atoms and/or molecules:

$O(^3P) + e(v') \rightarrow O(^1S) + e(v'')$ (6-28)

$O_2(X\ ^3\Sigma_g^-) + e(v') \rightarrow O(^3P) + O(^1S) + e(v'')$ (6-29)

Thus, the density of the metastable $^1S$ atoms or the intensity of the green forbidden line was found to be increasing with the electric current supplied to the discharge (see Fig. 6-4a). Also, as depicted by the straight line in Fig. 6-4b, the intensity was not proportional to any squared or exponential value of the electric current. This linear relationship is as expected from equation (4-3).

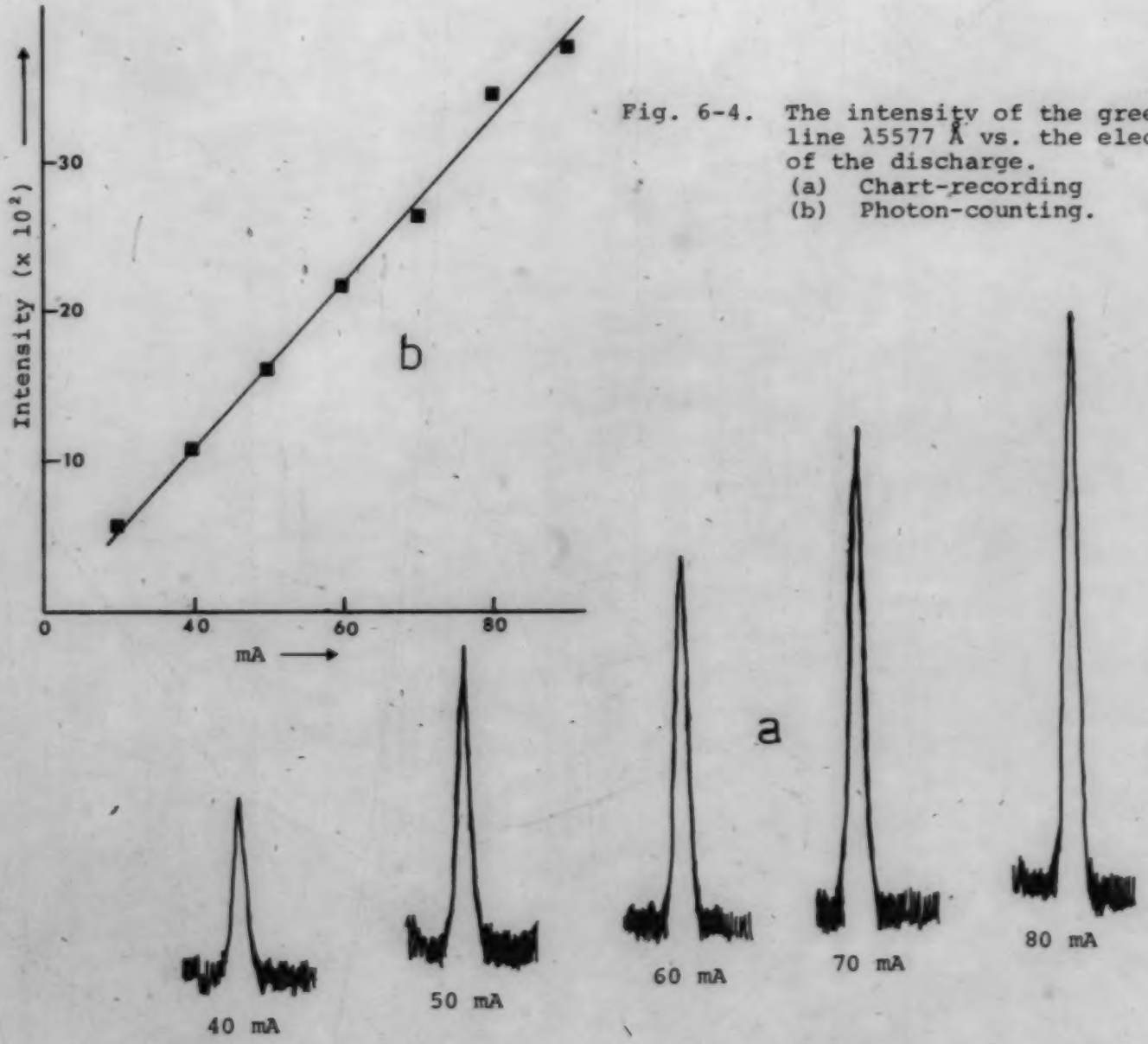


Fig. 6-4. The intensity of the green auroral line λ5577 Å vs. the electric current of the discharge.
(a) Chart-recording
(b) Photon-counting.

(v) Production through "Cascade" Transitions

Another possible populating process for the $O(^1S)$ state was through the cascading of such transitions as OI 1218 Å. However, through a particular range of oxygen partial pressures the cascading of 1218 Å turned out to be a depopulating process, as indicated in Table VI-1. In this table, through an increase of oxygen partial pressure from 0.02 to 0.10 torr, the intensity of OI 1218 Å would increase while, at the same time, OI 5577 Å would be decreasing. This paradox may indicate that the diffusion and collision processes, which also controlled the populating and deactivating processes for the metastable $^1S$ state, were playing a greater role than the cascading of transitions into that state. Actually, as the density of the $^1S$ state was increased, it would reduce the cascading and thus the intensity of 1218 Å, and would simultaneously increase spontaneous transition from itself, i.e. 5577 Å would then increase in intensity. Thus, under a given discharge condition, the density of the metastable $^1S$ state would be quantitatively connected to the intensities of both 1218 Å and 5577 Å, and this would allow for the normalisation process described in section 5.3c.

(c) OI 1218 Å

A problem encountered during the intensity measurements of 1218 Å was the fact that this line is very close to the ever-present hydrogen impurity line Lyman α at 1216 Å. To solve this problem it was found necessary to measure the intensity of OI 1218 Å in the second order, as is illustrated in Fig. 6-5. Since only relative intensity measurements of this line were undertaken, any diminished intensity incurred from the measurements in the second order would be cancelled out.

Furthermore, there was another possible problem in the intensity measurements of OI 1218 Å, stemming from the molecular absorption in the ultraviolet. Fortunately, as is well-known, there is a deep "window" in the molecular absorption spectrum of oxygen at the region next to Lyman α. Actually, the molecular absorption coefficient ($k_m$) at 1218 Å, as derived from Fig. 8 of Watanabe's "Ultraviolet Absorption Processes in Upper Atmospheres" (Wa 58), was less than 1.0 $cm^{-1}$. This value of $k_m$, as will be shown in section 6.4(d), would yield a negligible correction factor to the measured intensities of OI 1218 Å.

(d) The Absolute Transition Probability of [OI] 5577 Å

The experimental techniques developed for the measurement of the absolute A-value of forbidden lines have been applied here to the green line OI 5577 Å a

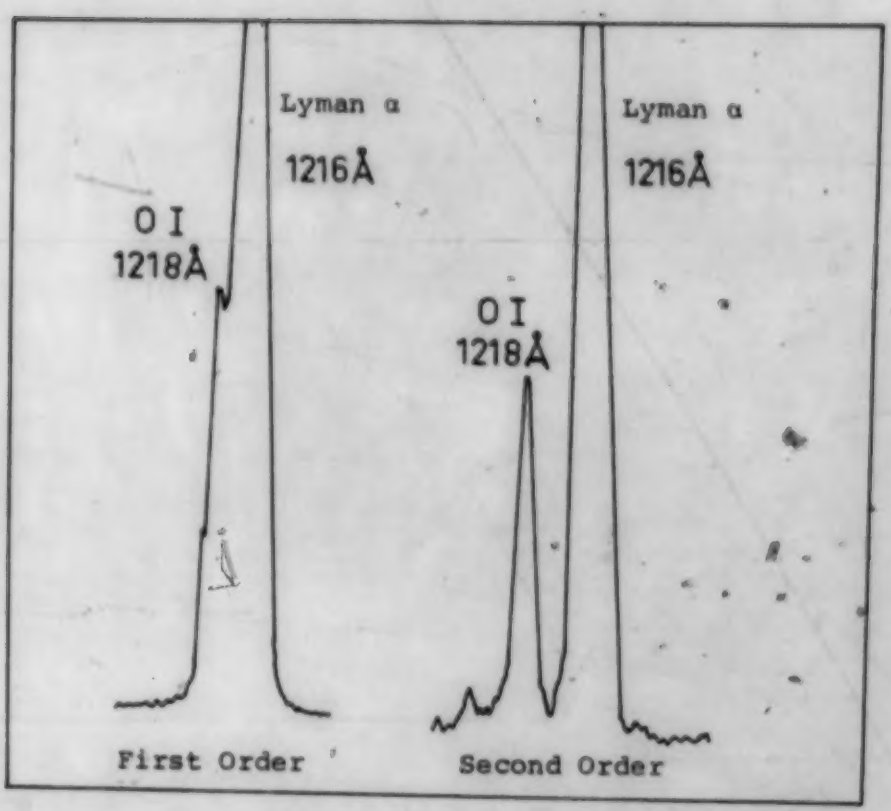


Fig. 6-5. Resolution of OI 1218 Å from Lyman α, 1216 Å.
(Sensitivity: First Order → 1 μA and 5 V
Second Order → 0.1 μA and 5 V)

total of 50 times, the runs being taken with total pressures of 15, 20 and 25 torr (helium was used as the buffer gas) while varying the oxygen partial pressure with each total pressure from 0.02 to 0.10 torr. The results are shown in Table VI-1.

The temperatures T, shown in column 3, were all obtained by probing a thermometer into the discharge that was uniformly diffuse and that satisfied the optimum conditions discussed in the previous chapter. The values of $k_o$ (column 6) for OI 1218 Å were obtained by interpolation from the computed graph shown in Fig. 4-4 (where $L = 2.031\ell$ and the upper limit of the integrations was $|\omega| = 3.0$). The $N_i$-values, obtained from equation (4-45), were first obtained by using the f-value of OI 1218 Å as taken from the work of Ott (Ot 71), i.e. f = 0.13 and then making the following substitutions (all in c.g.s. units): $e = 4.803 \times 10^{-10}$ e.s.u.; $m = 9.11 \times 10^{-28}$ gm; $c = 3.0 \times 10^{10}$ cm/sec; M = 32, and $R = 8.31 \times 10^{7}$ ergs/mole °K. The values of $(C_F/C_L)$ in the last but one column were then obtained by making the following substition in equation (4-45): r = 1.25 cm; L' = 7.0 cm; E(5577 Å) = $4.75 \times 10^{7}$ ergs/steradian-micron-cm²-sec (obtained by multiplying the value for λ5577 Å in Table IV-2 by $10^6$); $a_L = 4.427 \times 10^{-1}$ cm²; $h = 6.62 \times 10^{-27}$ ergs-cm; $(d_F/d_L)^2 = 0.97$; $\lambda = 5.577 \times 10^{-5}$ cm; $\Delta\lambda = 1.07 \times 10^{-6}$ μ

| | | | OI 1218 Å | | | OI 5577 Å | |
|---|---|---|---|---|---|---|---|
| Helium (Torr) | Oxygen (Torr) | $\sqrt{T}$ ($\sqrt{°K}$) | $I_L/I_\ell$ | $k_o\ell$ | $k_o$ ($cm^{-1}$) | $C_F/C_L$ ($\times 10^{-3}$) | A($sec^{-1}$) |
| 15 | 0.100 | 21.7 | 1.369 | 1.80 | 0.14 | 1.525 | 1.18 |
| 15 | 0.100 | 21.7 | 1.361 | 1.85 | 0.14 | 1.593 | 1.23 |
| 15 | 0.100 | 21.7 | 1.369 | 1.80 | 0.14 | 1.382 | 1.07 |
| 15 | 0.075 | 21.3 | 1.354 | 1.90 | 0.15 | 1.662 | 1.22 |
| 15 | 0.075 | 21.3 | 1.371 | 1.79 | 0.14 | 1.449 | 1.14 |
| 15 | 0.075 | 21.3 | 1.350 | 1.93 | 0.15 | 1.611 | 1.18 |
| 15 | 0.075 | 21.3 | 1.312 | 2.25 | 0.17 | 1.991 | 1.29 |
| 15 | 0.050 | 21.6 | 1.276 | 2.62 | 0.20 | 1.813 | 1.00 |
| 15 | 0.050 | 21.6 | 1.280 | 2.58 | 0.20 | 2.183 | 1.19 |
| 15 | 0.050 | 21.6 | 1.287 | 2.50 | 0.19 | 1.725 | 0.99 |
| 15 | 0.050 | 21.6 | 1.283 | 2.55 | 0.20 | 1.823 | 0.99 |
| 15 | 0.035 | 21.7 | 1.219 | 3.54 | 0.27 | 2.297 | 0.92 |
| 15 | 0.035 | 21.7 | 1.254 | 2.93 | 0.23 | 2.069 | 0.97 |
| 15 | 0.035 | 21.7 | 1.272 | 2.68 | 0.21 | 2.261 | 1.17 |
| 15 | 0.035 | 21.7 | 1.301 | 2.35 | 0.18 | 2.131 | 1.28 |
| 15 | 0.020 | 21.2 | 1.223 | 2.45 | 0.26 | 2.340 | 1.00 |
| 15 | 0.020 | 21.2 | 1.233 | 3.32 | 0.26 | 2.194 | 0.94 |
| 15 | 0.020 | 21.2 | 1.227 | 3.38 | 0.26 | 2.315 | 0.99 |
| 15 | 0.020 | 21.2 | 1.254 | 2.92 | 0.23 | 2.449 | 1.18 |

Table VI-1. Results on the absolute transition probability A of the green forbidden line. (Continued)

| | | | OI 1218 Å | | | OI 5577 Å | |
|---|---|---|---|---|---|---|---|
| Helium (Torr) | Oxygen (Torr) | $\sqrt{T}$ ($\sqrt{°K}$) | $I_L/I_\ell$ | $k_o\ell$ | $k_o$ ($cm^{-1}$) | $C_F/C_L$ ($\times 10^{-3}$) | A ($sec^{-1}$) |
| 20 | 0.100 | 22.3 | 1.366 | 1.82 | 0.14 | 1.705 | 1.28 |
| 20 | 0.100 | 22.3 | 1.377 | 1.75 | 0.14 | 1.702 | 1.28 |
| 20 | 0.100 | 22.3 | 1.339 | 2.02 | 0.16 | 1.495 | 0.98 |
| 20 | 0.075 | 22.2 | 1.296 | 2.40 | 0.19 | 1.686 | 0.94 |
| 20 | 0.075 | 22.2 | 1.287 | 2.50 | 0.19 | 1.655 | 0.92 |
| 20 | 0.075 | 22.2 | 1.317 | 2.20 | 0.17 | 1.597 | 0.99 |
| 20 | 0.050 | 22.2 | 1.287 | 2.50 | 0.19 | 1.877 | 1.05 |
| 20 | 0.050 | 22.2 | 1.283 | 2.55 | 0.20 | 1.836 | 0.97 |
| 20 | 0.035 | 22.1 | 1.300 | 2.36 | 0.18 | 1.956 | 1.16 |
| 20 | 0.035 | 22.1 | 1.300 | 2.36 | 0.18 | 1.892 | 1.12 |
| 20 | 0.035 | 22.1 | 1.303 | 2.33 | 0.18 | 1.938 | 1.15 |
| 20 | 0.035 | 22.1 | 1.290 | 2.46 | 0.19 | 2.093 | 1.17 |
| 20 | 0.020 | 21.2 | 1.226 | 3.40 | 0.26 | 2.179 | 0.93 |
| 20 | 0.020 | 21.2 | 1.227 | 3.40 | 0.26 | 2.149 | 0.92 |
| 20 | 0.020 | 21.2 | 1.235 | 3.25 | 0.25 | 2.260 | 1.00 |

Table VI-1 (continued)

| | | | OI 1218 Å | | | OI 5577 Å | |
|---|---|---|---|---|---|---|---|
| Helium (Torr) | Oxygen (Torr) | $\sqrt{T}$ ($\sqrt{°K}$) | $I_L/I_\ell$ | $k_o\ell$ | $k_o$ ($cm^{-1}$) | $C_F/C_L$ ($\times 10^{-3}$) | A ($sec^{-1}$) |
| 25 | 0.100 | 22.6 | 1.341 | 2.00 | 0.16 | 1.650 | 1.07 |
| 25 | 0.100 | 22.6 | 1.381 | 1.73 | 0.13 | 1.335 | 1.07 |
| 25 | 0.075 | 22.7 | 1.334 | 2.05 | 0.16 | 1.701 | 1.10 |
| 25 | 0.075 | 22.7 | 1.291 | 2.55 | 0.20 | 1.801 | 0.93 |
| 25 | 0.075 | 22.7 | 1.357 | 1.88 | 0.15 | 1.762 | 1.22 |
| 25 | 0.075 | 22.7 | 1.287 | 2.50 | 0.19 | 1.864 | 1.02 |
| 25 | 0.050 | 22.3 | 1.232 | 3.31 | 0.26 | 2.128 | 0.85 |
| 25 | 0.050 | 22.3 | 1.243 | 3.10 | 0.24 | 2.138 | 0.94 |
| 25 | 0.050 | 22.3 | 1.279 | 2.59 | 0.20 | 2.107 | 1.11 |
| 25 | 0.035 | 22.7 | 1.222 | 3.46 | 0.27 | 2.289 | 0.88 |
| 25 | 0.035 | 22.7 | 1.254 | 2.92 | 0.23 | 2.180 | 0.98 |
| 25 | 0.035 | 22.7 | 1.232 | 3.31 | 0.26 | 2.407 | 1.25 |
| 25 | 0.035 | 22.7 | 1.222 | 3.46 | 0.27 | 2.270 | 0.87 |
| 25 | 0.020 | 22.6 | 1.213 | 3.70 | 0.29 | 2.439 | 0.87 |
| 25 | 0.020 | 22.6 | 1.243 | 3.10 | 0.24 | 2.401 | 1.04 |
| 25 | 0.020 | 22.6 | 1.232 | 3.30 | 0.26 | 2.289 | 0.92 |
| Mean | | | | | | | 1.06 ± 0.13 |

Table VI-1 (continued)

and $T_F = 0.99$. Finally, the A-values in the last column were obtained by substituting the $N_i$- and the $(C_F/C_L)$-values into equation (4-44), which turned out to be the following:

$$A(5577\ \text{Å}) = \left(\frac{2.35}{k_o \sqrt{T}}\right)\left(\frac{C_F}{C_L}\right) \times 10^3\ \text{sec}^{-1}$$

The mean A-value of OI 5577 Å was thus found to be 1.06 $\text{sec}^{-1}$, with a standard deviation $\sigma$[†] of ±0.13. The standard deviation was, in fact, well within the total experimental error which will be discussed later in this chapter.

(e) Error Estimation for A(5577 Å)

The major source of error in this experiment involves the assumed f-value of OI 1218 Å, which was taken from Ott (Ot 71). He used a wall-stabilized arc discharge operating in a mixture of argon and oxygen, and obtained the value 0.12 with an error "estimated to be approximately ±23%". (Another recent experimental result by Forsman and Clark (Fo 73) was at least 50% smaller than other experimental values reported, and has not been used in this work.)

---

[†] The standard deviation $\sigma = \left[\frac{1}{n}\sum_{i=1}^{n}(x_i - \bar{x})\right]^{1/2}$ where n is the number of runs and $\bar{x}$ is the mean value and $x_i$ is the individual value obtained.

The error in the temperature measurements, as explained in section 5.2, had an upper limit of ±5%, while the intensity measurements should be good to better than ±10% and finally, ±5% error was allowed for the miscellaneous measurements such as those on the geometrical dimensions, etc. Thus, we estimate an overall uncertainty of about ±30%, giving the result

$$A(5577\ \text{Å}) = 1.06 \pm 0.32\ \text{sec}^{-1}$$

As may be noticed here, the standard deviation of ±0.13 found in the 50 runs was well within this estimated error limit.

(f) Obtaining the f-value of OI 1218 Å from the Current Results

One of the main sources of uncertainty in the present experimental result for A(5577 Å) is still in the f-value of OI 1218 Å. If we reversed the procedure, i.e. assumed the A-value (= 1.183 $\text{sec}^{-1}$) for 5577 Å obtained through the NCMET calculation of Nicolaides et al. (Ni 71), and substituted it in the current measurements, we would then obtain, for each run,

$$f = \frac{(6.54 \times 10^{-5})\ k_o \sqrt{T}}{(C_F/C_L)} .$$

The resulting mean f-value of OI 1218 Å is then 0.134 ± 0.013, as compared to 0.120 and 0.051 obtained experimen-

tally by Ott (Ot 71) and Forsman and Clark (Fo 73) respectively.

(g) The Absolute Transition Probability of the Forbidden Oxygen Line at λ2972 Å

Since the forbidden lines of oxygen at 2972 Å and 5577 Å have the same upper state ($^1S_0$), one can obtain the ratio of their A-coefficients by comparing their intensities under the same overall conditions (see equation 4-39).

The [OI] 2972 Å line (known as the transauroral line) was too weak to observe side-on from the discharge tube; the intensity comparison was therefore made by observing the forbidden lines end-on, i.e. with the tube fitted end-on to the Spex monochromator slit. However, even when the tube was end-on, [OI] 2972 Å was found to be photoelectrically measurable only when the buffer gas used in the discharge mixture was argon, instead of helium. Yet the transauroral line was so weak and the Spex response and the photographic plate emulsion were so low at that wavelength that it was not possible to obtain its spectrogram, even after long exposures. However, with a cooled 9658R photomultiplier it was found to be photoelectrically detectable. Figs. 6-6a & b illustrate the chart-recording of the two forbidden lines which as expected,

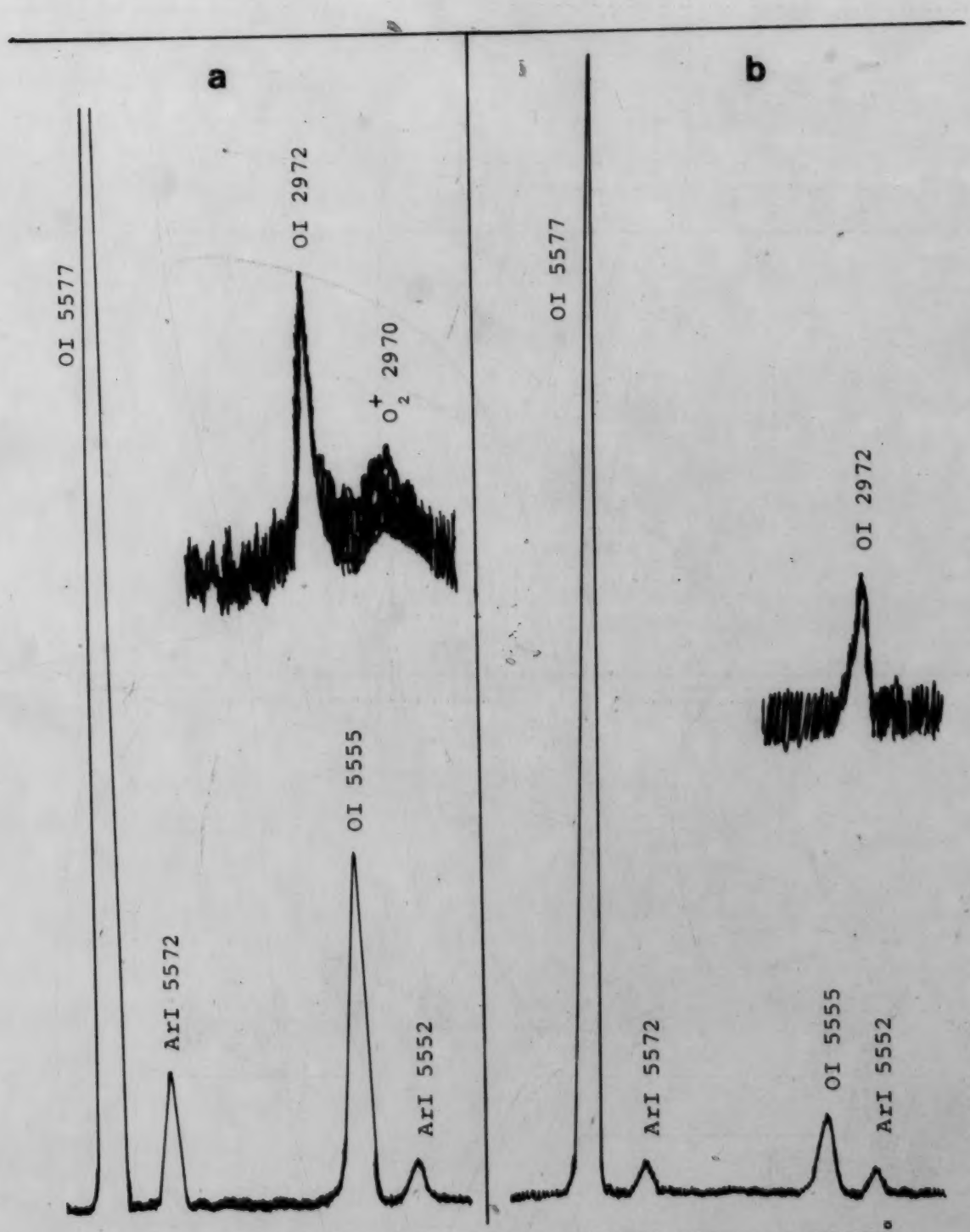


Fig. 6-6. Chart-recorded spectra of [OI] 2972 and 5577 Å.
(a) Mixture: 0.2 torr $O_2$ + 15 torr Ar (b) Mixture: 1 torr $O_2$ + 15 torr Ar
Sensivity: OI 5577:(3 μA & 5 V)
OI 2972:(0.3 μA & 2 V)
Other Conditions: same.

were found to diminish in intensity as the partial pressure of oxygen was increased.

The Spex monochromator and detection system was then calibrated at the two wavelengths (5577 and 2972 Å) in the following way:

The mean number of counts/sec from the standard lamp, run at the calibrated current (35 amperes) and under the same overall spectrophotometric conditions, were first obtained. These counts were then corrected for the background and scattering light (done by using the appropriate filters). Say, then

$$\frac{\text{mean counts/sec from lamp for } \lambda 5577 \text{ Å}}{\text{mean counts/sec from lamp for } \lambda 2972 \text{ Å}} = \frac{x}{y} \qquad (6\text{-}30)$$

and, from Table IV-2,

$$\frac{\text{spectral radiance of lamp (35 Amps.) at } \lambda 5577 \text{ Å}}{\text{spectral radiance of lamp (35 Amps.) at } \lambda 2972 \text{ Å}} = \frac{a}{b} \qquad (6\text{-}31)$$

Then,

$$\frac{\text{Response of Spex detection system at } \lambda 5577 \text{ Å}}{\text{Response of Spex detection system at } \lambda 2972 \text{ Å}} = \frac{(x/y)}{(a/b)} = \frac{z}{1} \qquad (6\text{-}32)$$

Thus, if

$$\frac{\text{measured intensity of [OI] 5577 Å}}{\text{measured intensity of [OI] 2972 Å}} = \frac{C(5577 \text{ Å})}{C(2972 \text{ Å})} \times \frac{h \times 2972}{h \times 5577}$$

$$= \frac{C'(5577 \text{ Å})}{C'(2972 \text{ Å})} \qquad (6\text{-}33)$$

Then the true intensity ratio

$$\frac{I(5577\ \text{Å})}{I(2972\ \text{A})} = \frac{C'(5577\ \text{Å})}{C'(2972\ \text{Å})} \times \frac{1}{z} \qquad (6\text{-}34)$$

The values of $C'(\lambda)$ obtained by photon-counting; the peaks of the two photon-counting profiles through the same slit width were compared, and the comparison was repeated several times, each with a mixture of different argon or oxygen partial pressures. The photon-counting profiles of [OI] 5577 Å and [OI] 2972 Å for one of those mixtures are illustrated in Fig. 5-5, and the results are shown in Table VI-2.

Table VI-2. Results for the true intensity ratio I(5577 Å)/I(2972 Å).

| Mixture Number | $\frac{C'(5577\ \text{Å})}{C'(2972\ \text{Å})} \times 10^2$ | $\frac{I(5577\ \text{Å})}{I(2972\ \text{Å})}$ | Mean $\frac{A(5577\ \text{Å})}{A(2972\ \text{Å})}$ |
|---|---|---|---|
| 1 | 2.81 | 23.1 | |
| 2 | 2.85 | 23.5 | |
| 3 | 2.93 | 24.1 | 23.7 ± 1.1 |
| 4 | 3.10 | 25.5 | |
| 5 | 2.70 | 22.2 | |

In this table, the values shown in the third column were obtained by multiplying those in the second column with

the z-value that was obtained as follows:

Using the calibrated standard lamp and equation (6-30), it was found that

$$\frac{x}{y} = 2565$$

and from equation (6-31),

$$\frac{a}{b} = 211$$

so that $z = 12.16$

Thus, as shown in the fourth column of Table VI-2,

$$\text{Mean } \frac{A(5577\ \text{Å})}{A(2972\ \text{Å})} = 23.7 \pm 1.1$$

However, as previously obtained in the present work,

$$A(5577\ \text{Å}) = 1.06 \pm 0.013\ \text{sec}^{-1}$$

$$\therefore A(2972\ \text{A}) = 0.045 \pm 0.008\ \text{sec}^{-1}$$

Allowing an upper limit of ±10% error in the intensity measurements, we would then obtain

$$\frac{A(5577\ \text{Å})}{A(2972\ \text{Å})} = 23.7 \pm 2.4$$

Adding the ±10% error to the previous ±30% error estimated for A(5577 Å), we would finally obtain

$$A(2972\ \text{Å}) = 0.045 \pm 0.014\ \text{sec}^{-1}$$

where the standard deviation (±0.008) for Å(2972 Å) is still within the estimated "most probable" error of ±0.014.

Due to the fact that [OI] 5577 Å arises from

pure EQ and [OI] 2972 from pure MD radiation, both having the same upper $^1S$ level, the constancy of their measured ratios from mixtures of varying pressures can but confirm the assumption that collisional stimulation of the $^1S$ level was absent, i.e. the measured 5577 Å line intensity did in fact correspond to photons arising from spontaneous emission only.

The theoretical and experimental results for the A coefficients of [OI] 5577 Å and [OI] 2972 Å, that have been reported by previous workers, are listed in Table VI-3. Omholt's result (Om 56) was deduced from studies on several types of rapidly changing auroras, while the values for the ratio A(5577)/A(2972) obtained by LeBlanc et al. (Le 66) and McConkey et al. (Mc 66) were from laboratory studies. McConkey and Kernahan (Mc 69) measured the A-value of the green line reliable, however, only to a factor of two, due mainly to a 50% uncertainty at that time in the f-value of OI 1218 Å. The result of Corney and Williams (Co 72) was obtained by recording the time dependence of the decay of [OI] 5577 Å during the afterglow of a pulsed discharge in an inert gas-oxygen mixtures. As for the theoretical results, the methods used were as mentioned in section 2.6 of this thesis.

Thus, the new experimental determination of the

| REFERENCE | A(5577) | A(2972) | $\frac{A(5577)}{A(2972)}$ | A(5577) + A(2972) |
|---|---|---|---|---|
| Theoretical | | | | |
| Condon (Co 34) | 2.0 | 0.18 | 11.1 | 2.18 |
| Pasternack (Pa 40) | 2.2 | 0.09 | 24.4 | 2.29 |
| Yamanouchi and Horie (Ya 52) | 2.04 | 0.067 | 30.4 | 2.11 |
| Garstang (Ga 51) | 1.28 | 0.078 | 16.4 | 1.36 |
| Garstang (Ga 56) | 1.25 | 0.071 | 17.6 | 1.32 |
| Nicolaides et al. (Ni 71) | 1.183 | - | - | - |
| Experimental | | | | |
| Omholt (Om 56) | - | - | - | 1.43 ± 0.20 |
| LeBlanc et al. (Le 66) | - | - | 22 ± 2 | |
| McConkey et al. (Mc 66) | - | - | 18.6 ± 3.7 | - |
| McConkey and Kernahan (Mc 69) | 1.0 | - | - | - |
| Corney and Williams (Co 72) | - | - | - | 1.31 ± 0.05 |
| Present work | 1.06 ± 0.32 | 0.045 ± 0.014 | 23.7 ± 2.4 | 1.11 |

Table VI-3. Theoretical and experimental results for the A-coefficients of the forbidden OI lines at λλ5577 and 2972 Å ($sec^{-1}$).

A coefficient of the 5577 Å is in good agreement with the latest sophisticated theoretical calculation (see section 2.6). Moreover, in obtaining a value for the ratio A(5577)/A(2972) we find good agreement with other results, both theoretical and experimental.

## 6.4 Results and Analysis on the Forbidden [OI] Lines at λλ6300 and 6364 Å

### (a) Laboratory Production of the Red Auroral Lines at λλ6300 and 6364 Å

The red forbidden lines at λλ6300 and 6364 Å were produced in a similar way to the green forbidden line, except that here it was necessary to use a higher partial pressure of oxygen (thus a higher probability of bringing up a "cored" discharge) and argon had to be used as the buffer gas in the discharge mixture - they did not show up in mixtures using helium as a buffer. Futhermore, the red [OI] line at λ6300 Å was found to be produced to an extent that was photoelectrically measurable only in a restricted number of mixture compositions, and that was only for conditions of an "optimum dishcarge" where the molecular oxygen and impurity bands were absent. Figs. 6-7a & b illustrate an example of how the red [OI] line at λ6300 Å appearing in a certain type of mixture (1.5 torr of oxygen and 30 torr of argon), would simply

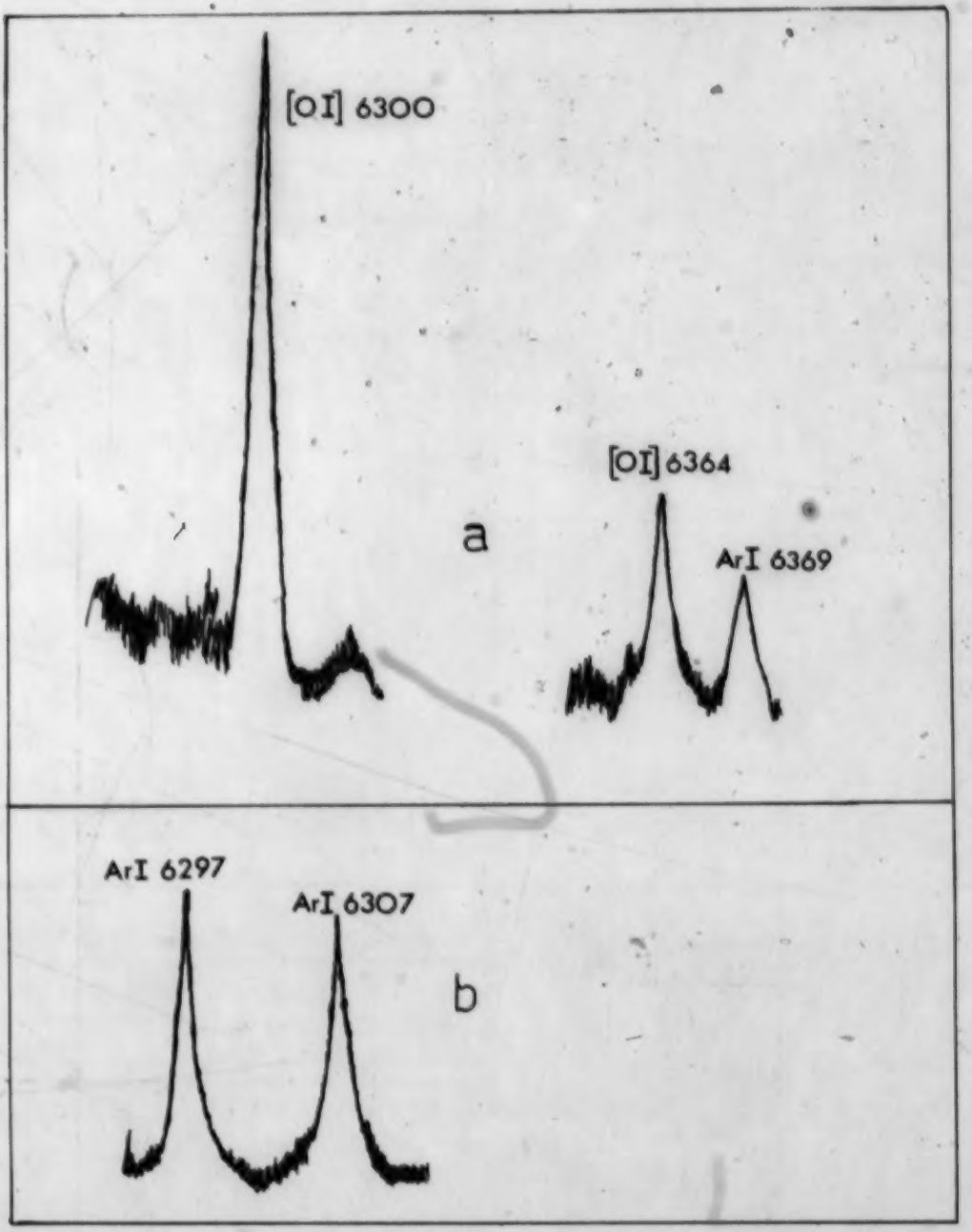


Fig. 6-7. The red forbidden lines were:
(a) present in a mixture of 1.5 torr of oxygen and 30 torr of argon.
(b) absent in a mixture of 2.0 torr of oxygen and 20 torr of argon.

dissappear in another mixture of different composition (20 torr oxygen and 15 torr of argon). Also, in Fig. 6-7a, both [OI] 6300 and 6364 Å showed up while ArI 6927 and 6307 Å were absent, whereas in Fig. 6-7b, the reverse effect occurred. Thus, unlike the green line, we were restricted to runs using oxygen partial pressures of 1.25 torr or 1.50 torr, and argon pressures of 25, 30 and 35 torr. Through each discharge a current of 90 mA and a p.d. of about 6000 volts were used.

(b) Processes Involved in the Production of the Metastable $O(^1D)$ Atoms and the Red Forbidden Lines

The same mechanism as that considered in section 6.2(b) can be proposed to explain the production of the metastable $O(^1D)$ atoms. Thus, here we can replace He by Ar throughout equations (6-9) to (6-13) which would represent one of the main processes by which $O(^1D)$ atoms are produced.

Another main production process for the $O(^1D)$ atoms is represented by equation (6-13) with x being substituted by the $B\ ^3\Sigma_u^-$ state (see Fig. 6-3):

$$O_2(B\ ^3\Sigma_u^-) + h\nu \rightarrow O(^3P) + O(^1D) + K.E.$$

(dissociation limit = 7.08 eV)

The $(B\ ^3\Sigma_u^- - X\ ^3\Sigma_g^-)$ transition is the well-known Shumann-

Range system whose continuum and absorption bands have been observed quite a long time ago (Fü 25, Le 26), with the continuum maximum situated at about 1750 Å. The most accurate convergence (theoretical) limit for the system was actually determined by Brix and Herzberg (Br 54) and found to be 57128 ± 5 $cm^{-1}$ or 7.08 eV.

There is also a dissociation continuum maximum at λ1349 Å (≈ 9.19 eV) which is just above the dissociation limit at 9.00 eV ($^1D + {}^1D$) (see Fig. 6-3). This would suggest the existence of an unknown, unstable state x with a dissociation limit ($^1D + {}^1D$) at 9.00 eV. Photodissociation of this unstable state would yield a further amount of $O(^1D)$ atoms:

$$O_2'(x) + h\nu \rightarrow {}^1D + {}^1D + K.E. \qquad (6\text{-}35)$$

Barrow and Parcq (Ba 68) and Carleer and Colin (Ca 70) observed a f $^1\Delta_u$ - a $^1\Delta_g$ band system in absorption for sulphur molecules whereby they establish that the dissociation products of f $^1\Delta_u$ should be necessarily ($^1D + {}^1D$). This result would suggest that the unknown state x in equation (6-35) may also be f $^1\Delta_u$, so that a f $^1\Delta_u$ - a $^1\Delta_g$ band system in absorption in oxygen molecules would also exist. However, no literature on such a band system for oxygen exists yet. The assignment of this state (f $^1\Delta_u$) as shown in Fig. 6-3 is therefore tentative here.

Production by Direct Collisions with Electrons

Again here, it was found that the most probable mechanisms for the $^1D$ atoms would be through direct collisions between energetic electrons and ground state atoms and/or molecules:

$$O(^3P) + e(v') \rightarrow O(^1D) + e(v'')$$

$$O_2(X\ ^3\Sigma_g) + e(v') \rightarrow O(^3P) + O(^1D) + e(v'')$$

Thus, the density of the metastable $^1D$ atoms or the intensity of the red forbidden line $\lambda$6300 Å was again found to be directly proportional to the electric current supplied to the discharge mixture (see Figs. 6-8a & b).

(c) OI 1152 Å

Like the oxygen line at 1218 Å, that at 1152 Å was found to increase in intensity with the oxygen partial pressure while at the same time the intensity of the forbidden line at 6300 Å would be decreasing, thus indicating the same connection between the density of the $^1D$ state with the line intensities of $\lambda$1152 Å and $\lambda$6300 Å as that between the density of the $^1S$ state and the line intensities of $\lambda$1218 Å and $\lambda$5577 Å.

It was found necessary to measure the intensity of OI 1152.15 Å in the second order because it was always blended by the oxygen molecular bands at $\lambda$1151.46, 1151.67 and 1152.14 Å. These bands, shown in Fig. 6-9, were iden-

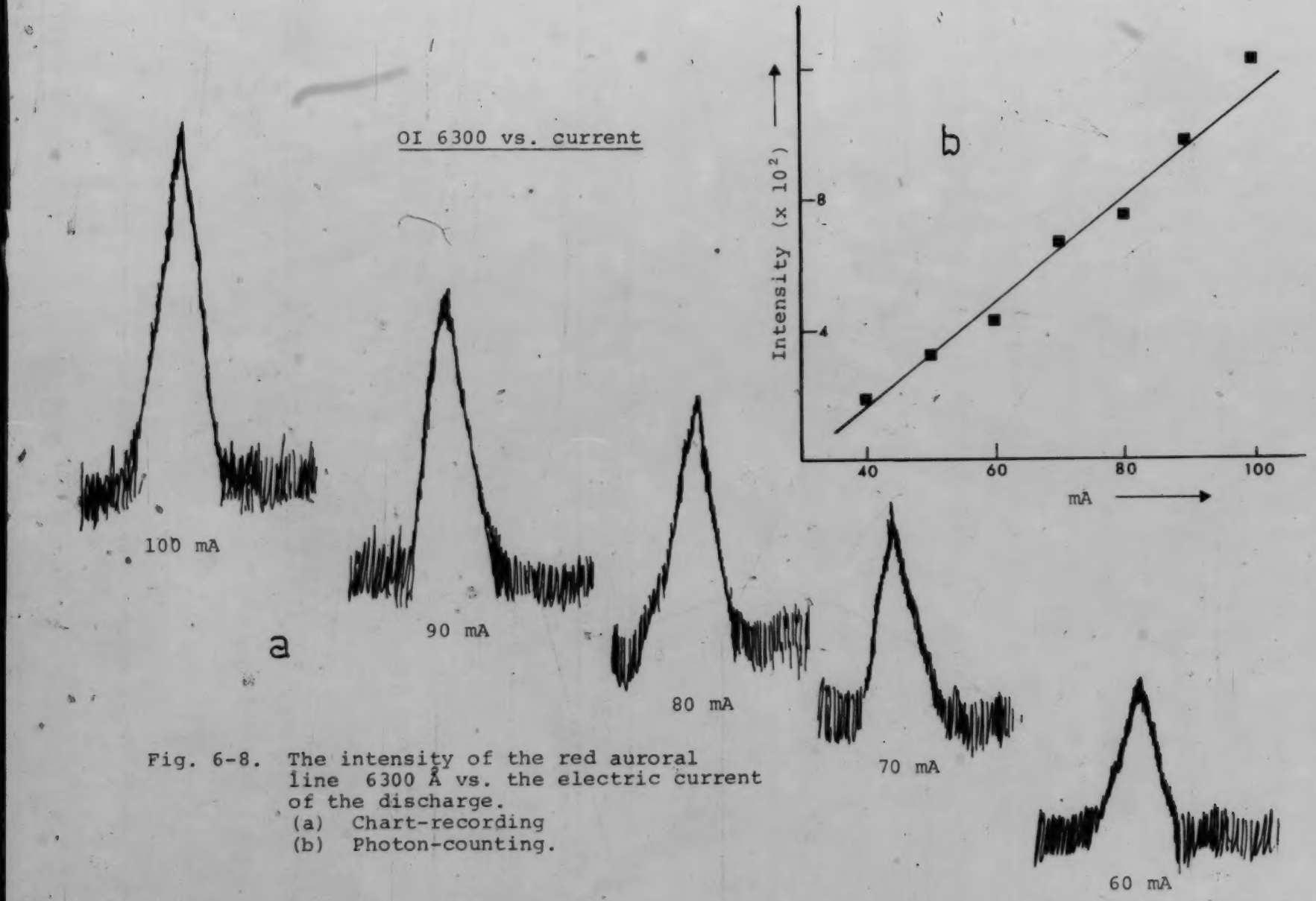


Fig. 6-8. The intensity of the red auroral line 6300 Å vs. the electric current of the discharge.
(a) Chart-recording
(b) Photon-counting.

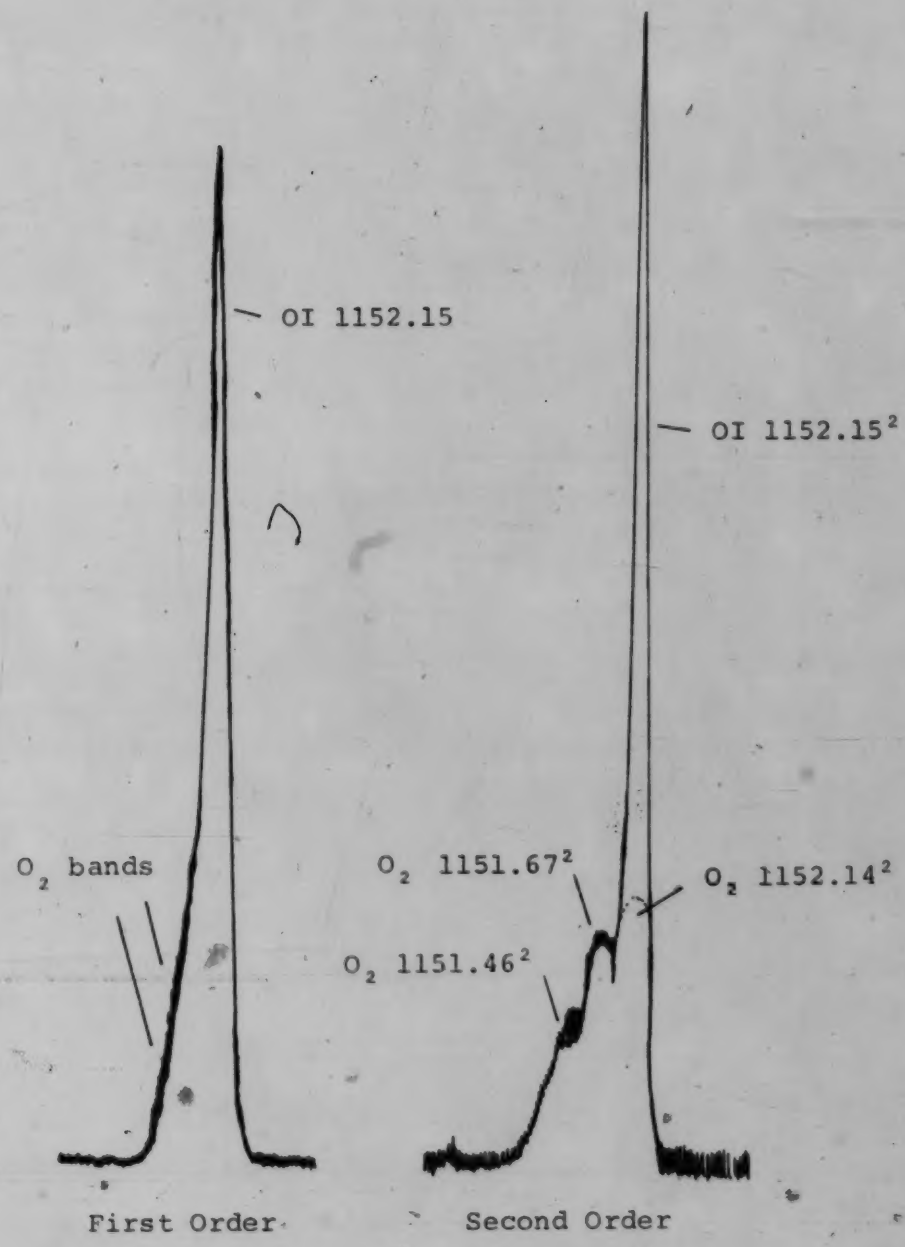


Fig. 6-9. Resolution of OI 1152 Å from $O_2$ bands at λ1151.46, 1151.67 and 1152.14 Å.

tified as group (a) by Tanaka (Ta 52) who assigned an intensity ratio of 8/7 to I(1152.14 Å)/(1151.67 Å). Thus, to obtain the baseline or continuum for OI 1152.15 Å which superposed $O_2$ 1152.14 Å, the peak intensity of λ1151.67 Å was measured and multiplied by 8/7.

The greatest problem involved in the intensity measurement of OI 1152 Å was that produced by the molecular absorption at that wavelength (there is not an optical window there, unlike the case for Lyman α). Thus a correction factor due to molecular absorption has to be applied to the measured intensity ratio $I_L/I_\ell$ of this line.

(d) The "Correction Factor" Due to Molecular Absorption

Unlike 1218 Å, the molecular absorption of oxygen at 1152 Å is not negligible. Thus, in measuring the intensity ratio ($I_L/I_\ell$) of 1152 Å, not only the atomic absorption coefficient ($k_\lambda$) but also the molecular absorption coefficient $k_m(\lambda)$ should be taken into account.

$K_m(\lambda)$ is defined by Lambert-Bouguer's law,

$$I = I_o \, e^{-k_m(\lambda) \cdot x} \qquad (6\text{-}36)$$

where $I_o$ and I are the light intensities before and after absorption in a path d reduced to N.T.P.

i.e. $$x = d \times \frac{P}{760} \times \frac{273}{T} \qquad (6\text{-}37)$$

The absorption cross section is then obtained from $k_m$ as follows:

$$\sigma_m(\lambda) = k_m(\lambda)/n_o \qquad (6\text{-}38)$$

where $n_o = 2.70 \times 10^{19}$ molecules/cm$^3$ (called the "Loschmidt's number). The values of $k_m(\lambda)$ for molecular oxygen can be deduced from curves relating $\sigma_m$ to $\lambda$, obtained by Watanabe (Wa 58), Metzer and Cook (Me 64) or Ogawa and Yamawaki (Og 70).

To obtain the correction factor due to molecular absorption let us consider the flux coming out of point A of a discharge tube (cross section = a) into the monochromator slit (see Fig. 6-10). If the flux per unit volume with no absorption at all were $I_u$, then that from a volume element a(dx) with no absorption would be $a(dx)(I_u)$. Then, from

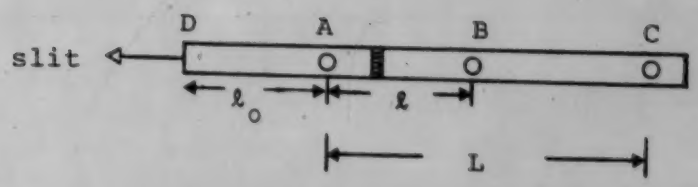


Fig. 6-10. The molecular absorption paths.

equation (6-36), the flux from volume element a(dx) after molecular absorption through a reduced length x would be

$$a(dx)(I_u)\ e^{-k_m(\lambda)\cdot x}$$

Hence, the flux from the volume AC after molecular absorption is

$$(I_L)_{mol.} = \int_0^{L_R} a(dx)(I_u)\ e^{-k_m(\lambda)\cdot x}$$

$$= a(I_u)\ [1 - \exp\{-k_m(\lambda)\cdot L_R\}] \qquad (6\text{-}39)$$

where $$L_R = L \times \frac{P}{760} \times \frac{273}{T} \qquad (6\text{-}40)$$

Similarly, from volume AB,

$$(I_\ell)_{mol.} = a(I_u)\ [1 - \exp\{k_m(\lambda)\cdot \ell_R\}] \qquad (6\text{-}41)$$

$$\therefore \left(\frac{I_L}{I_\ell}\right)_{mol.} = \frac{1 - \exp\{-k_m(\lambda)\cdot L_R\}}{1 - \exp\{-k_m(\lambda)\cdot \ell_R\}} = F(P,T,k_m(\lambda),L_R,\ell_R) \qquad (6\text{-}42)$$

Now, the flux coming from volume AC starting at point A would be attenuated, when it reached point D, by the same factor, $\exp\{-k_m\ \ell_{o_R}\}$, as that from volume AB starting at the same point A, i.e.

$$\left(\frac{I_L}{I_\ell}\right)_{mol.} \text{ at point A} = \left(\frac{I_L}{I_\ell}\right)_{mol.} \text{ at point D} = F \qquad (6\text{-}43)$$

However, if there were no absorption at all,

$$\frac{I_L}{I_\ell} = \frac{NA\ h\nu\ L}{NA\ h\nu\ \ell} = \left(\frac{L}{\ell}\right) \qquad (6\text{-}44)$$

$\therefore$ the correction factor due to molecular absorption is

$$C(P,T,k_m(\lambda),L_R,\ell_R) = \left(\frac{L}{\ell}\right) \Big/ F(P,T,k_m(\lambda),L_R,\ell_R)$$

$$= \left(\frac{L}{\ell}\right) \Big/ \frac{(1 - \exp\{-k_m(\lambda)\cdot L_R\}}{(1 - \exp\{-k_m(\lambda)\cdot \ell_R\}} \qquad (6\text{-}45)$$

Also, during the experiment, the measured ratio $(I_L/I_\ell)$ included both molecular and atomic absorption. Hence, for atomic absorption only,

$$\left(\frac{I_L}{I_\ell}\right)_{at.} = \left(\frac{I_L}{I_\ell}\right)_{meas.} \times C(P,T,k_m(\lambda),L_R,\ell_R)$$

$$= \left(\frac{I_L}{I_\ell}\right)_{meas.} \times \left(\frac{L}{\ell}\right) \Big/ \frac{1 - \exp\{-k_m(\lambda)\cdot L_R\}}{1 - \exp\{-k_m(\lambda)\cdot \ell_R\}} \qquad (6\text{-}46)$$

Case for the Oxygen "Windows"

At the oxygen windows, the molecular absorption coefficient $k_m(\lambda) \approx 0$, so that if we evaluate equation (6-42) accordingly, we would obtain

$$F = \frac{1 - \exp\{-k_m(\lambda)\cdot L_R\}}{1 - \exp\{-k_m(\lambda)\cdot \ell_R\}}$$

$$= \frac{1 - \{1 - k_m L_R + (k_m L_R)^2 \ldots\}}{1 - \{1 - k_m \ell_R + (k_m \ell_R)^2 \ldots\}} \qquad (6\text{-}47)$$

$$= \frac{L_R}{\ell_R} = \frac{L}{\ell}$$

Thus, for equation (6-45), the correction factor will then be

$$C = \left(\frac{L}{\ell}\right) \Big/ \left(\frac{L}{\ell}\right) = 1.0$$

i.e., when $k_m(\lambda) \approx 0$, as it is for OI 1218 Å ($k_m \approx 0.3$ cm$^{-1}$), the value of C would be unity, i.e. no correction due to molecular absorption is required at this wavelength (as was assumed).

(e) The Absolute Transition Probability of the Forbidden [OI] Line at λ6300 Å

The same technique as the one applied to the green forbidden line in section 6.2(d) was employed for the red one at λ6300 Å. The results are as shown in Table VI-4. The buffer gas used was argon and the number of runs was restricted to twelve for the reason mentioned previously. The total pressure of the gas mixture was generally higher than that used for the green line and a correspondingly higher temperature was obtained. Many values that were used for substitution in equation (4-44) and (4-45) for determining $N_i$ and $A_{ij}$ were the same as those for the green line, except for the following changes that were due to alterations on the tube's arrangement and the wavelengths: $L' = 8.0$ cm, $(d_F/d_L)^2 = 0.40$, $E(6300\ \text{Å}) = 7.75 \times 10^7$ ergs/steradian-micron-cm$^2$-sec, $\lambda = 6.300 \times 10^{-5}$cm and $f(1152\ \text{Å}) = 0.101$ (±8%). The f-value at 1152 Å was obtained in this laboratory by the beam-foil technique (Li 72).

To obtain the value of $k_o$, the measured intensity ratio $(I_L/I_\ell)_{meas.}$ was corrected for absorption by molecular oxygen by using equation (6-46). The molecular absorption coefficient, $k_m(1152\ \text{Å})$, was actually deduced from the work of Watanabe (Wa 58) and was found to be 32.4 cm$^{-1}$. Finally, as shown in the last column of Table VI-4, the value of

| Argon (Torr) | Oxygen (Torr) | OI 1152 Å | | | | OI 6300 Å | |
|---|---|---|---|---|---|---|---|
| | | $\frac{I_L}{I_\ell}$ meas. | $\frac{I_L}{I_\ell}$ at. | $k_o\ell$ | $k_o$ ($cm^{-1}$) | $C_P/C_L$ ($\times 10^{-5}$) | $A_{ij}$ ($\times 10^{-3}$) ($sec^{-1}$) |
| 35 | 1.25 | 1.050 | 1.195 | 4.20 | 0.33 | 3.46 | 4.54 |
| 35 | 1.25 | 1.061 | 1.207 | 3.85 | 0.30 | 3.57 | 5.15 |
| 35 | 1.50 | 1.054 | 1.249 | 3.00 | 0.23 | 2.89 | 5.44 |
| 35 | 1.50 | 1.052 | 1.247 | 2.93 | 0.23 | 2.03 | 3.82 |
| 30 | 1.25 | 1.062 | 1.209 | 3.80 | 0.29 | 3.82 | 5.70 |
| 30 | 1.25 | 1.060 | 1.206 | 3.88 | 0.30 | 3.65 | 5.27 |
| 30 | 1.50 | 1.058 | 1.253 | 2.93 | 0.22 | 2.79 | 5.48 |
| 30 | 1.50 | 1.063 | 1.260 | 2.83 | 0.22 | 2.90 | 5.70 |
| 25 | 1.25 | 1.048 | 1.193 | 4.26 | 0.33 | 4.82 | 6.32 |
| 25 | 1.25 | 1.066 | 1.213 | 3.70 | 0.29 | 4.75 | 7.09 |
| 25 | 1.50 | 1.067 | 1.264 | 2.79 | 0.22 | 3.07 | 6.04 |
| 25 | 1.50 | 1.063 | 1.260 | 2.86 | 0.22 | 3.45 | 6.79 |
| Mean | | | | | | | 5.61 ± 0.94 |

Table VI-4. Results on the absolute transition probability of the red forbidden OI line at λ6300 Å.

A(6300 Å) would be given by

$$A(6300\ \text{Å}) = \frac{43.25}{k_o} \cdot \frac{C_F}{C_L} \quad \text{sec}^{-1}$$

and the mean

$$A(6300\ \text{Å}) = 5.61 \times 10^{-3} \pm 0.94 \quad \text{sec}^{-1}$$

(f) Error Estimation for A(6300 Å)

The overall error involved here is around the same as that estimated for the green line, i.e. $\leq \pm 30\%$, if it were not for the additional uncertainty introduced by the value of the molecular absorption $k_m$ at 1152 Å. The latter was deduced from Watanabe's results (Wa 58) whose degree of uncertainty depended on the reliability of his photoelectric recordings. This type of uncertainty generally has an upper limit of 10%, so that the overall error on the A-value of OI 6300 Å would be ±33%, giving the result

$$A(6300\ \text{Å}) = 5.61 \pm 1.87$$

Again here, the standard deviation of ±0.94, obtained in the 12 runs, was still well within the estimated overall error.

(g) Obtaining the $k_m$-Value of Oxygen at λ1152 Å from the Current Results

The molecular absorption coefficient ($k_m$) of oxygen at λ1152 Å was found to be 32.4 $cm^{-1}$ from Watanabe's results (obtained from upper atmospheric observations), whereas in Metzer and Cook's results (obtained from laboratory observations) it was found to be around 200 $cm^{-1}$. Such a wide discrepancy can but cast doubt as to whether the choice of Watanabe's results in the determination of A(6300 Å) was indeed the right one. Consequently, to ascertain that a reasonable choice was made; the procedure by which Table IV-4 was established, was here reversed by assuming initially the best available theoretical A-value of OI 6300 Å (= $6.29 \times 10^{-3}$ $sec^{-1}$), which is the mean of those obtained by Garstang (Ga 51) and Yamanouchi and Horie (Ya 52), and then substituting it into the present measurements; the $k_m$-values for each run were then computed from a program that also incorporated the correction factors defined in equation (6-45) or (6-46), the results being as shown in Table VI-5. The resulting mean $k_m$-value for oxygen at 1152 Å turned out to be 45.0 $cm^{-1}$ ± 7.1, which is much nearer to Watanabe's rather than Metzer and Cook's result, thus supporting the current choice for the $k_m$-value.

| Argon (Torr) | Oxygen (Torr) | OI 6300 Å | | OI 1152 Å | | | | |
|---|---|---|---|---|---|---|---|---|
| | | Mean A(6300 Å) ($sec^{-1}$) | $C_P/C_L$ ($\times 10^{-5}$) | $k_o$ ($cm^{-1}$) | $k_o \ell$ | $\left(\frac{I_L}{I_\ell}\right)$ at. | $\left(\frac{I_L}{I_\ell}\right)$ meas. | $k_m$ ($cm^{-1}$) |
| 35 | 1.25 | $6.29 \times 10^{-3}$ | 3.46 | 0.24 | 3.10 | 1.243 | 1.050 | 53.5 |
| 35 | 1.25 | | 3.57 | 0.25 | 3.22 | 1.236 | 1.061 | 49.0 |
| 35 | 1.50 | | 2.89 | 0.20 | 2.58 | 1.280 | 1.054 | 42.8 |
| 35 | 1.50 | | 2.03 | 0.14 | 1.81 | 1.370 | 1.052 | 60.8 |
| 30 | 1.25 | | 3.82 | 0.26 | 3.35 | 1.229 | 1.062 | 47.0 |
| 30 | 1.25 | | 3.65 | 0.25 | 3.22 | 1.236 | 1.060 | 49.2 |
| 30 | 1.50 | | 2.79 | 0.19 | 2.45 | 1.291 | 1.058 | 44.0 |
| 30 | 1.50 | | 2.90 | 0.20 | 2.58 | 1.280 | 1.063 | 41.8 |
| 25 | 1.25 | | 4.82 | 0.33 | 4.26 | 1.193 | 1.048 | 42.6 |
| 25 | 1.25 | | 4.75 | 0.33 | 4.26 | 1.193 | 1.066 | 38.0 |
| 25 | 1.50 | | 3.07 | 0.21 | 2.71 | 1.269 | 1.067 | 37.8 |
| 25 | 1.50 | | 3.45 | 0.24 | 3.10 | 1.243 | 1.063 | 33.8 |
| Mean | | | | | | | | $45.0 \pm 7.1$ |

Table VI-5. Results on the molecular absorption coefficient $k_m$ of OI 1152 Å, assuming a mean A(OI 6300 Å) of $6.29 \times 10^{-3}$ $sec^{-1}$.

(h) Obtaining the f-Value of OI 1152 Å from the Current Results

The most recent and accurate f-value of OI 1152 Å was found to be 0.11 ± 20% in the measurements of Ott (Ot 71) and 0.101 ± 10% in those of Lin et al. (Li 72). Here, assuming the mean theoretical A-value of OI 6300 Å ($= 6.29 \times 10^{-3}$) obtained from the references (Ga 51) and (Ya 52) and substituting it into the current measurements, we would obtain, for each run,

$$f = \frac{k_o}{(C_F/C_L)} \times 1.47 \times 10^3$$

The resulting mean value of f(1152 Å) was then found to be 0.116 ± 0.024.

(i) The Absolute Transition Probability of the Forbidden [OI] Line at λ6364 Å

The two red oxygen forbidden lines [OI] 6300 Å and [OI] 6364 Å have a common parent state in $2p^4\ {}^1D_2$, so that, by comparing their intensities under the same overall conditions one can obtain the ratio of their A coefficients.

The [OI] 6364 Å line (also known as a red auroral line) was too weak to observe side-on from the discharge tube; the intensity comparison was therefore carried out by observing the lines end-on. However, unlike the [OI] 2972 Å line the forbidden line at λ6364 Å could be photographed.

The spectrogram shown in Fig. 6-11 illustrates the green (λ5577 Å) and the red (λ6300/64 Å) forbidden lines, taken on a strip of Kodak film EH-135 and with a 45 minutes exposure; the discharge mixture, consisting of 1.50 torr oxygen and 30 torr argon, was run at a constant current of 90 mA.

To obtain the intensity ratio I(6364 Å)/I(6300 Å) the response of the Spex monochromator and detection system at these wavelengths was calibrated as explained in section 5.3(g). The peaks of their photon-counted profiles were compared for six different argon-oxygen mixtures. The final results on the true intensity ratio are as shown in Table VI-6.

Table VI-6. Results on the true intensity ratio I(6364 Å)/I(6300 Å).

| Mixture Number | $\frac{C'(6364\ Å)}{C'(6300\ Å)}$ | $\frac{I(6364\ Å)}{I(6300\ Å)}$ | Mean $\frac{A(6300\ Å)}{A(6364\ Å)}$ |
|---|---|---|---|
| 1 | 0.331 | 0.331 | |
| 2 | 0.329 | 0.329 | |
| 3 | 0.310 | 0.310 | |
| 4 | 0.340 | 0.340 | 0.32 ± 0.01 |
| 5 | 0.306 | 0.306 | |
| 6 | 0.315 | 0.315 | |

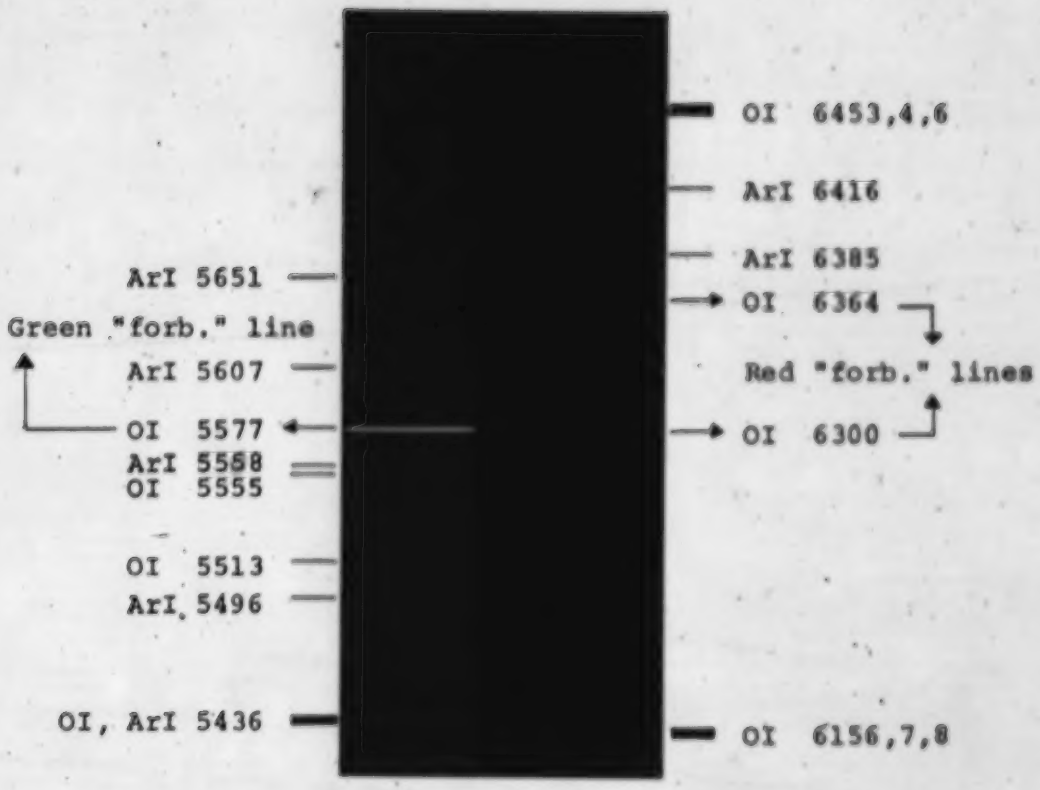


Fig. 6-11. Photographs of the green (5577 Å) and the red (6300/64 Å) forbidden lines of oxygen.

Since the responses at 6300 Å and 6364 Å are equal to the extent where they cannot be exactly distinguished, their z-value (see equation 6-32) is therefore unity and the values in the second and third columns of Table VI-6 would then be equal. We would then obtain, as denoted in the fourth column,

$$\text{Mean } \frac{A(6364\ \text{Å})}{A(6300\ \text{Å})} = 0.32 \pm 0.01$$

However, from the previous result,

$$A(6300\ \text{Å}) = (5.61 \pm 0.94) \times 10^{-3}\ \text{sec}^{-1}$$

$$\therefore A(6364\ \text{Å}) = (1.80 \pm 0.36) \times 10^{-3}\ \text{sec}^{-1}$$

Allowing an upper limit of ±10% error in the intensity ratio measurements, we would then obtain

$$\frac{A(6364\ \text{Å})}{A(6300\ \text{Å})} = 0.32 \pm 0.03$$

Adding the ±10% uncertainty to the previous ±33% error estimated for A(6300 Å), we would finally obtain

$$A(6364\ \text{Å}) = (1.80 \pm 0.62) \times 10^{-3}\ \text{sec}^{-1}$$

Again here, as for I(5577)/I(2972), the constancy of the ratio I(6364)/I(6300) indicates the absence of collisional stimulation in the $^1D$ level, i.e. the measured 6300 Å line intensity did correspond to photons arising from spontaneous emission only.

In Table VI-7, the comparison between the various

| REFERENCE | A(6300) | A(6364) | $\frac{A(6364)}{A(6300)}$ | $\frac{A(6300)+}{A(6364)}$ |
|---|---|---|---|---|
| Theoretical | | | | |
| Condon (Co 34) | 7.5 | 2.5 | 0.33 | 10.0 |
| Pasternack (Pa 40) | 7.8 | 2.6 | 0.33 | 10.4 |
| Garstang (Ga 51) | 6.9 | 2.2 | 0.32 | 9.1 |
| Yamanouchi and Horie (Ya 52) | 5.69 | 1.85 | 0.325 | 7.54 |
| Experimental | | | | |
| Kvifte and Vegard (Kv 47) | - | - | 0.33 | - |
| Omholt (Om 60) | - | - | - | 5.3 |
| Stoffregen and Derblom (St 60b) | - | - | - | 8.3 |
| McConkey et al. (Mc 66) | - | - | 0.33 | - |
| Present work | 5.61±1.87 | 1.80±0.62 | 0.32±0.03 | 7.41 |

Table VI-7. Theoretical and experimental results for the forbidden A-values of [OI] lines at λλ6300 and 6364 Å (in $sec^{-1} \times 10^{-3}$).

experimental and theoretical values that have been previously reported for the A-coefficients of [OI] 6300 Å and [OI] 6364 Å and the present experimental results is summarized. Stoffregen and Derblom (St 60b) and Omholt (Om 60) estimated the lifetime of the $^1D_2$ level from studies of aurorae, while the ratio A(6364)/A(6300) was measured in the laboratory by Kvifte and Vegard (Kv 47) and McConkey et al. (Mc 66). The theoretical results were all based on the perturbation method described in section 2.6.

Thus, to date the only determination made on the A-coefficients of the red forbidden lines was based on a perturbation theory. However, in these theoretical calculations, which were done about 20 years ago, it is acknowledged (see comments on section 2.6(a)) that the correct wavefunctions were not used - only a few pertinent wavefunctions were then available and there were no electronic computers as nowadays to deduce them. Consequently, the size of the error involved in these theoretical A-coefficients was not estimated. As mentioned previously, the more sophisticated NCMET method of Sinanoğlu and co-workers has not yet been applied to the red forbidden lines. Thus, the present experimental A-coefficients on both those lines are in fact the first ever reported and their agreement to the limited theoretical and experimental results previously reported appears satisfactory (Table VI-6).

(j) Obtaining the "Deactivation Probabilities" of the Metastable $^1S$ and $^1D$ Oxygen Atoms in the Upper Atmosphere

In the upper atmosphere, the lifetime $\tau(t)$ of the metastable $^1S$ and $^1D$ states are constantly being modified by collisional deactivation through neighbouring atoms, molecules and electron. The rate of population change of the metastable level (whose initial density is $N_i$), is given by

$$\frac{dN_i}{dt} = Q(t) - \frac{1}{\tau(t)} N_i \qquad (6\text{-}47)$$

where Q is the excitation rate of the metastable level at the time t; and $\tau(t)$ is given by

$$\frac{1}{\tau(t)} = [\sum_j A_{ij} + D_i(t)] \qquad (6\text{-}48)$$

where $D_i(t)$ is the collisional deactivation probability of the metastable level at the time t; and $\sum_j A_{ij}$ is the sum of the spontaneous transition probabilities from the metastable level to its lower ones.

Case with $^1S$ Atoms:

$$\sum_j A_{ij} = A(5577) + A(2972) + A(2958)$$

where A(2958) is negligible as compared to A(2972). Thus, using the current results,

$$\sum_j A_{ij} = 1.06 + 0.045 = 1.05 \text{ sec}^{-1}$$

Also, using the result for the lifetime of $^1S$ at a certain instant t, such as one of those measured by Omholt (Om 56)

i.e. $$\tau(t) = 0.7 \text{ sec}$$

Then, substituting in equation (6-48), we obtain

$$\frac{1}{0.7} = 1.105 + D_i(t)$$

or, $$D_i(t) = 0.32 \text{ sec}^{-1}$$

Similarly, the deactivation probabilities of the $^1D$ level at any instant t can be deduced from our results. It may be noticed here that $D_i(t)$ may be a negative value, in which case we have a collisional stimulation.

(k) Obtaining the Oxygen Abundance in the Solar Atmosphere from the Present Results

A crucial test for theories on the formation of elements from protons and neutrons and thus on the composition of stars and galaxies, is that obtained by comparing the predicted relative elemental abundances with those observed in astrophysical sources. The exciting developments now taking place in this type of work make it imperative to determine accurately these abundances. The sun, of course, is the most obvious object for these investigations, and its composition presumably corresponds to that of the solar system at the time it was formed.

The obstacles which can bar the way to a quantitative determination of solar elemental abundances are numerous; they are described in detail by Goldberg et al. (Go 60). However, since the development of the curve-of-growth method, which can now make use of accurate photometric measurements of equivalent widths and improved f-values, the reliability of the abundance results has been largely improved.

The main discrepancy involved in the curve-of-growth method lies, as mentioned in Chapter I of this thesis, in the solar model atmospheres that were assumed. Thus, forbidden lines, which have the advantage of being less sensitive to the turbulence and damping constants - parameters which differ among the various model atmospheres - are frequently employed together with allowed lines, in the determination of the solar abundances. However, these forbidden lines, which may be present in the solar spectrum, are usually faint and/or blended and thus can also introduce a source of uncertainty in the final results.

Like many others, Müller et al. (Mü 68) derived the oxygen abundance in the solar atmosphere by iteration from the observed equivalent widths of the forbidden lines at λλ5577, 6300 and 6364 Å and other weak and strong allowed lines. However, unlike other workers, they seem

to have undertaken a more thorough analysis in that their observations were made at several positions on the solar disk ($\mu$ = 1.0, 0.7, 0.5, 0.4 and 0.3), and moreover they applied three models - Holweger (Ho 67), Mutslecner (Mü 64) and Utrecht (He 64) - to their data. The results of their center-to-limb analysis of the solar oxygen lines are collected in Tables VI-8, IV-9 and VI-10. These abundances were normalised to that of hydrogen, log $N_H$ = 12.00. The values followed by (:) were due to larger random scatter of the measured equivalent widths and were given a half weight when the values were averaged out. The last column of each table lists the mean of the abundances for each line across the solar disk. For the forbidden lines these abundances were obtained with the A-values calculated by Garstang (Ga 51) whereas those inside the brackets are obtained when the current results on the forbidden A-values are applied.

Thus, the mean of the oxygen abundances, applying the same weight to individual lines as Müller et al. (Mü 68), is (in this work) 8.84, 8.93 or 8.88 for the models of Holweger, Mutslecner or Utrecht respectively. As the Holweger model was found to provide the best fit to the observed profiles of the OI lines both at the centre and near the limb, the oxygen abundance value log N = 8.84 is therefore considered as the most reliable of the three.

Some results on the oxygen abundance, which were

| λ(Å) | log N | | | | | log N |
|---|---|---|---|---|---|---|
| | μ = 1.0 | 0.7 | 0.5 | 0.4 | 0.3 | |
| 7772 | 8.78 | 8.80 | 8.80 | 8.88 | 8.88 | 8.85 |
| 7774 | 8.72 | 8.73 | 8.75 | 8.80 | 8.91 | 8.78 |
| 7775 | 8.67 | 8.69 | 8.69 | 8.75 | 8.83 | 8.73 |
| 6157 | 8.90: | 9.00: | 9.09: | 9.22: | 9.35: | 9.11: |
| 6158 | 8.76 | 8.69 | 8.77 | 8.89 | 9.03 | 8.83 |
| 6364 | 8.81:(8.90) | 8.73:(8.82) | 8.76:(8.85) | 8.72:(8.81) | 8.81:(8.90) | 8.77:(8.86) |
| 6300 | 8.81 (8.90) | 8.72 (8.81) | 8.71 (8.80) | 8.69 (8.78) | 8.70 (8.79) | 8.73 (8.82) |
| 5577 | 9.10:(9.18) | 9.11:(9.19) | 9.12:(9.20) | 9.04:(9.12) | 9.10:(9.18) | 9.09:(9.17) |
| Weighted Mean | | | | | | 8.83 (8.84) |

Table VI-8. Oxygen abundance results (Holweger Model).

| λ(Å) | log N | | | log N |
|---|---|---|---|---|
| | μ = 1.0 | 0.5 | 0.3 | |
| 7772 | 8.85 | 9.00 | 9.10 | 8.98 |
| 7774 | 8.78 | 8.91 | 9.04 | 8.91 |
| 7775 | 8.73 | 8.84 | 8.95 | 8.84 |
| 6157 | 9.19: | 9.19: | 9.41: | 9.17: |
| 6158 | 8.87 | 8.87 | 9.09 | 8.91 |
| 6364 | 8.75:(8.84) | 8.75:(8.84) | 8.77:(8.86) | 8.76:(8.85) |
| 6300 | 8.71 (8.80) | 8.71 (8.80) | 8.68 (8.77) | 8.71 (8.80) |
| 5577 | 9.12:(9.20) | 9.12:(9.20) | 9.14:(9.22) | 9.12:(9.20) |
| Weighted Mean | | | | 8.90 (8.93) |

Table VI-9. Oxygen abundance results (Mutschlecner Model).

| λ(Å) | log N | | | log N |
|---|---|---|---|---|
| | μ = 0.10 | 0.5 | 0.3 | |
| 7772 | 8.92 | 8.93 | 8.98 | 8.94 |
| 7774 | 8.86 | 8.88 | 8.93 | 8.89 |
| 7775 | 8.81 | 8.81 | 8.85 | 8.82 |
| 6157 | 8.93: | 9.12: | 9.36: | 9.14: |
| 6158 | 8.78 | 8.79 | 8.98 | 8.85 |
| 6364 | 8.79:(8.88) | 8.65:(8.74) | 8.72:(8.81) | 8.72:(8.81) |
| 6300 | 8.77 (8.86) | 8.63 (8.72) | 8.62 (8.71) | 8.67 (8.76 |
| 5577 | 9.19:(9.27) | 8.06:(9.14) | 9.09:(9.17) | 9.11:(9.19) |
| Weighted Mean | | | | 8.87 (8.88) |

Table VI-10. Oxygen abundance results (Utrecht Ref. Model).

obtained from observations made on both allowed and forbidden lines are shown in Table VI-11. Most of the authors used the A-values of Garstang in their calculations.

| Authors | Log N |
|---|---|
| Cabannes and Dufay (Ca 48) | 8.73 |
| Claas (Cl 51) | 8.65 |
| Goldberg et al. (Go 60) | 8.96 |
| Swings (Sw 66) | 9.00 |
| Müller et al. (Mü 68) | 8.83 |
| Malia (Ma 68) | 7.80 |
| Present work | 8.84 |

Table VI-11. Oxygen abundance results from various authors.

The different abundance results obtained are generally due to the different measured equivalent widths, models and weighted means employed by each author. Thus, using the forbidden A-values obtained from the current results, the mean oxygen abundance was found to be 8.84, which deviates by < 5% from the mean of the other six results shown in Table VI-11.

## SULPHUR RESULTS

### 6.5 The Spectra

The simplified term scheme shown in Fig. 6-12 illustrates the forbidden and allowed transitions of SI that were of interest in this project. The A-value of [SI] 4589 Å was determined by measuring its absolute intensity and simultaneously carrying out the optical absorption experiment on SI 1782 Å.

As for [SI] 7725 Å, its A-value was obtained from a measurement of its intensity relative to that of [SI] 4589 Å, since both of these forbidden lines have a common $3p^4\ {}^1S_0$ parent level. Unfortunately, the other forbidden transitions in [SI] which occur around 11,000 Å are not accessible to our detection system.

### 6.6 Results and Analysis on the Forbidden Lines of Atomic Sulphur at λλ4589 and 7725 Å

#### (a) Laboratory Production of [SI] 4589 and 7725 Å

To produce these forbidden lines, the procedure mentioned in section 5.1, was followed rigorously. These lines were, in fact, produced only over a limited range of pressures and/or currents, and with krypton being used as the buffer gas. Using a discharge tube that was slightly different in dimensions to that shown in Fig. 3-2, current

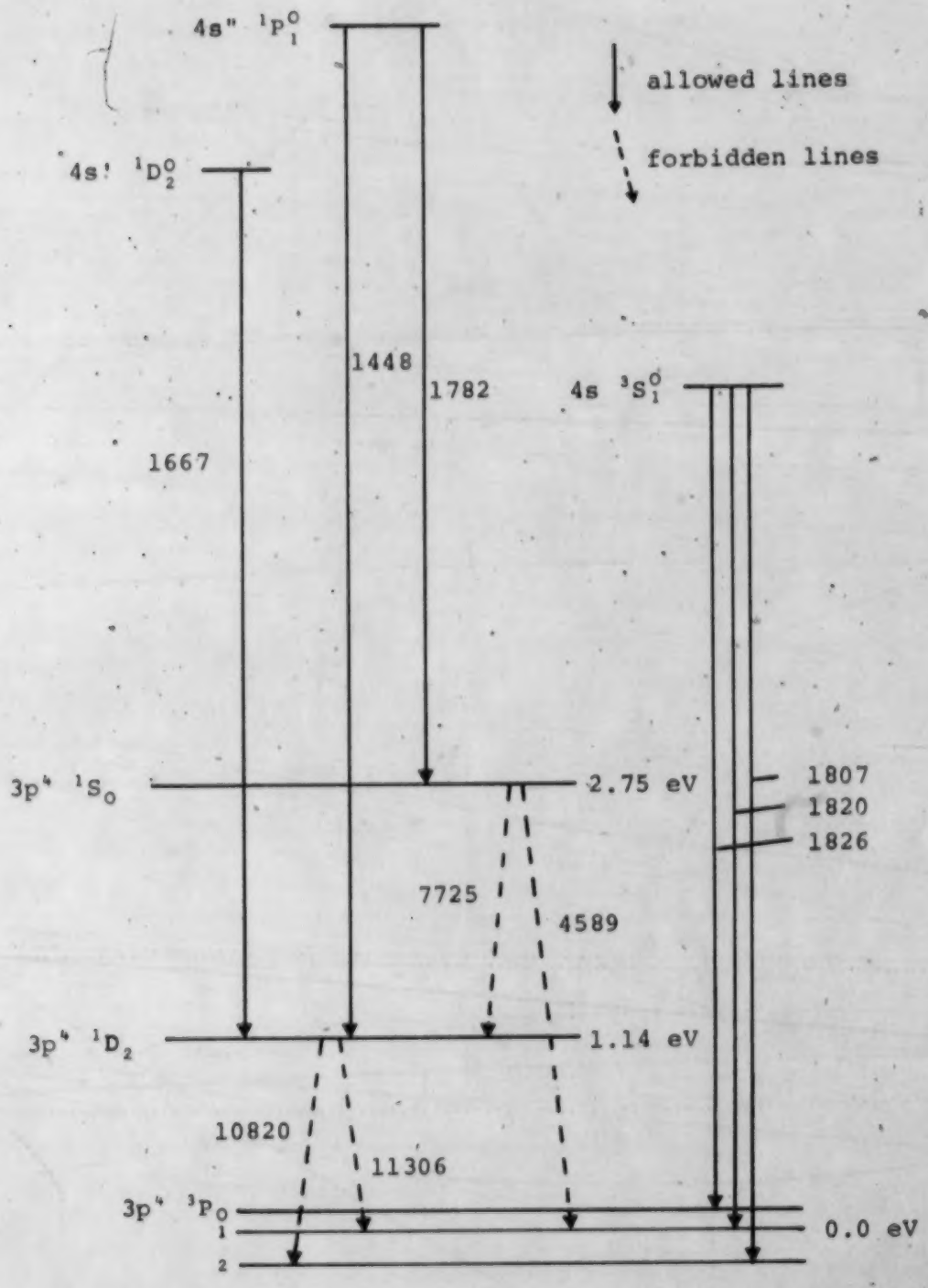


Fig. 6-12. Partial term scheme of SI (not to scale).

levels of 15 to 30 mA and pressures of 3 to 8 torr of krypton were used in the excitation of the S($^1$S) metastable states.

Below these current and pressure limits, the forbidden lines were found to be too weak for meaningful measurements, whereas above them, these lines were blended with molecular $S_2$ bands. Fig. 6-13a illustrates these features around [SI] 4589 Å in a 30 torr krypton-sulphur discharge mixture. Furthermore, under the high-pressure condition, the discharge became "cored" and the lines were found to diminish in intensity as the current was increased (see Fig. 6-13b).

(b) Processes Involved in the Production of the Metastable S($^1$S) Atoms and the Corresponding Forbidden Lines

It is believed here that the production mechanism of the S($^1$S) atoms is analogous to that proposed in section 6.3(b) for the O($^1$S) atoms, i.e. with the main process involving the photodissociation of an excited $S_2$ molecular state. Thus, as in $O_2$, to determine the unknown state(s) whose dissociation products include the $^1$S atoms, a knowledge of the dissociation limits of $S_2$ would be essential, besides the usual consideration of Wigner-Witmer rules, the ordinary Selection rules and energy resonance, in the elimination of the other possible mechanisms.

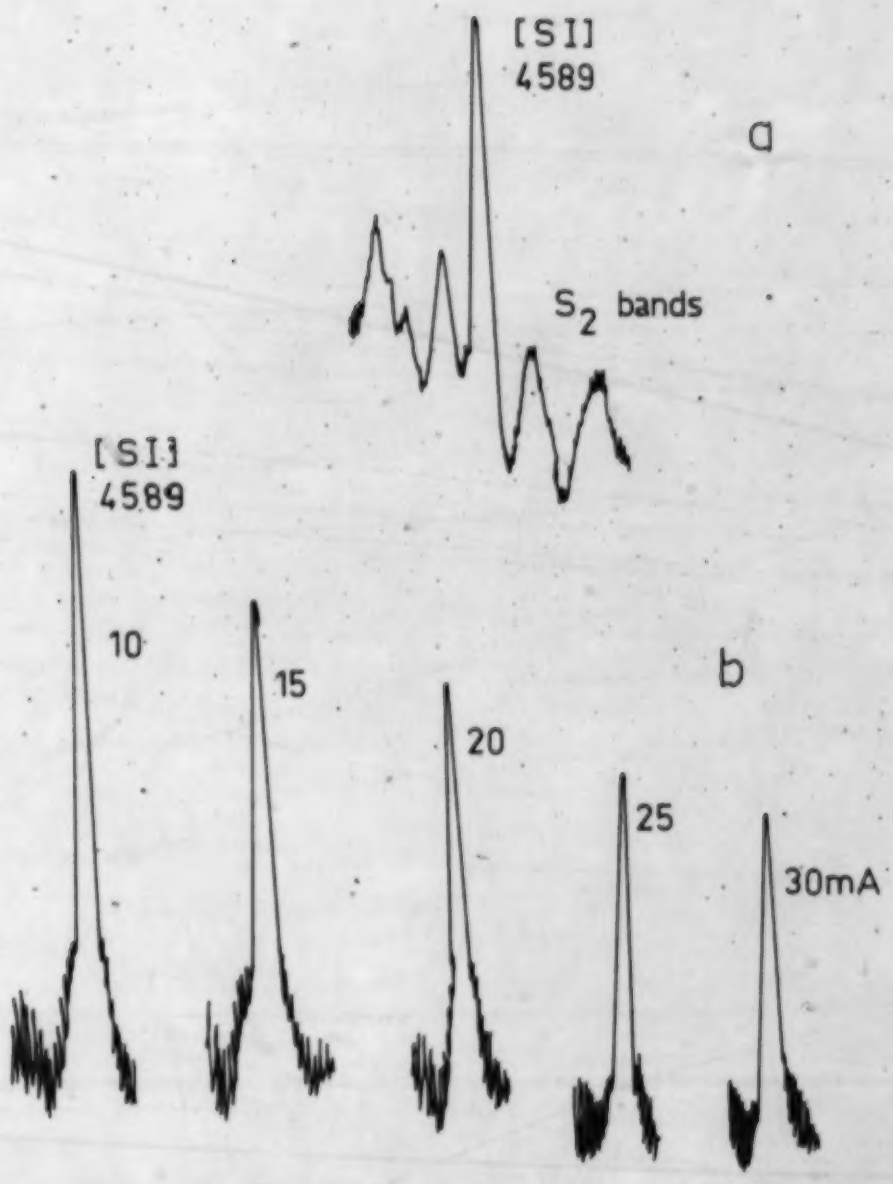


Fig. 6-13. The forbidden [SI] line at λ4589 Å in a high-pressure (30 torr krypton) discharge medium:
(a) [SI] 4589 blended by molecular $S_2$ bands.
(b) [SI] 4585 decreasing with current increase.

Since the dissociation limit for the ground state $S_2(X\ ^3\Sigma_g^-)$ is 4.4 eV and the atomic energy levels of $S(^1S)$ and $S(^1D)$ are 2.75 and 1.14 eV respectively (see Fig. 6-12), the following photodissociation processes and the corresponding dissociation limits can be written:

$$S_2(a\ ^1\Delta_g) \text{ or } S_2(X\ ^3\Sigma_g^-) + h\nu \rightarrow S(^3P) + S(^3P) + K.E. \quad (6\text{-}49)$$

(Dissociation Limit: 4.4 eV)

$$S_2(B\ ^3\Sigma_u^-) + h\nu \rightarrow S(^1D) + S(^3P) + K.E. \quad (6\text{-}50)$$

(Dissociation Limit: 5.54 eV)

$$S_2(x?) + h\nu \rightarrow S(^1S) + S(^3P) + K.E. \quad (6\text{-}51)$$

(Dissociation Limit: 7.15 eV)

$$S_2(y?) + h\nu \rightarrow S(^1S) + S(^1D) + K.E. \quad (6\text{-}52)$$

(Dissociation Limit: 8.29 eV)

As for $O_2$, the unknown state x whose dissociation products are $(^1S + ^3P)$, i.e. which satisfies equation (6-51) was found to be a $D\ ^3\Pi_u$ state. In support of this we may refer to the $^3\Pi_u - X^3\Sigma_g$ transitions which were observed in absorption by Maeder and Miescher (Ma 48). They identified three distinct dissociation continuum maxima at 1694.6, 1702.3 and 1707.9 Å, which differ energetically from the dissociation limit $(^1S + ^3P)$ by only 0.11, 0.13 and 0.17 eV respectively. Thus, it can be deduced here that the $S_2(D\ ^3\Pi_u)$ state would be unstable and that its potential curve would have a shallow minimum.

Similarly, the unknown state y whose dissociation products are ($^1S + {}^1D$), i.e. which satisfies equation (6-52), can be deduced as being a g $^1\Pi_u$ or a g $^1\Delta_u$ state. However, unlike $O_2$, no (g $^1\Pi_u$ - a $^1\Delta_u$) or (g $^1\Delta_u$ - a $^1\Delta_u$) transitions have yet been identified in absorption (or emission). The only other absorption bands so far identified are those belonging to the (5$'\Delta_u$ - a $^1\Delta_u$) transitions (Ca 70), which correspond to the dissociation pro-products ($^1D + {}^1D$).

Thus, in the present case where krypton was used as the buffer gas, the proposed mechanism for the excitation of the S($^1S$) atoms, i.e. of the forbidden [SI] lines at λλ4589 and 7725 Å, is as follows:

$$Kr(^1S) + e(v') \rightarrow Kr'' + e(v'') \qquad (6\text{-}53)$$

The excited Kr" would then excite ground state $S_2$ molecules:

$$Kr'' + S_2(X\ ^3\Sigma_g^-) \begin{cases} \rightarrow Kr' + S_2'(D\ ^3\Pi_u) & (6\text{-}54a) \\ \rightarrow Kr' + S_2'(g\ ^1\Delta_u) & (6\text{-}54b) \\ \rightarrow Kr' + S_2'(g\ ^1\Pi_u) & (6\text{-}54c) \end{cases}$$

where Kr" > Kr' > Kr($^3P_2$) ≡ metastable Kr state = 9.915 eV and, through spontaneous radiation,

$$Kr' \rightarrow Kr(^3P_2) + h\nu\ (Kr\ lines) \qquad (6\text{-}55)$$

Thus, through photodissociation:

$$S_2'(D\ ^3\Pi_u) + h\nu \rightarrow S(^1S) + S(^3P) + K.E. \qquad (6\text{-}56a)$$

$$S_2'(g\ ^1\Delta_u) + h\nu \rightarrow S(^1S) + S(^1D) + K.E. \qquad (6\text{-}56b)$$

$$S_2'(g\ ^1\Pi_u) + h\nu \rightarrow S(^1S) + S(^1D) + K.E. \qquad (6\text{-}56c)$$

Finally, through spontaneous radiation,

$$S(^1S) \rightarrow S(^3P) + h\nu \text{ (SI 4589)} \qquad (6\text{-}57a)$$

$$S(^1S) \rightarrow S(^1D) + h\nu \text{ (SI 7725)} \qquad (6\text{-}57b)$$

Production by Direct Collisions with Electrons

Besides the above processes it was found that direct collisions between energetic electrons and ground state atoms and/or molecules would represent another productive mechanism for the $S(^1S)$ atoms:

$$S(^3P) + e(v') \rightarrow S(^1S) + e(v'') \qquad (6\text{-}58)$$

$$S_2(X\ ^3\Sigma_g^-) + e(v') \rightarrow S(^3P) + S(^1S) + e(v'') \qquad (6\text{-}59)$$

In fact, the density of the metastable $^1S$ atoms or the intensity of the [SI] line at λ4589 Å was found to be linearly proportional to the electric current through an "optimum" krypton-sulphur discharge (see Fig. 6-14).

(c) SI 1782 Å

The SI line at λ1782 Å, which was used in the atomic absorption experiment was always found to be partially blended with the high wavelength side of the CO band at λ1776 Å, even for the cleanest krypton-sulphur discharge (see Fig. 6-15). This is due to the fact that

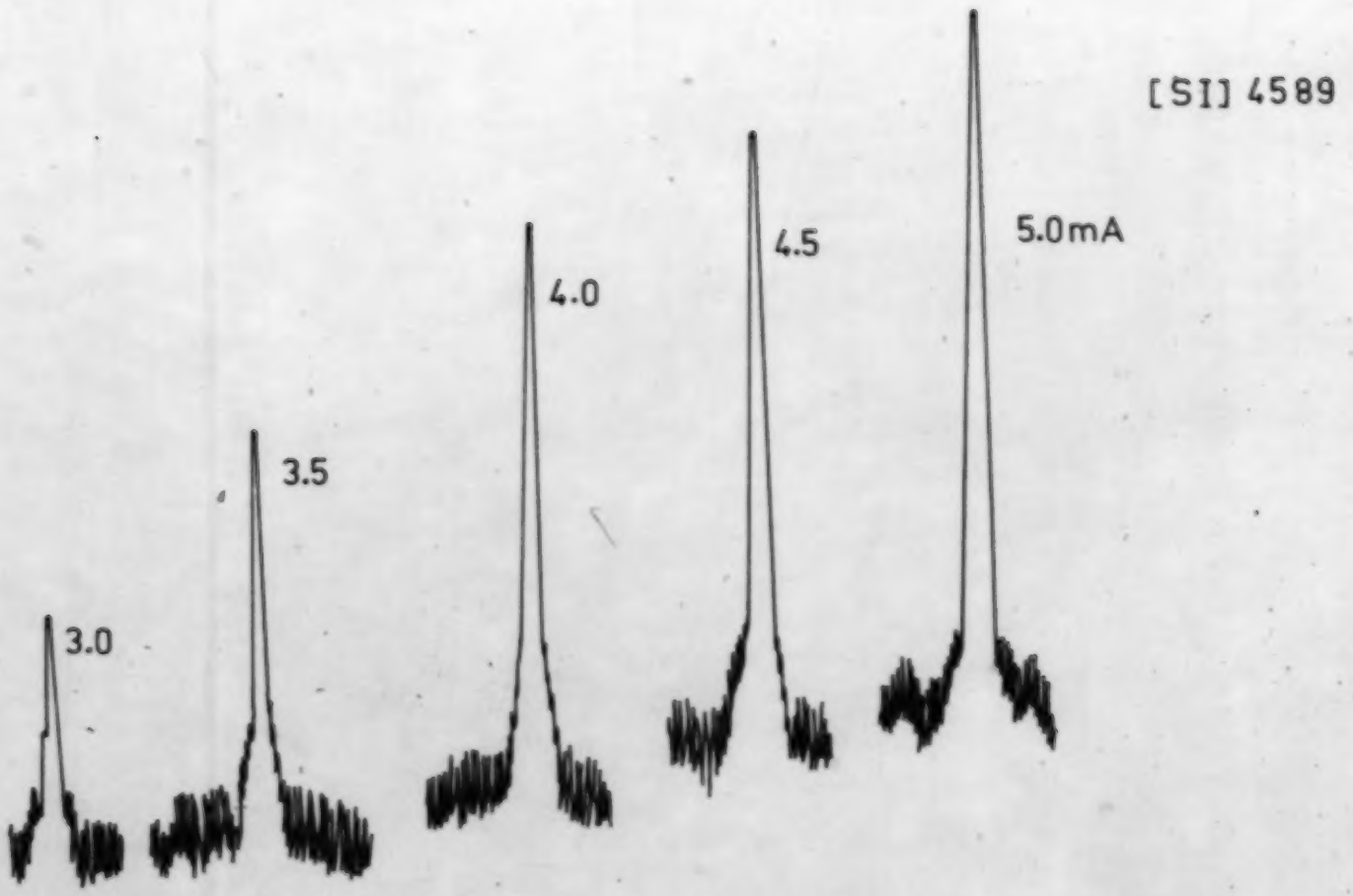


Fig. 6-14. The intensity of the forbidden [SI] line at λ4589 Å vs. the electric current supplied to an optimum sulphur-krypton discharge (5 torr of Kr).

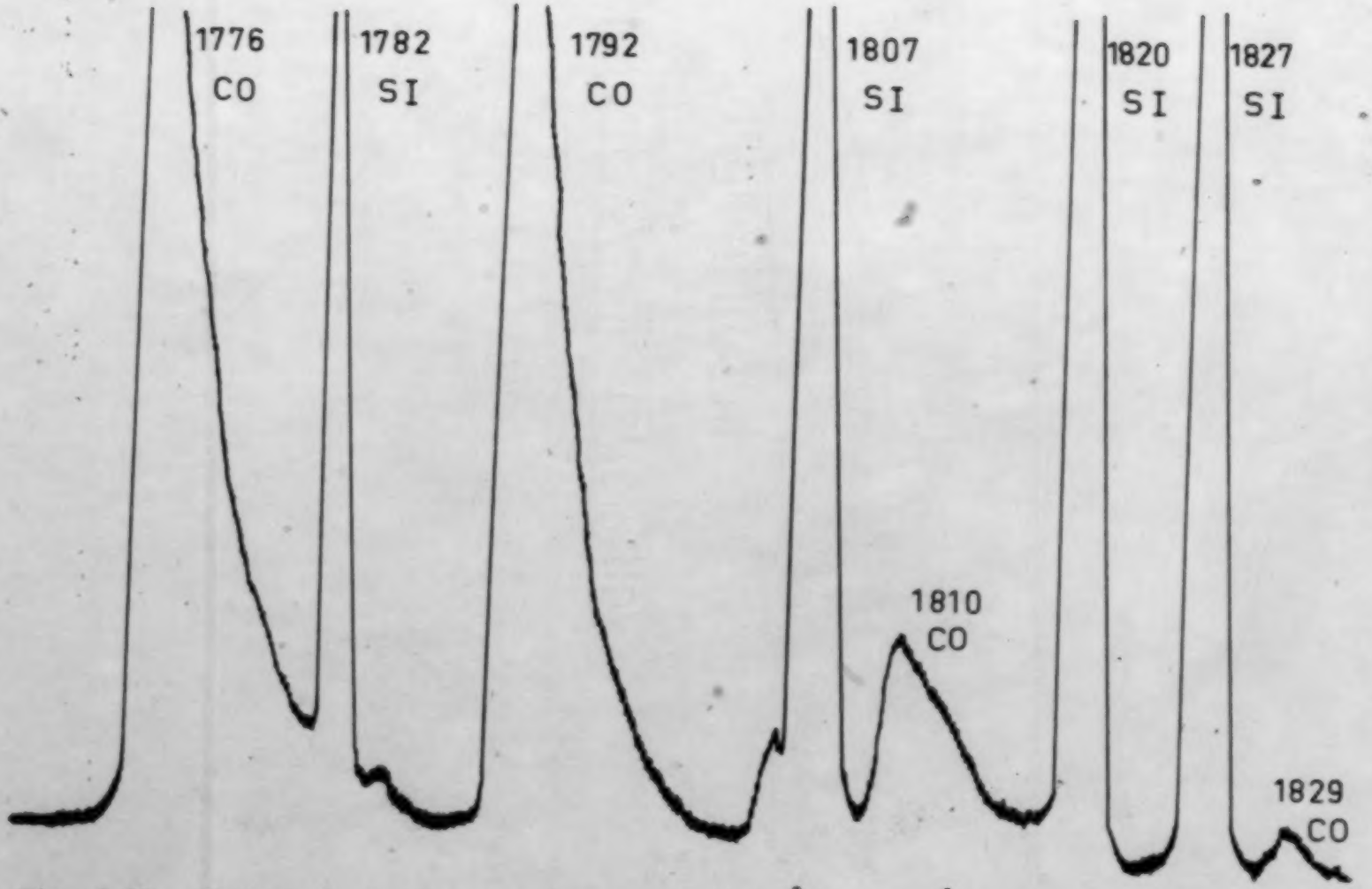


Fig. 6-15. The spectral scan of sulphur from 1770 Å to 1830 Å from a sulphur-krypton (5 torr) mixture run at 10 mA.

even the 99.9% pure sulphur powder (that was distilled into the discharge tube) was probably contaminated with a slight trace of impurity carbon. However, as explained in section 5.3(d), the intensity contribution from the impurity CO band to that of the SI line at λ1782 Å could be computed by means of a best-fit Lagrangian interpolation polynomial, and its percentage calculated. Assuming this percentage to be constant, the intrinsic intensity of SI 1782 Å was readily deduced from the total intensity measured at 1782 Å .

The $S_2$ bands in the region 1600-1870 Å were observed in absorption by Wieland et al. (Wi 34), and Maeder and Miescher (Ma 48), and in emission by Tanaka and Ogawa (Ta 62). Fortunately, there are no absorption $S_2$ bands around λ1782 Å, the nearest being at λλ1771 and 1797 Å. Thus, no correction factor, as for OI 1152 Å, was required in the intensity measurement of SI 1782 Å. Also, any molecular absorption by CO molecules was neglected here because (1) the region at λ1782 Å falls right on the wing of the CO band whose head is at 1776 Å, and (2) the low CO partial pressure would, in any case, yield a correction factor approaching unity.

A spectral scan covering the region 1770-1830 Å, which includes the CO bands, SI 1782 Å and the resonance SI lines at λλ1807, 1820 and 1826 Å, is illustrated in Fig. 6-15.

(d) The Absolute Transition Probability of the Forbidden [SI] Line at λ4589 Å

The same experimental technique as was applied to the forbidden [OI] lines has been employed for [SI] 4589 Å. The results are as shown in Table VI-12.

The pressure range of the buffer gas (krypton) used was from 3 to 8 torr and a lower current (10-30 mA), as compared to that used for oxygen (90 mA), was employed in the krypton-sulphur discharge. The values of $k_o$ (column 6) for SI 1782 Å were obtained by interpolation from a computed graph (see Fig. 4-4) that was obtained with L = 2.020ℓ . The values of $(C_P/C_L)$ in the last but one column were obtained, after deducing the $N_i$-values from equation (4-45) with the following substitutions: $\lambda = 1.782 \times 10^{-5}$, M = 64; e, m, c and R as usual, and the f-value of SI 1782 Å was taken as the weighted mean of the values obtained (theoretically through an intermediate coupling method) by Aymar (Ay 73) and (experimentally with a wall-stabilised arc) by Müller (Mü 68b), i.e. f(1782 Å) = 0.235. The other values to be substituted in equation (4-44) for obtaining $(C_P/C_L)$ were: r = 0.75 cm; L' = 7.0 cm; E(4589 Å) = $1.04 \times 10^7$ units of radiance; $(d_P/d_L)^2 = (110.8/127.9)^2$; $\lambda = 4.589 \times 10^{-5}$ and $\Delta\lambda = 2.14 \times 10^{-4}$ μ. After the final substitutions in equation (4-44), the A-values denoted in the last column of Table VI-12 would then be

| Kr (Torr) | Current (mA) | $\sqrt{T}$ ($\sqrt{°K}$) | SI 1782 Å | | | SI 4589 Å | |
|---|---|---|---|---|---|---|---|
| | | | $I_L/I_\ell$ | $k_o\ell$ | ($cm^{-1}$) | $C_F/C_L$ ($\times 10^{-4}$) | A(4589 Å) ($sec^{-1}$) |
| 8 | 17 | 19.0 | 1.282 | 2.58 | 0.17 | 1.21 | 0.26 |
| 8 | 17 | 19.0 | 1.318 | 2.20 | 0.14 | 1.17 | 0.30 |
| 8 | 17 | 19.0 | 1.302 | 2.38 | 0.16 | 1.19 | 0.27 |
| 8 | 20 | 19.2 | 1.309 | 2.30 | 0.15 | 1.31 | 0.31 |
| 8 | 20 | 19.2 | 1.244 | 3.05 | 0.20 | 1.48 | 0.27 |
| 8 | 20 | 19.2 | 1.270 | 2.70 | 0.18 | 1.51 | 0.30 |
| 8 | 23 | 19.0 | 1.248 | 3.11 | 0.20 | 1.47 | 0.27 |
| 8 | 23 | 19.0 | 1.249 | 3.10 | 0.20 | 1.40 | 0.25 |
| 8 | 23 | 19.0 | 1.251 | 3.06 | 0.20 | 1.26 | 0.23 |
| 8 | 27 | 19.3 | 1.243 | 3.20 | 0.21 | 2.49 | 0.42 |
| 8 | 27 | 19.3 | 1.224 | 3.30 | 0.23 | 2.60 | 0.40 |
| 8 | 27 | 19.3 | 1.230 | 3.35 | 0.22 | 2.40 | 0.39 |

Table VI-12. Results on the absolute transition probability of forbidden SI line at λ4589 Å. (Continued)

| Kr (Torr) | Current (mA) | $\sqrt{T}$ ($\sqrt{°K}$) | SI 1782 Å | | | SI 4589 Å | |
|---|---|---|---|---|---|---|---|
| | | | $I_L/I_\ell$ | $k_0\ell$ | $k_0$ ($cm^{-1}$) | $C_F/C_L$ ($\times 10^{-4}$) | A(4589 Å) ($sec^{-1}$) |
| 6 | 23 | 19.1 | 1.215 | 3.67 | 0.24 | 2.07 | 0.31 |
| 6 | 23 | 19.1 | 1.208 | 3.82 | 0.25 | 2.18 | 0.32 |
| 6 | 23 | 19.1 | 1.214 | 3.67 | 0.24 | 2.14 | 0.32 |
| 6 | 27 | 19.2 | 1.207 | 3.83 | 0.25 | 2.28 | 0.33 |
| 6 | 27 | 19.2 | 1.203 | 3.98 | 0.26 | 2.34 | 0.32 |
| 6 | 27 | 19.2 | 1.208 | 3.82 | 0.25 | 2.52 | 0.36 |
| 5 | 27 | 18.9 | 1.216 | 3.75 | 0.24 | 1.74 | 0.26 |
| 5 | 27 | 18.9 | 1.208 | 3.82 | 0.25 | 1.91 | 0.28 |
| 5 | 27 | 18.9 | 1.210 | 3.78 | 0.25 | 1.85 | 0.27 |
| 3 | 27 | 19.4 | 1.243 | 3.20 | 0.21 | 1.87 | 0.32 |
| 3 | 27 | 19.4 | 1.224 | 3.45 | 0.23 | 2.03 | 0.31 |
| 3 | 27 | 19.4 | 1.211 | 3.67 | 0.24 | 1.73 | 0.26 |
| Mean | | | | | | | 0.31 ± 0.05 |

Table VI-12 (continued)

$$A(4589\ \text{Å}) = \frac{6.91}{k_o \sqrt{T}} \left(\frac{C_F}{C_L}\right) \times 10^3\ \text{sec}^{-1}$$

Thus, the mean A-value of [SI] 4589 Å was found to be 0.31 with a standard deviation of ±0.05. The overall experimental error involved would be about the same as that estimated for the green forbidden OI line, i.e. $\leq$ ±30%, giving the experimental result

$$A(4589\ \text{Å}) = 0.31 \pm 0.09\ \text{sec}^{-1}$$

(e) Obtaining the f-value of SI 1782 Å from the current Results

A significant source of error that may exist in the present result on the A-value of [SI] 4589 Å comes from the f-value assumed for SI 1782 Å. We may, however, check the reliability of this f-value by reversing the procedure, i.e. by assuming initially the A-value (= 0.35 $\text{sec}^{-1}$) for [SI] 4589 Å obtained through theoretcal calculations by Czyzak and Krueger (Cz 63), and then substituting it into the current measurements. It was then found that, for each run,

$$f(1782\ \text{Å}) = \frac{1.19 \times k_o \sqrt{T}}{(C_F/C_L)} \times 10^{-5}$$

and the resulting mean f(1782 Å) = 0.28 ± 0.06.

The overall estimated error limit for this f-value would, of course, depend on the A-value obtained by Czyzak

and Krueger (Cz 63). Previous f-values obtained for SI 1782 Å were 0.20 by Müller (Mü 68), 0.27 by Aymar (Ay 73) and 0.58 by Lawrence (La 67). Thus, the f-value obtained here, is close to those of Aymar and Müller (the mean of which was here assumed in the determination of the A-value of [SI] 4589 Å.

(f) The Absolute Transition Probability of the [SI] Line at λ7725 Å

The spectrogram shown in Fig. 6-16 illustrates the forbidden [SI] lines at λλ7725 and 4589 Å, taken on hypersensitized I-N kodak plates during a three-hour exposure using a krypton-sulphur mixture run at 5 mA. Although the line at λ7725 Å is intrinsically stronger than that at λ4589 Å, on the photoelectric detection system its response was much less. In fact, it was barely detectable from the discharge tube when viewed side-on; its transition probability was therefore determined by comparing its "end-on" intensity to that of [SI] 4589 Å, since these lines have the same $3p^4\ {}^1S_0$ parent level.

After calibrating the Spex detection system at the two wavelengths and comparing the peak intensities of their photon-counted profiles for 10 different krypton-sulphur mixtures, the results shown in Table VI-13 were obtained:

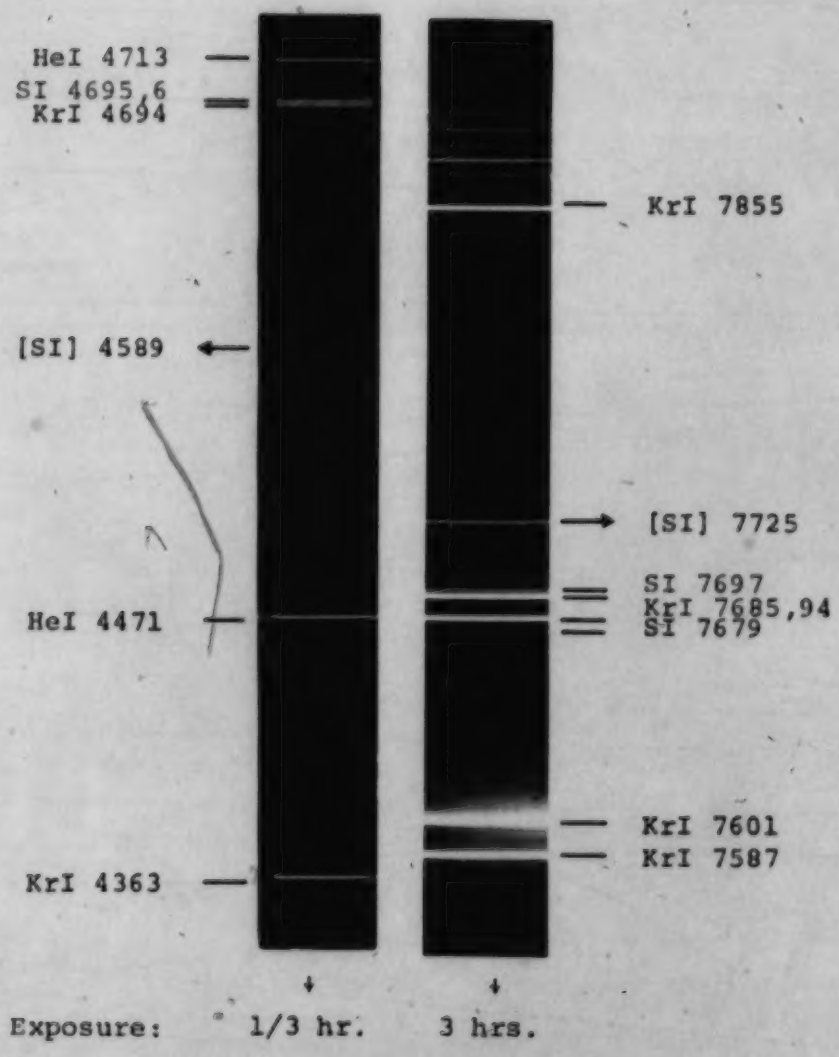


Fig. 6-16. Photographs of the forbidden [SI] lines at λλ4589 and 7725 Å from a Kr-S discharge.

| Mixture Number | $\frac{C'(7725\ \text{Å})}{C'(4589\ \text{Å})}$ | $\frac{I(7725\ \text{Å})}{I(4589\ \text{Å})}$ | Mean $\frac{A(7725\ \text{Å})}{A(4589\ \text{Å})}$ |
|---|---|---|---|
| 1 | 0.36 | 4.9 | |
| 2 | 0.36 | 4.9 | |
| 3 | 0.35 | 4.8 | |
| 4 | 0.35 | 4.8 | |
| 5 | 0.38 | 5.2 | |
| 6 | 0.34 | 4.7 | 4.9 ± 0.19 |
| 7 | 0.34 | 4.7 | |
| 8 | 0.38 | 5.2 | |
| 9 | 0.35 | 4.8 | |
| 10 | 0.38 | 5.2 | |

Table VI-13. Results on the A-ratios of the [SI] lines at λλ7725 and 4589 Å.

In this table, the values shown in the third column were obtained by dividing those in the second with the z-value (equation 6-32) obtained, which was 0.073. Thus, as shown in the fourth column,

$$\text{Mean}\ \frac{A(7725\ \text{Å})}{A(4589\ \text{Å})} = 4.9 \pm 0.19$$

However, from the previous result,

$$A(4589\ \text{Å}) = 0.31 \pm 0.09\ \text{sec}^{-1}$$

$$\therefore A(7725\ \text{Å}) = 1.52 \pm 0.28\ \text{sec}^{-1}$$

Allowing an upper limit of ±10% error in the intensity-ratio measurements, we would have

$$\frac{A(7725\ \text{Å})}{A(4589\ \text{Å})} = 4.9 \pm 0.5$$

Adding this ±10% error to the previous ±30% error estimated for A(4589 Å), we would finally obtain

$$A(7725\ \text{Å}) = 1.52\ \text{sec}^{-1}$$

with a "most probable error" ($\sqrt{30^2 + 10^2}$ %) of ± 0.49.

Futhermore, the constancy of the ratio I(7725)/I(4589) indicates here the absence of collisional stimulation, i.e. the measured 4589 Å line intensity did correspond to photons arising from spontaneous emission only.

The new A-values are compared with those from other workers in Table VI-14. The A-values obtained by Czyzak and Krueger (Cz 63) were based on Garstang's perturbation method, and the relative A-value of McConkey et al. (Mc 68) was obtained experimentally using a krypton-sulphur discharge. It can be seen that the agreement among the results is very satisfactory.

| REFERENCE | A(4589 Å) | A(7725 Å) | $\frac{A(7725\ Å)}{A(4589\ Å)}$ |
|---|---|---|---|
| Theoretical | | | |
| Czyzak and Krueger (Cz 63) | 0.35 | 1.78 | 5.09 |
| Experimental | | | |
| McConkey et al. (Mc 68) | - | - | 5.1 ± 0.7 |
| Present work | 0.31 ± 0.09 | 1.52 ± 0.49 | 4.9 ± 0.5 |

Table VI-14. Comparison of the previous and present A-values on [SI] 4589 and 7725 Å (in $sec^{-1}$).

(g) The Solar Abundance of Sulphur

The absence of precise wavelength assignments for the forbidden [SI] lines has delayed their identification in the Fraunhofer spectrum where they are blended to a great extent with several other lines and bands.

Sattarov (Sa 65) identified the [SI] line at λ4589 Å and apparently used an incorrectly assigned wavelength and equivalent width (Sw 68), whereby he obtained a solar abundance of sulphur of log $N_S$ = 8.20, as compared to that (log $N_S$ = 7.30) obtained from the permitted high-excitation lines by Goldberg et al. (Go 60). The region

around 4589 Å was scanned with the Oxford photoelectric spectrometer by Blackwell et al. (Bl 67), which indicated complex blending there. No other direct attempt has been made to find the proper equivalent width of [SI] 4589 Å; thus, no other result on the sulphur abundance based on this line, except that by Sattarov, is available.

The region at λ7725 Å was scanned at the Jungfraujoch station (Switzerland) by L. Delbouille and G. Roland (De 63). The forbidden line there was identified by Swings et al. (Sw 68) from a blended neighbourhood consisting of a SiI line and bands from $O_2$ and CN. Using the mean of the wavelengths assigned to this line by Kaufman (Ka 67) and McConkey et al. (Mc 68), Swings et al. (Sw 68) deduced a sulphur abundance of log $N_S$ = 7.10. This value was based on the A-value obtained by Czyzak and Krueger (Cz 63); using the A-value obtained in the present work, this abundance now turns out to be log $N_S$ = 7.17.

## SELENIUM RESULTS

### 6.7 The Spectra

The corresponding forbidden lines that were of interest in the SeI spectrum are illustrated in the simplified terms scheme shown in Fig. 6-17. The same technique as described in section 6.2(d) was applied in the determination of the A-value of [SeI] 4887 Å, i.e. its absolute intensity was measured, and, at the same time, the optical absorption experiment was carried on the ultraviolet line of SeI at 1994 Å which was feeding the $4p^4\ {}^1S_0$ upper level of 4487 Å.

As for the forbidden [SeI] line at λ7768 Å, its A-value was obtained by comparing its intensity to that of λ4887 Å, since these lines have the same parent level.

The absorption experiment was also applied to the SeI resonance lines at λλ1855, 1691, 2040 and 2075 Å to determine the atomic densities of the ${}^1D_0$ and $P_{0,1,2}$ levels respectively.

### 6.8 Results and Analysis on the Forbidden [SeI] Lines at λλ4887 and 7768 Å

#### (a) Laboratory Production of [SeI] 4887 Å

During the preliminary work undertaken for the production of the forbidden [SeI] lines, it was found that, if an inert gas such as helium or krypton was used as the

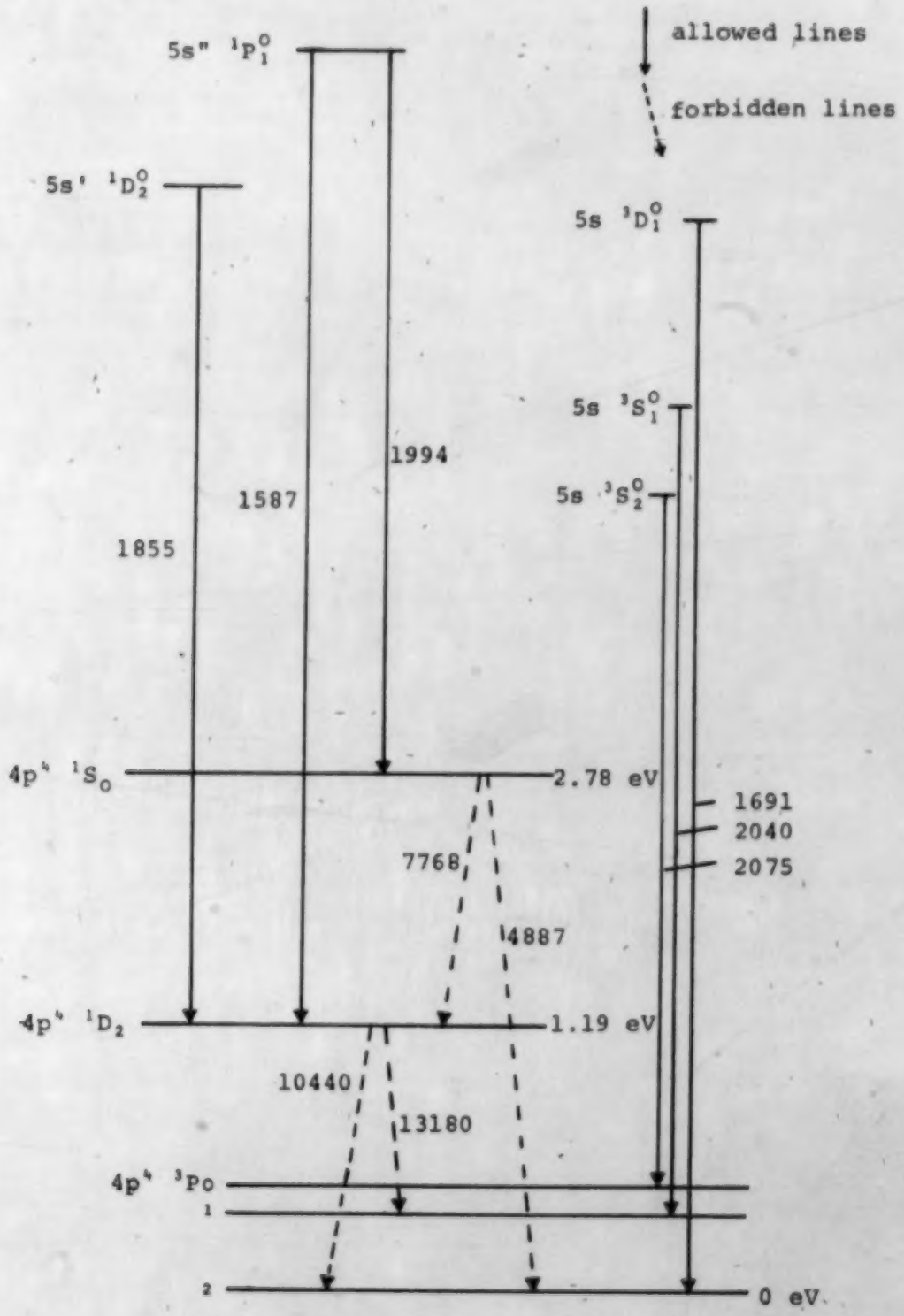


Fig. 6-17. Partial term scheme of SeI (not to scale).

buffer, these lines would not be excited. Also, although argon gave a fairly good result, neon was preferentially used because the forbidden lines appeared stronger in the Ne-Se discharge.

As in the case for sulphur, the forbidden lines of [SeI] can only be produced under limited discharge conditions for the Se-Ne mixture. First of all, when the discharge was not clean the forbidden line produced would be partially blended by impurity bands and less accuracy would then be expected in the intensity measurement - this is illustrated in the spectrograms shown in Fig. 6-18, where (a) the [SeI] line at λ4887 Å was not clearly resolved from the impurity CO bands and (b) the [SeI] line at λ4887 A was resolved in a correspondingly clean discharge. Secondly, when the neon partial pressure was relatively too high, the $Se_2$ bands would appear and partially blend the forbidden line, as illustrated in Fig. 6-19a.

Another problem involved with the intensity measurements of [SeI] 4887 Å was that, even when the discharge is optimum, this line might not be clearly resolved from the neighbouring NeI line at λ4885 Å. However, during the photon-counting of [SeI] 4887 Å, an appropriate slit width in the Spex (≃ 120 μ) was employed so that the corresponding waveband (≃ 1.3 Å) would then accept only the light coming from the [SeI] line at λ4887 Å, i.e. no intensity countribution from NeI 4885 Å would be included (see Fig. 6-19b).

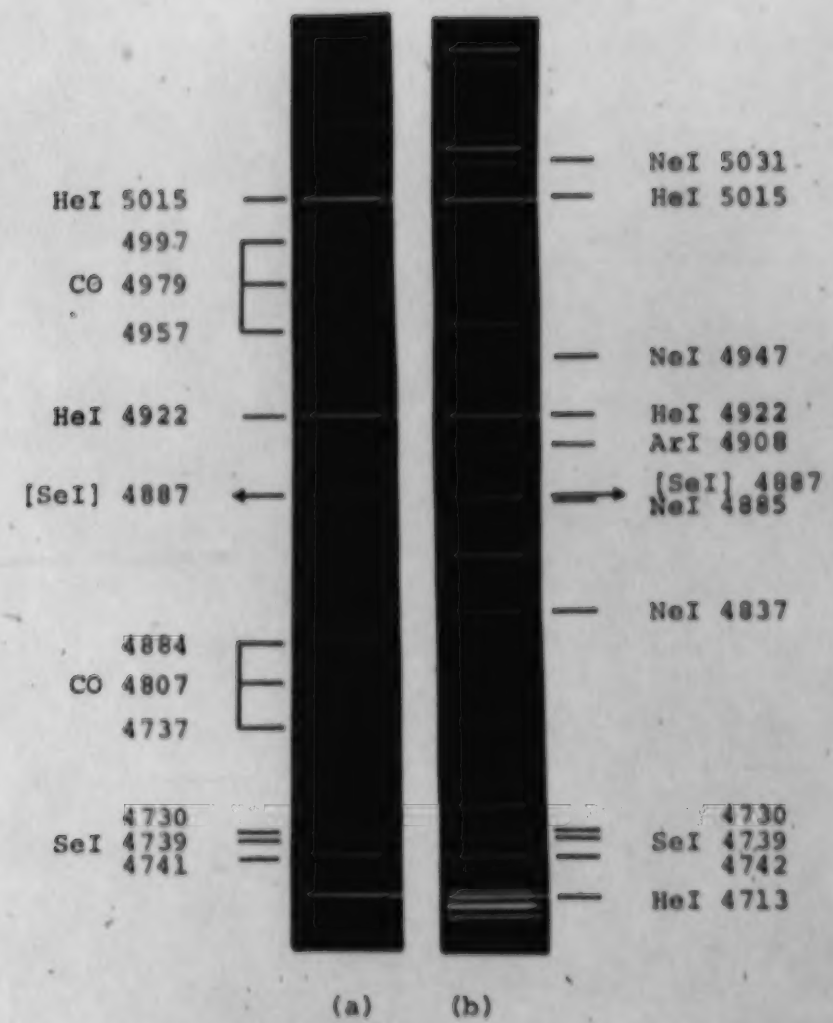


Fig. 6-18. Photographs of the forbidden [SeI] line at λ4887 Å from a Ne-Se discharge which is (a) impure and (b) clean.

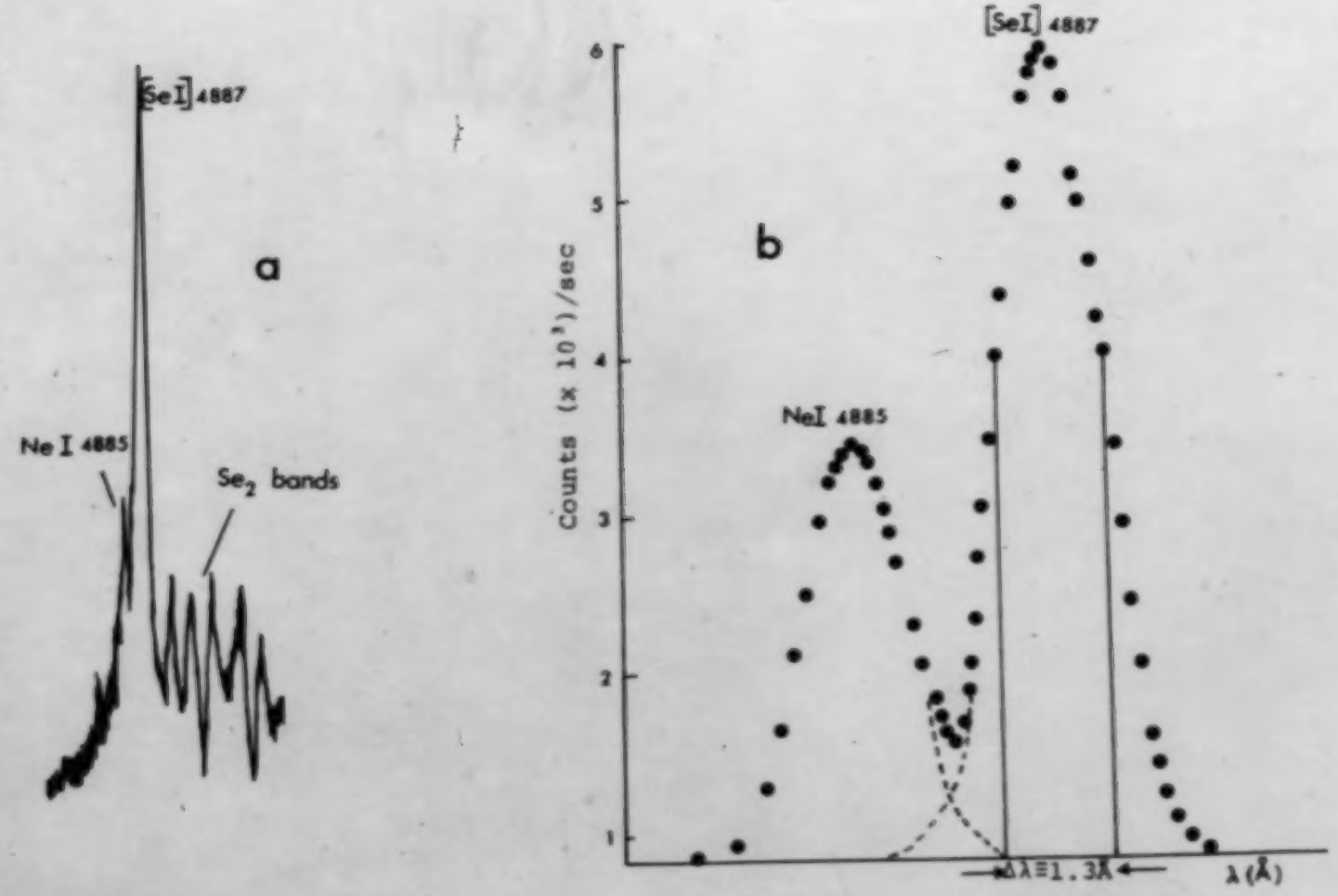


Fig. 6-19. [SeI] from a Ne-Se discharge run at 30 mA.
(a) Pen-chart profile of [SeI] 4887 with a relatively high partial neon pressure (≈ 30 torr).
(b) Photon-counting profile of [SeI]4887 through a slit width of 120 μ.

(b) Processes Involved in the Production of the Metastable Se($^1$S) Atoms

As with oxygen and sulphur, to ascertain whether the metastable $^1$S atoms of selenium are also produced through the photodissociation of excited molecular states, it was necessary to know the energy potential curves of the states and the dissociation limits, besides the ordinary Selection and Wigner-Witmer rules and the energy resonance.

Early analyses of the main band spectrum of $Se_2$, apparently indicating a $^1\Sigma$ ground state, have been reviewed by Barrow et al. (Ba 66), who found that the system is again B $^3\Sigma_u^-$ - X $^3\Sigma_g^-$, as in $O_2$ and $S_2$. The dissociation energy of $Se_2$ (i.e. the dissociation limit for ($^3$P + $^3$P) has since been established at 3.2 ± 0.1 eV. Thus the dissociation limit of ($^1$S + $^3$P) would be 5.98 eV and that of ($^1$S + $^1$D), 7.17 eV. However, the absorption spectrum and the excited $Se_2$ states with dissociation limits at ($^1$S + $^3$P) and ($^1$S + $^1$D) have not yet been subject to experimental investigation. The lack of such knowledge has prevented further discussion on the production mechanism of Se($^1$S) atoms in the present work, although a mechanism analogous to that for O($^1$S) and S($^1$S) atoms may be proposed.

Again, however, the production of Se($^1$S) atoms from direct collisions between energetic electrons and ground state atom and/or molecules was important here;

the intensity of the forbidden [SeI] line at λ4887 Å was found to be increasing linearly with the electric current through the Se-Ne discharge.

(c) SeI 1994 Å

The ultraviolet lines which could have been used in the absorption experiment for the determination of the $^1S$ state densities of selenium are situated at λλ1994, 2050, 2548 and 3501 Å. The last three lines were not used because they could not be produced with reasonable intensity in the present work; even the line at λ1994 Å was produced only after prolonged cleaning of the discharge system (see Fig. 5-3).

The f-value of the SeI line at λ1994 Å was theoretically calculated through an intermediate coupling and quantum defect method by Lawrence (La 67) and Gruzdev (Gr 69). However, Lawrence made an error in his quantum defect calculation for the configuration $np^3$ 5s (Gr 69) and so the f-value of Gruzdev (= 0.17) was used in the present work. This f-value should be good to better than ±10% since the energy levels (and wavelengths) predicted from this method agree to within 0.1% of the experimental data of some ionized lines (NeIII, MgV and AlIV) from the tables of Striganov and Sventitskii (St 66).

As in the case of the SI line, the molecular

absorption of SeI at λ1994 Å was assumed to be negligible, and no $Se_2$ bands were ever recorded in that wavelength region.

(d) The Absolute Transition Probability of the Forbidden [SeI] Line at λ4887 Å

The absolute transition probability of the [SeI] line at λ4887 Å was determined experimentally, using the same technique as for the forbidden lines of [SI] and [OI]. The results are shown in Table VI-15.

The first column of this table indicates the pressure range of neon, which was used as the buffer gas, and the discharge was run at a constant current of 30 mA through all the (26) discharge mixtures. The values of $k_o$ (column 5) for [SeI] 1994 Å were obtained by interpolation from a computed graph of $k_o\ell$ vs. $I_L/I_\ell$, where $L = 2.013\ell = 31.0$ cm. The values of $(C_F/C_L)$ in the last but one column were obtained after making the following substitutions: $\lambda = 1.994 \times 10^{-5}$ cm; M = 157.92; f(1994 Å) = 0.17, r = 1.25 cm, E(4887 Å) = $2.32 \times 10^7$ ergs/.....; $(d_F/d_L) = (101.5/124.5)$, $\Delta\lambda = 1.316 \times 10^{-4}$ μ and the other parameters were as usual. After the final substitutions in equation (4-44), the A-values denoted in the last column of Table VI-15 would then be

$$A(4887\ \text{Å}) = \frac{3.99}{k_o \sqrt{T}} \left(\frac{C_F}{C_L}\right) \times 10^3\ \text{sec}^{-1}$$

| Neon (Torr) | √T (°K) | SeI 1994 Å | | | SeI 4887 Å | |
|---|---|---|---|---|---|---|
| | | $I_L/I_\ell$ | $k_o\ell$ | $k_o$ ($cm^{-1}$) | $C_F/C_L$ ($\times 10^{-3}$) | A(4887 Å) ($sec^{-1}$) |
| 12 | 18.5 | 1.873 | 0.22 | 0.014 | 0.541 | 8.34 |
| 12 | 18.5 | 1.830 | 0.28 | 0.018 | 0.523 | 6.87 |
| 12 | 18.5 | 1.834 | 0.28 | 0.018 | 0.548 | 6.57 |
| 12 | 18.5 | 1.832 | 0.28 | 0.018 | 0.594 | 7.11 |
| 10 | 18.4 | 1.857 | 0.24 | 0.016 | 0.638 | 8.64 |
| 10 | 18.4 | 1.846 | 0.25 | 0.016 | 0.652 | 8.83 |
| 8 | 18.5 | 1.723 | 0.50 | 0.032 | 1.348 | 9.08 |
| 7 | 18.5 | 1.622 | 0.74 | 0.048 | 1.506 | 6.76 |
| 7 | 18.5 | 1.618 | 0.75 | 0.049 | 1.591 | 7.01 |
| 7 | 18.5 | 1.668 | 0.63 | 0.041 | 1.634 | 7.20 |
| 7 | 18.5 | 1.644 | 0.69 | 0.045 | 1.671 | 8.07 |

Table VI-15. Results on the absolute transition probability of forbidden SeI line at λ4887 Å. (Continued)

| Neon (Torr) | $\sqrt{T}$ (°K) | SeI 1994 Å | | | SeI 4887 Å | |
|---|---|---|---|---|---|---|
| | | $I_L/I_\ell$ | $k_0\ell$ | $k_0$ ($cm^{-1}$) | $C_F/C_L$ ($\times 10^{-3}$) | A(4887 Å) ($sec^{-1}$) |
| 6 | 18.3 | 1.506 | 1.13 | 0.073 | 2.156 | 6.44 |
| 6 | 18.3 | 1.518 | 1.07 | 0.069 | 2.205 | 6.97 |
| 6 | 18.3 | 1.480 | 1.23 | 0.080 | 2.209 | 6.02 |
| 6 | 18.3 | 1.595 | 0.80 | 0.052 | 2.124 | 8.91 |
| 4 | 18.3 | 1.406 | 1.58 | 0.103 | 2.449 | 5.18 |
| 4 | 18.3 | 1.417 | 1.50 | 0.097 | 2.340 | 5.26 |
| 4 | 18.3 | 1.416 | 1.50 | 0.097 | 2.366 | 5.32 |
| 3 | 18.4 | 1.572 | 0.89 | 0.058 | 2.434 | 9.09 |
| 3 | 18.4 | 1.465 | 1.29 | 0.084 | 2.407 | 6.24 |
| 3 | 18.4 | 1.495 | 1.17 | 0.076 | 2.402 | 6.89 |
| 3 | 18.4 | 1.523 | 1.06 | 0.069 | 2.314 | 7.30 |
| 2 | 18.2 | 1.594 | 0.80 | 0.052 | 2.074 | 8.74 |
| 2 | 18.2 | 1.454 | 1.33 | 0.086 | 2.117 | 5.40 |
| 2 | 18.2 | 1.553 | 0.95 | 0.062 | 2.051 | 7.25 |
| 2 | 18.2 | 1.614 | 0.77 | 0.050 | 1.826 | 8.00 |
| Mean | | | | | | 7.31 ± 1.22 |

Table VI-15 (continued)

Thus, the mean A-value of [SeI] 4887 Å was found to be 7.31 $sec^{-1}$ with a standard deviation of ±1.22. The overall experimental error involved would be about the same as that estimated for the other forbidden lines, i.e. $\leq$ ±30%, giving the experimental result

$$A(4887\ \text{Å}) = 7.31 \pm 2.19\ sec^{-1}$$

(e) Obtaining the f-value of SeI 1994 Å from the Current Results

The f-value of SeI 1994 Å was also determined by assuming the A-value of [SeI] 4887 Å as obtained by Garstang (Ga 64) through a semiempirical and perturbation method, and then substituting it into the current measurements. The following relation was then obtained for each run:

$$f(1994\ \text{Å}) = \frac{k_0 \sqrt{T}}{(C_F/C_L)} \times 4.26 \times 10^{-5}$$

and it was then found that the mean f-value was

$$f(1994\ \text{Å}) = 0.24 \pm 0.06$$

The overall estimated error for this f-value would depend on the assumed A-value of [SeI] 4887 Å. This f-value may be compared to those obtained by Gruzdev (Gr 69) and Lawrence (La 67), which are 0.17 and 0.41 respectively.

(f) The Absolute Transition Probability of the [SeI] Line at λ7768 Å

The pen-chart and photon-counting profiles of the forbidden [SeI] line at λ7768 Å are illustrated in Figs. VI-20a and VI-20b respectively. The Ne-Se discharge (10 torr Ne) was run at a current of 30 mA. The A-value of this line was obtained by comparing its intensity with that of [SeI] 4887 Å, under the same conditions.

The asymmetric photon-counting profile shown in Fig. VI-20b indicates the presence of a weak blended line on the longer wavelength side. However, on choosing a slit width of 80 μ in the Spex, it was ascertained that the corresponding waveband of 0.86 Å - obtained with a grating dispersion of 10.7 Å/mm - would only allow a negligible contribution (dark area D), if any at all, from the weak blended line.

The results for the intensity or A-ratios for 10 runs are summarized in Table VI-16, after the response ratio, $z(= 1.09 \times 10^{-1})$, for the regions at λλ7768 and 4887 Å was determined.

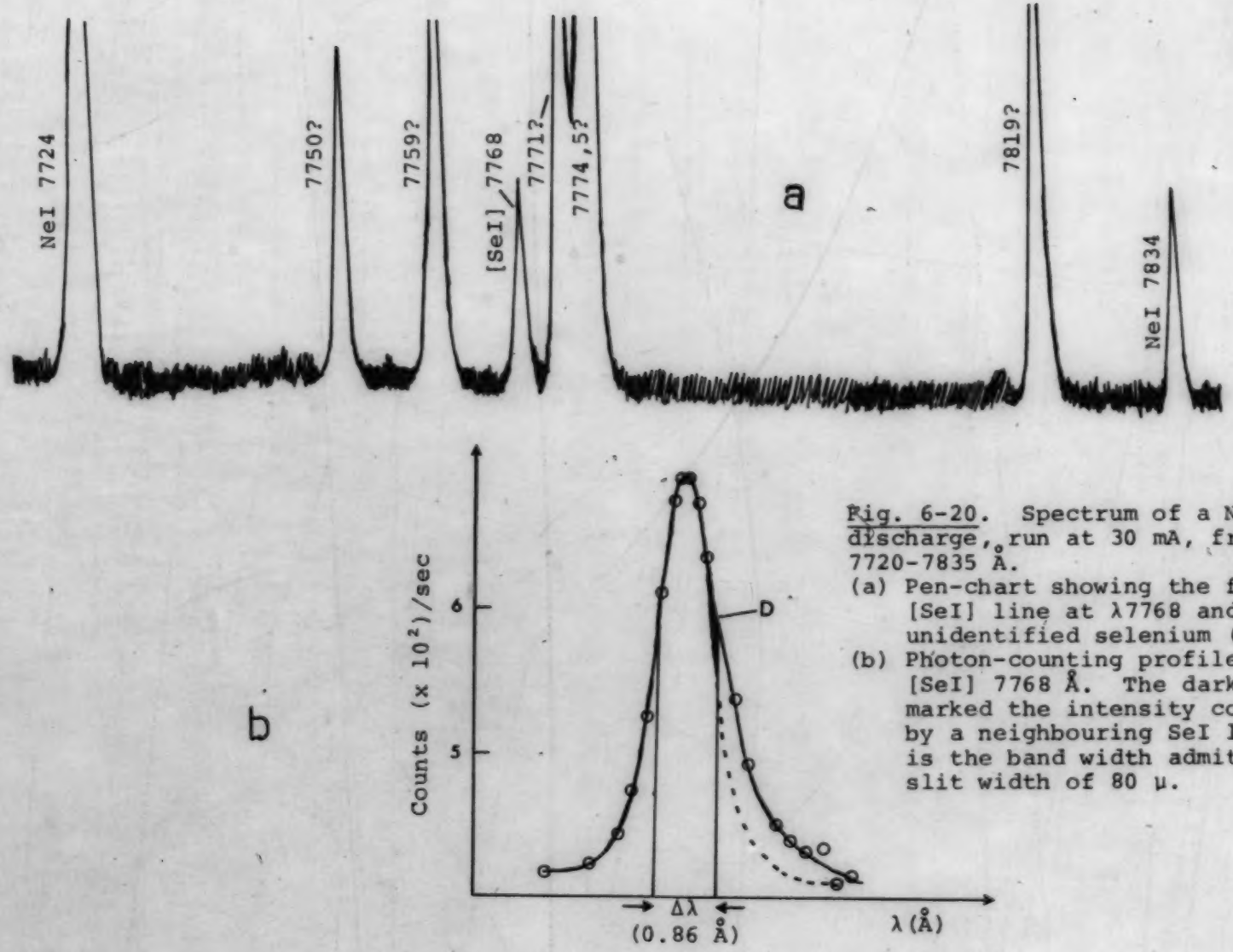


Fig. 6-20. Spectrum of a Ne-Se discharge, run at 30 mA, from 7720-7835 Å.
(a) Pen-chart showing the forbidden [SeI] line at λ7768 and other unidentified selenium (?) lines.
(b) Photon-counting profile of [SeI] 7768 Å. The dark area D marked the intensity contributed by a neighbouring SeI line. Δλ is the band width admitted by a slit width of 80 μ.

Table VI-16. Results on the A-ratios of the forbidden [SeI] lines at λλ4887 and 7768 Å.

| Neon (torr) | $\frac{C'(7768\ \text{Å})}{C'(4887\ \text{Å})}$ (x $10^{-2}$) | $\frac{I(7768\ \text{Å})}{I(4887\ \text{Å})}$ |
|---|---|---|
| 8 | 3.12 | $\frac{3.12 \times 10^{-2}}{1.09 \times 10^{-2}} = 0.286$ |
| 8 | 2.69 | 0.247 |
| 6.0 | 2.82 | 0.259 |
| 6.0 | 2.84 | 0.261 |
| 4.0 | 3.11 | 0.258 |
| 4.0 | 2.86 | 0.262 |
| 2.0 | 3.02 | 0.277 |
| 2.0 | 3.28 | 0.300 |
| 0.8 | 3.20 | 0.294 |
| 0.8 | 3.16 | 0.290 |
| Mean A(7768 Å)/A(4887 Å) | | 0.276 ± 0.017 |

Allowing an upper limit of ±10% error in the intensity-ratio measurements, we would have

$$\frac{A(7768\ \text{Å})}{A(4887\ \text{Å})} = 0.28 \pm 0.03$$

However, from the previous result

$$A(4887\ \text{Å}) = 7.31 \pm 2.19\ \text{sec}^{-1}$$

$$\therefore \quad A(7768\ \text{Å}) = 2.05\ \text{sec}^{-1}.$$

with a most probable error of ±0.65.

The new experimental A-values of [SeI] are the first ever measured and they are compared with those obtained by Garstang (Ga 64) in Table VI-17. Again here, it can be seen that the agreement among the results is very satisfactory.

| REFERENCE | A(4887 Å) ($sec^{-1}$) | A(7768 Å) ($sec^{-1}$) | A(7768 Å) / A(4887 Å) |
|---|---|---|---|
| Theoretical | | | |
| Garstang (Ga 64) | 7.7 | 2.3 | 0.30 |
| Experimental | | | |
| Present work | 7.31 ± 2.19 | 2.05 ± 0.65 | 0.28 ± 0.03 |

Table VI-17. Comparison of the experimental and theoretical A-values on [SeI] 4887 and 7768 Å (in $sec^{-1}$).

(g) Measuring the Atomic Populations of the Ground States of Selenium

In the search for new materials for gas lasers, Bokhan (Bo 69) suggested the favourably situated energy levels of the selenium ground state configuration - "the presence of groups of three levels due to splitting of the $^3P$ state can lead to rapid relaxation by means of

collisions, while the absence of an electric dipole transition between the $^3P$ and $^1D$ and $^1S$ states, in association with the larger energy differences of $^1S$ - $^3P$ and $^1D$ - $^3P$ transitions, leads to long lifetimes for the $^1S$ and $^1D$ levels".

The optical line-absorption technique has also been applied here to determine the population densities of the selenium ground states from the point of view of investigating population inversion among them. This technique (described in section 4.2) differs from the usual absorption technique in that the absorption cell is simultaneously used as the light source; thus the disadvantages associated with unequal thermal source and absorber temperature are automatically eliminated.

In general, to obtain the population densities N by this absorption method, all the other parameters (besides N) involved in equation (4-45) must be known:

$$\frac{1}{N_i} = \left(\frac{\pi e^2}{mc}\right)\sqrt{\frac{M}{2\pi R}} \cdot \frac{\lambda_{ih}\, f_{ih}}{k_{o_{ih}}} \qquad (4\text{-}45)$$

After making the numerical substitutions in this equation, the following general relationship for selenium energy states are obtained

$$N = \left(\frac{k_o \sqrt{T}}{\lambda_o\, f}\right) (6.86 \times 10^4) \text{ atoms/cm}^3$$

where the parameters are as defined previously.

In selenium, the optical line-absorption studies were carried out on the ultraviolet lines at λλ1994, 1855, 1691, 2040 and 2075 Å (see Fig. 6-21), to obtain the population density of the $^1S_0$, $^1D_2$, $^3P_0$, $^3P_1$ and $^3P_2$ levels respectively (i.e. all states within the ground configuration). The f-values of these lines were all taken from the "intermediate-coupling" calculations of Gruzdev (Gr 69), i.e. f(1994 Å) = 0.17, f(1855 Å) = 0.13, f(1691 Å) = 0.068, f(2040 Å) = 0.054 and f(2075 Å) = $2.3 \times 10^{-4}$.

The results on the atomic densities of these ground states are summarized in Table VI-18. The pressure range used for the $^1D$ and $^3P$ states was 10 to 20 torr, so that the normalisation process for the intensity values of $I_\ell$, as described in section 5.3(c), was not required. The pressure range used for the $^1S$ state was lower (2 to 10 torr) and the normalisation procedure was applied there whenever necessary. (It was possible to do this since the intensity of the forbidden [SeI] line at λ4887 Å was being measured at the same time.)

However, it was impossible to correlate the results with the change of pressure or any other discharge conditions because the partial pressure of the selenium vapour varied according to that exerted by the neon gas (which differred for each discharge condition), and no effective way of measuring the selenium partial pressure was possible.

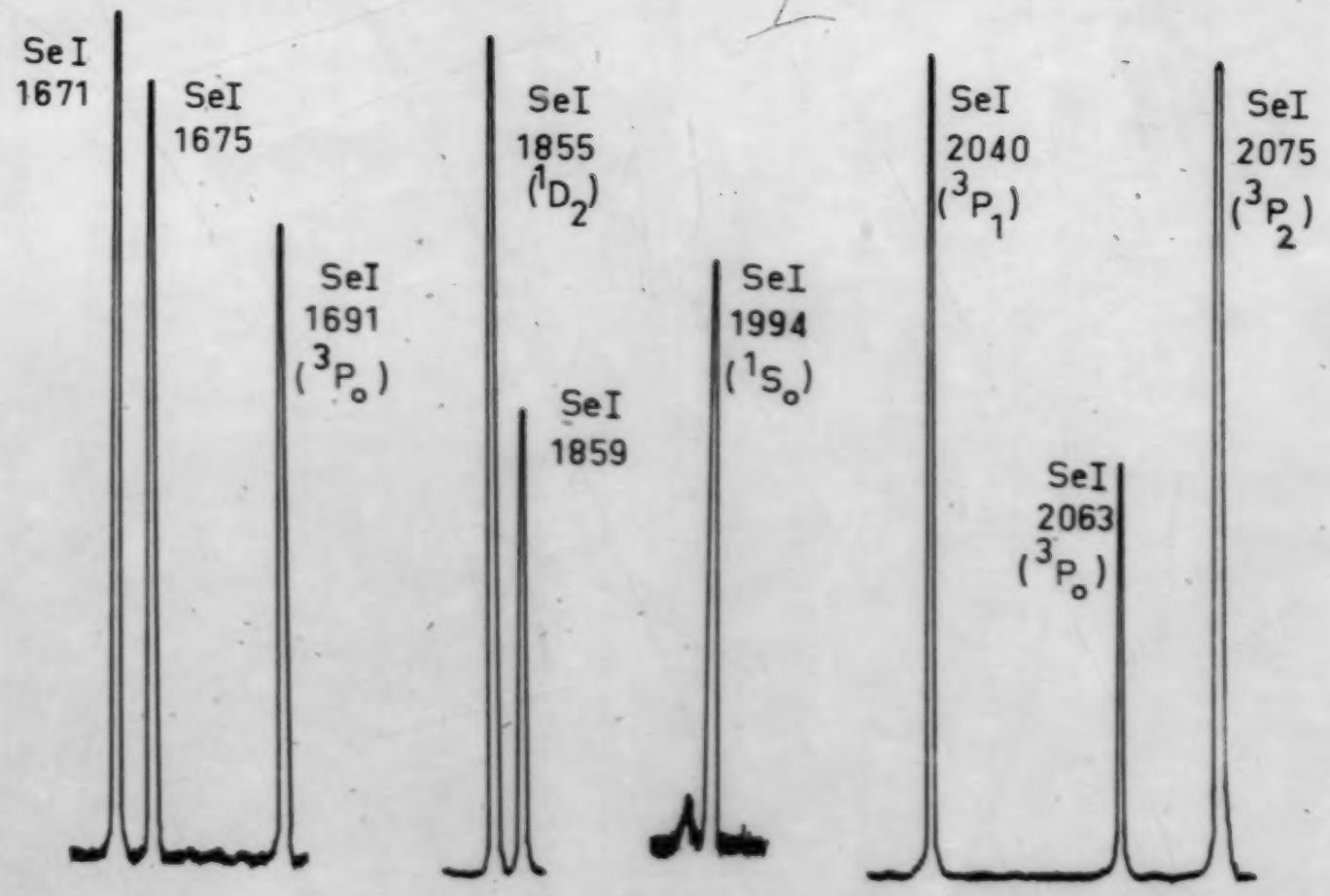


Fig. 6-21. The uv SeI lines used in the absorption experiment for determining the atomic state densities of the ground states $^1S$, $^1D$ and $^3P$.

| Neon (Torr) | Selenium (Torr) | $\sqrt{T}$ ($\sqrt{°K}$) | SeI 1994 Å | | | $N(^1S_0)$ (x $10^{10}$) |
|---|---|---|---|---|---|---|
| | | | $I_L/I_\ell$ | $k_o\ell$ | $k_o$ ($cm^{-1}$) | |
| 12 | $P_a$ | 18.5 | 1.832 | 0.28 | 0.018 | 0.67 |
| 10 | $P_b$ | 18.4 | 1.857 | 0.24 | 0.016 | 0.59 |
| 8 | $P_c$ | 18.5 | 1.723 | 0.50 | 0.032 | 1.19 |
| 6 | $P_d$ | 18.3 | 1.518 | 1.07 | 0.069 | 2.55 |
| 4 | $P_e$ | 18.3 | 1.416 | 1.50 | 0.097 | 3.59 |
| Neon (Torr) | Selenium (Torr) | $\sqrt{T}$ ($\sqrt{°K}$) | SeI 1855 Å | | | $N(^1D_2)$ (x $10^{10}$) |
| | | | $I_L/I_\ell$ | $k_o\ell$ | $k_o$ ($cm^{-1}$) | |
| 20 | $P_1$ | 18.08 | 1.892 | 0.18 | 0.012 | 0.62 |
| 15 | $P_2$ | 18.22 | 1.484 | 1.20 | 0.078 | 4.04 |
| 12 | $P_3$ | 18.30 | 1.477 | 1.26 | 0.082 | 4.26 |
| 10 | $P_4$ | 18.11 | 1.727 | 0.50 | 0.032 | 1.65 |

Table VI-18. Atomic state densities of the ground states of selenium per $cm^3$. (Continued)

| Neon (Torr) | Selenium (Torr) | $\sqrt{T}$ ($\sqrt{°K}$) | SeI 1691 Å | | | $N(^3P_0)$ (x $10^{10}$) |
|---|---|---|---|---|---|---|
| | | | $I_L/I_\ell$ | $k_o\ell$ | $k_o$ ($cm^{-1}$) | |
| 20 | $P_1$ | 18.08 | 1.769 | 0.42 | 0.027 | 2.91 |
| 15 | $P_2$ | 18.22 | 1.427 | 1.45 | 0.094 | 10.22 |
| 12 | $P_3$ | 18.30 | 1.550 | 0.96 | 0.062 | 6.77 |
| 10 | $P_4$ | 18.11 | 1.532 | 1.02 | 0.066 | 7.14 |
| | | | SeI 2040 Å | | | $N(^3P_1)$ (x $10^{10}$) |
| 20 | $P_1$ | 18.08 | 1.770 | 0.51 | 0.033 | 3.72 |
| 15 | $P_2$ | 18.22 | 1.388 | 1.70 | 0.110 | 12.49 |
| 12 | $P_3$ | 18.30 | 1.479 | 1.23 | 0.080 | 9.12 |
| 10 | $P_4$ | 18.11 | 1.462 | 1.30 | 0.084 | 9.48 |
| | | | SeI 2075 Å | | | $N(^3P_2)$ (x $10^{13}$) |
| 20 | $P_1$ | 18.08 | 1.714 | 0.52 | 0.034 | 0.89 |
| 15 | $P_2$ | 18.22 | 1.374 | 1.78 | 0.116 | 3.04 |
| 12 | $P_3$ | 18.30 | 1.503 | 1.13 | 0.073 | 1.92 |
| 10 | $P_4$ | 18.11 | 1.657 | 0.67 | 0.043 | 1.12 |

Table VI-18 (continued)

Nevertheless, the results indicate that the population of the $^3P_2$ level was generally about a factor of 100 higher than either of the levels $^1S_0$, $^1D_2$, $^3P_0$ and $^3P_1$, and that $N(^3P_1) > N(^3P_0) > N(^1D_2) > N(^1S_0) \approx 10^{10}$ atoms/cm$^3$ for the same selenium partial pressure (see results for the mixtures consisting of 12 torr of neon). Thus, these results would indicate that population inversion does not exist among these ground states with the present conditions; selective optical-pumping of the energy levels would be required to produce the inversion, but no further studies in this direction were made in the present study.

# CHAPTER VII

## SUMMARY

The present studies on the forbidden transitions in the first three elements with a $np^4$ ground configurations have included, in brief, the following:

(1) A study of the basic characteristics of the "forbidden" radiation and the special techniques employed for producing the lines in the laboratory, whereby their most interesting property - transition probability - was experimentally determined.

(2) A comprehensive survey of the two theoretical approaches that were introduced to calculate the A-values of forbidden lines was made. In the first approach a semiempirical approximation based on an intermediate coupling and thus perturbative method was employed, whereas a non-closed shell many electron theory was used in the second.

(3) The chemical processes involved in the production mechanism(s) of the metastable atoms and thus of the forbidden lines were investigated and a resulting production mechanism that applies to forbidden transitions from both the upper atmospheric as well as the laboratory sources, was proposed in this work.

(4) An optical line-absorption technique was employed on the allowed ultraviolet lines to determine the population densities of the metastable energy levels. This technique, when carried out simultaneously with the absolute intensity measurements of forbidden lines, have here produced a successful method for measuring the absolute A-values of forbidden lines.

By analogous considerations this method has also been used to determine the f-values of the allowed ultraviolet lines, which were feeding the upper metastable levels of forbidden lines, whose A-values were initially assumed (from theoretical sources).

(5) Applications of the experimental results from the present work were directed towards such studies in astrophysics as the determination of the solar elemental abundances and partially towards laser physics from the point of view of studing population inversion. The most important use from the results was obtained through a comparison to theoretical results that were based on approximations where the fact that an estimate of the overall error involved from them cannot be obtained, represents a shortcoming.

The results of the improved experimental techniques employed in this work represent the only source for the experimental (forbidden) A-values which are often needed in many important studies. Thus, apart from 5577 Å, the results

for the [OI], [SI] and [SeI] lines are the first ever determined experimentally. These A-values and the f-values of some related ultraviolet lines are summarized in Tables VII-1 and VII-2.

It is now hoped that the present studies on forbidden transitions can be extended to the heavier $np^4$ elements, such as tellurium and polonium, and to those with a $np^2$ or $np^3$ ground configuration. Again here, the problem associated with these further studies would depend on the individual lines and the atomic-molecular structure of the elements. Also, other improvements in the instrumentation, the design of the discharge tube and the f-values assumed, among other possible factors, would help to reduce the experimental errors involved.

| | $np^4(^1S_0 - {}^3P_1)$, MD | $np^4(^1S_0 - {}^1D_2)$, EQ | |
|---|---|---|---|
| OI (n = 2) | A(2972) $sec^{-1}$ | A(5577) $sec^{-1}$ | A(5577)/A(2972) |
| Present work | 0.045 ± 0.014 | 1.06 ± 0.32 | 23.7 ± 2.4 |
| SI (n = 3) | A(4589) $sec^{-1}$ | A(7725) $sec^{-1}$ | A(7725)/A(4589) |
| Present work | 0.31 ± 0.09 | 1.52 ± 0.49 | 4.9 ± 0.5 |
| SeI (n = 4) | A(4887) $sec^{-1}$ | A(7768) $sec^{-1}$ | A(7768)/A(4887) |
| Present work | 7.31 ± 2.19 | 2.05 ± 0.65 | 0.28 ± 0.03 |
| | $np^4(^1D_2 - {}^3P_2)$, MD & EQ | $np^4(^1D_2 - {}^3P_1)$, MD & EQ | |
| OI (n = 2) | A(6300) $sec^{-1}$ | A(6364) $sec^{-1}$ | A(6300)/A(6364) |
| Present work | 5.61 ± 1.87 | 1.80 ± 0.62 | 0.32 ± 0.03 |

Table VII-1. Summary of the forbidden A-values obtained in the present work.

| Transitions | f-values |
|---|---|
| OI 1218 Å ($2p^4\ ^1S_0 - 2p^3\ 3s''\ ^1P^o_1$) | 0.134 |
| OI 1152 Å ($2p^4\ ^1D_2 - 2p^3\ 3s'\ ^1D^o_2$) | 0.116 |
| SI 1782 Å ($3p^4\ ^1S_0 - 3p^3\ 4s''\ ^1P^o_2$) | 0.28 |
| SeI 1994 Å ($4p^4\ ^1S_0 - 4p^3\ 5s''\ ^2P^o_1$) | 0.24 |

Table VII-2. Summary of the allowed f-values obtained in the present work.

# BIBLIOGRAPHY


(Al 49) L. H. Aller, C. W. Ufford, and J. H. Van Vleck, Astrophys. J. 109, 42 (1949).

(Al 53) L. H. Aller, "The Atmospheres of the Sun and Stars", Ronald Press, New York, 142 (1953).

(Al 68) F. Alberti, R. A. Ashby and A. E. Douglas, Can. J. Phys. 46, 337 (1968).

(Ar 48) G. Araki, Prog. Theor. Phys., vol III, no. 2, 152 (1948).

(Ar 65a) L. A. Arzimovich, "Elementary Plasma Physics", Blaisdell Publ. Co., 57 (1965).

(Ar 65b) Ibid., p. 108.

(Ay 73) M. Aymar, Physica 66, 364 (1973).

(Ba 66) R. F. Barrow, G. G. Chandler, and C. B. Meyer, Phil. Trans. Roy. Soc. London A260, 395 (1966).

(Ba 68) R. F. Barrow and R. P. Parcq, J. Phys. B 1, 283 (1968).

(Be 65) W. R. Bennett, Jr., Appl. Opt., Suppl. on Chem. Lasers, 12 (1965).

(Be 72) D. R. Beck and O. Sinanoğlu, Phys. Rev. Lett. 28, 945 (1972).

(Bl 67) D. E. Blackwell, A. D. Pelford, and E. A. Mallia, Monthly Not. Roy. Astron. Soc. 136, 365 (1967).

(BO 28) I. S. Bowen, Astrophys. J. 67, 1 (1928).

(Bo 69) P. A. Bokhan, Opt. and Spect. XXVIII, no. 5, 459 (1970).

(Br 54) P. Brix and G. Herzberg, Can. J. Phys. 32, 110 (1954).

(Ca 48) J. Cabannes and J. Dufay, Comptes Rendus Ac. Sc. 226, 1569 (1948).

(Ca 56) J. Cabannes and J. Dufay, "The Airglow and the Aurorae", Permagon Press, London, 73 (1956).

(Ca 70) M. Carleer and R. Colin, J. Phys. B 3, 1715 (1970)

(Ch 30) S. Chapman, Mem. Roy. Meteor. Soc. 3, 103 (1930).

(Cl 51) W. J. Claas, Rech. Astrophys. Obs. Utr. 12, (1951).

(Co 34) E. U. Condon, Astrophys. J. 79, 217 (1934).

(Co 35) E. U. Condon and G. H. Shortley, "The Theory of Atomic Spectra", Cambridge, 98 (1935).

(Co 62) D. R. Corson and P. Lorrain, "Introduction to Electromagnetic Fields and Waves", Freeman, San Francisco, 446 (1962).

(Cz 63) S. J. Czyzak and T. K. Krueger, Astrophys. J. 126, 177 (1963).

(Da 67) A. Dalgarno and S. P. Khare, Planet. Space Sc. 15, 938 (1967).

(De 54) J. C. De Vos, Physica 20, 690 (1954).

(De 63) L. Delbouille and G. Roland, "Photometric Atlas of the Solar Spectrum from 7498 to 12016 Å", Liège (1963).

(Ea 69) R. H. Eather, J. Geophys. Res. 74, 153 (1969).

(Em 39) K. G. Emeleus, R. H. Sloane and E. B. Cathcart, Proc. Phys. Soc. London 51, 987 (1939).

(Er 65) K. B. S. Eriksson, Arkiv Fys. 16, 199 (1965).

(Er 72) K. B. S. Eriksson, Phys. Lett. 41A, 97 (1972).

(Er 73) K. B. S. Eriksson, J. Opt. Soc. Am. 63, 632 (1973).

(Fo 73) E. N. Forsman and K. C. Clark, Phys. Rev. A 7, 1203 (1973)

(Fr 30) R. Fredricks and J. S. Campbell, Phys. Rev. 36, 151, 1460 (1930).

(Fü 25) C. Füchtbauer and E. Holm, Z. phys. 26, 245 (1925).

(Ga 51) R. H. Garstang, Monthly Not. Roy. Astron. Soc. 111, 115 (1951).

(Ga 56) R. H. Garstang, "The Airglow and the Aurorae", Permagon Press, New York (1956).

(Ga 64) R. H. Garstang, J. Res., NBS-68A, 61 (1964).

(Ga 68) A. G. Gaydon, "Dissociation Energies", London, 69 (1968).

(Ga 74) R. H. Garstang, Private Communication (1974).

(Ge 41) E. Gerjuoy, Phys. Rev. 60, 233 (1941).

(Gi 69) F. R. Gilmore, E. Bauer, J. W. McGowan, J. Quant. Spect. Rad. Transf. 9, 157 (1969).

(Go 60) L. Goldberg, E. A. Müller and L. H. Aller, Astrophys. J. Suppl. Ser. 5, 1 (1960).

(Go 65) G. Gould, Appl. Opt., Suppl. on Chem. Lasers, 60 (1965).

(Gr 69) P. F. Gruzdev, Opt. Spect. XXVII, no. 6, 479 (1969).

(Ha 33) D. R. Hartree and M. M. Black, Proc. Roy. Soc. A 139, 311 (1933).

(Ha 39) D. R. Hartree, W. Hartree, and B. Swirles, Phil. Trans. Roy. Soc. A 238, 229 (1939).

(Ha 59) J. A. Harrison, Proc. Phys. Soc. London 73, 841 (1959).

(He 50) G. Herzberg, "Molecular Spectra and Structure Spectra of Diatomic Molecules", vol. I, 316-321 (1950).

(He 64) J. R. W. Heintze, H. Hubenet and C. De Jager, Bull. Astrophys. Inst. Neth. 17, 442 (1964).

(He 65) J. R. W. Heintze, Rech. Astron. Obs. Utr. 17, 1 (1965).

(Hi 66) R. L. Hilliard and C. G. Shepherd, Planet. Space Sc. 14, 383 (1966).

(Ho 67) H. Howelger, Z. Astrophys. 65, 365 (1967).

(Je 41) F. A. Jenkins and S. Mrozowski, Phys. Rev. 59, 808 (1941).

(Ka 69) V. Kaufman and L. J. Radziemski, Jr., J. Opt. Soc. Am. 59, 227 (1969).

(Ke 68) J. A. Kernahan, Ph.D. Thesis, The Queen's University of Belfast (1968).

(Ke 75a) J. A. Kernahan and P. H. L. Pang, Can. J. Phys. 53, 455 (1975)

(Ke 75b) J. A. Kernahan and P. H. L. Pang, Can. J. Phys. 53, 1114 (1975).

(Ke 75c) J. A. Kernahan and P. H. L. Pang, Can. J. Phys. (To be published).

(Kr 72) P. H. Krupenie, J. Phys. and Chem. Ref. Data, vol. 1, no. 2, 520 (1972).

(Kv 47) G. Kvifte and L. Vegard, Geophys. Publ. Oslo 17, 3 (1947).

(La 67) G. M. Lawrence, Astrophys. J. 148, 261 (1967).

(Le 26) S. W. Leifson, Astrophys. J. 63, 73 (1926).

(Le 66) F. S. LeBlanc, O. Oldenberg, and N. P. Carleton, J. Chem. Phys. 45, 2200 (1966).

(Li 72) C. C. Lin, D. J. G. Irwin, J. A. Kernahan, A. E. Livingston and E. H. Pinnington, Can. J. Phys. 50, 2496 (1972).

(Ma 48) R. Maeder and E. Miescher, Helv. Phys. Acta 21, 441 (1948).

(Ma 60) W. C. Martin and C. H. Corliss, J. Res. NBS 64A, 443 (1960).

(Ma 68) E. A. Mallia, Solar Physics 3, 505 (1968).

(Mc 25) J. C. McLennan and G. M. Shrum, Proc. Phys. Soc. London A108, 501 (1925).

(Mc 28) J. C. McLennan, Proc. Phys. Soc. London A120, 327 (1928).

(Mc 64) McKoy and O. Sinanoğlu, J. Chem. Phys. 41, 2689 (1964).

(Mc 64a) E. W. McDaniel, "Collision Phenomena in Ionized Gases", Wiley, New York, 506 (1964).

(Mc 64b) Ibid., p. 50.

(Mc 66) J. W. McConkey, D. J. Burns, K. A. Moran, and K. G. Emeleus, Phys. Lett. 22, 416 (1966).

(Mc 68) J. W. McConkey, D. J. Burns, K. A. Moran, and J. A. Kernahan, Nature 217, 538 (1968).

(Mc 69) J. W. McConkey and J. A. Kernahan, Planet. Space Sc. 17, 1297 (1969).

(Mc 70) J. W. McConkey, R. E. W. Pettifer and K. A. Moran, Planet Space Sc. 17, 1429 (1969).

(Me 64) P. H. Metzer and G. R. Cook, J. Quant. Spect. Rad. Trans. 4, 107 (1964).

(Me 69) J. A. Meyer, D. W. Setser and D. H. Stedman, Astrophys. J. 157, 1023 (1969).

(Mi 34a) A. C. G. Mitchell and M. W. Zeemansky, "Resonance Radiation and Excited Atoms", Cambridge, 99 (1934).

(Mi 34b) Ibid., p. 96.

(Mo 49) C. E. Moore, "Atomic Energy Levels", NBS 467, 1949).

(Mr 44) S. Mrozowski, Rev. Mod. Phys. 16, 153 (1944).

(Mü 64) E. A. Müller and J. P. Mutschlecner, Astrophys. J. suppl. 9, 1 (1964).

(Mü 68) E. A. Müller, B. Baschek and H. Howelger, Solar Physics 3, 125 (1968).

(Mü 68b) D. Müller, Z. Naturf. 23a, 1707 (1968).

(Mu 69) W. Murcray, Planet. Space Sc. 17, 1429 (1969).

(Ni 61) J. H. Nilson and G. G. Shepherd, Planet. Space Sc. 5, 229 (1961).

(Ni 70) C. Nocolaides and O. Sinanoğlu, J. Physique C4, nos. 11-12, Tome 31, 117 (1970).

(Ni 71) C. Nicolaides, O. Sinanoğlu and P. Westhaus, Phys. Rev. A 4, 1400 (1971).

(Ni 72) C. A. Nicolaides, D. R. Beck and O. Sinanoğlu, J. Phys. B 6, 62 (1973).

(Og 68) M. Ogawa, Can. J. Phys. 46, 312 (1968).

(Og 70) M. Ogawa and K. R. Yamawaki, Appl. Opt. 9, 1709 (1970).

(Ök 69) I. Öksüz and O. Sinanoğlu, Phys. Rev. 181, 42 (1969).

(Om 56) A. Omholt, "The Airglow and the Aurorae", Permagon Press, New York (1956).

(Om 71) A. Omholt, "The Optical Aurorae", Permagon Press, New York, 143 (1971).

(Or 36) L. S. Orstein, Physica 3, 561 (1936).

(Ot 71) W. R. Ott, Phys. Rev. A 4, 245 (1971).

(Pa 30) F. Pascheu, Z. Physik 65, 1 (1930).

(Pa 40) S. Pasternak, Astrophys. J. 92, 129 (1940).

(Pa 70) T. D. Parkinson, E. C. Zipf, Jr., and T. M. Donohue, Planet. Space Sc. 18, 187 (1970).

(Ra 52) G. Racah, Phys. Rev. 85, 381 (1952).

(Re 67) M. H. Rees and A. Dalgarno, Planet. Space Sc. 15, 1097 (1967).

(Ro 63) C. C. J. Roothan and P. S. Bagus, "Methods in Computational Physics", New York (1963).
C. C. J. Roothan and P. S. Kelly, Phys. Rev. 131, 1177 (1963)
E. Clementi, "Tables of Atomic Functions, IBM Res. Lab., California (1967).

(Ru 34) J. E. Ruedy and R. C. Gibbs, Phys. Rev. 46, 880 (1934).

(Ru 44) A. Rubinowicz, Rep. Prog. Phys. 12, 233 (1944).

(Ru 54) G. A. W. Rutgers and J. C. De Vos, Physica 20, 715 (1954).

(Sa 65) I. Sattarov, Astrophys. J. 114, 469 (1965).

(Sc 55a) L. I. Schiff, "Quantum Mechanics", McGraw-Hill, 280-285, 400-403 (1955).

(Sc 55b) Ibid., p. 251.

(Sc 68) K. Schurer, Optik 28, 400 (1968).

(Se 54) M. J. Seaton, J. Atm. Terrest. Phys. 4, 295 (1954).

(Sh 41) G. H. Shortley, L. H. Aller, J. G. Baker, and D. H. Menzel, Astrophys. J. 93, 178 (1941).

(Si 68) O. Sinanoğlu and I. Öksüz, Phys. Rev. Lett. 21, 507 (1968).

(Si 73) O. Sinanoğlu and D. R. Beck, Chem. Phys. Lett. 24, 20 (1973).

(Sl 66) H. T. Silverstone and O. Sinanoğlu, J. Chem. Phys. 44, 1899, 3608 (1966).

(St 60) R. Stair, R. G. Johnston, and E. W. Halbach, J. Res. NBS-A, 64A, 291 (1960).

(St 60b) W. Stofregen and H. Derblom, Nature 185, 28 (1960).

(St 66) A. R. Striganov and N. S. Sventitskii, "Tables of Spectral Lines", Atomizdat, Moscow (1966).

(Sw 66) J. P. Swings, Ann. d'Astrophys. 29, 371 (1966).

(Sw 69) J. P. Swings, D. L. Lambert and N. Grevesse, Solar Physics 6, 3 (1969).

(Ta 52) Y. Tanaka, J. Chem. Phys. 20, 1728 (1952).

(Ta 62) Y. Tanaka and M. Ogawa, J. Chem. Phys. 36, 726 (1962).

(To 60) Y. G. Toresson, Arkiv Fysik 18, 417 (1960).

(Tr 52) R. E. Trees, Phys. Rev. 85, 382 (1952).

(Tu 62) E. C. Turgeon and G. G. Shepherd, Planet. Space Sc. 9, 295 (1962).

(Ve 34) L. Vegard, Geofys. Publ. Oslo 11, 1 (1934).

(Wa 58) K. Watanabe, Adv. Geophys. 5, 153 (1958).

(Wa 59) L. Wallace and J. W. Chamberlain, Planet. Space Sc. 2, 60 (1959).

(Wa 61) R. E. Watson and A. J. Freeman, Phys. Rev. 124, 1117 (1961).

(Wa 72) K. Watadani, J. Geomag. Geoelect. 24, 153 (1972).

(We 69) P. Westhaus and O. Sinanoğlu, Phys. Rev. 183, 56 (1969).

(Wh 34a) H. E. White, "Introduction to Atomic Spectra", McGraw-Hill Co., New York and London, 420 (1934).

(Wh 34b) Ibid., p. 422.

(Wh 34c) Ibid., p. 430.

(Wi 28) E. Wigner and E. E. Witmer, Z. Physik 51, 859 (1928).

(Wi 34) K. Wieland, M. Wehrli and E. Miescher, Helv. Phys. Acta 7, 841 (1934).

(Wi 61) W. L. Wiese and J. B. Shumaker, Jr., J. Opt. Soc. Am. 51, 937, 1009 (1961).

(Wi 66) W. L. Wiese, M. W. Smith, and B. M. Glennon, Nat. Stand. Ref. Data Ser., NBS 4, 82 (1966).

(Ya 52) T. Yamanouchi and H. Horie, J. Phys. Soc. Japan 7, no. 1, 52 (1952).

(Zi 69) E. C. Zipf, Can. J. Chem. 47, 1863 (1969).